0830-L-02 NAS1.29/3-2.97-06

NASA Tech Briefs

National Aeronautics and
Space Administration

Electronic Components and Circuits

Electronic Systems

Physical Sciences

Materials

Computer Programs

Mechanics

Machinery

Fabrication Technology

Mathematics and Information Sciences

Life Sciences

97-06
1999-035331
June 1997

C

INTRODUCTION

Tech Briefs are short announcements of new technology derived from the research and development activities of the National Aeronautics and Space Administration. These Briefs emphasize information considered likely to be transferable across industrial, regional, or disciplinary lines and are issued to encourage commercial application.

Availability of NASA Tech Briefs and TSP's

Distribution of NASA Tech Briefs, a monthly periodical publication, is limited to engineers in U.S. industry and to other domestic technology transfer agents. Requests for individual Tech Briefs or for Technical Support Packages (TSP's) announced herein should be addressed to

NASA Center for AeroSpace Information
Technology Transfer Office
800 Elkridge Landing Rd.
Linthicum Heights, MD 21090-2934
Telephone No. (301) 621-0245

Please reference the three-letter, five-digit control number located at the end of each Tech Brief. Information on NASA's Technology Utilization Program, its documents, and services is also available at the same facility.

Technology Utilization Officers and Patent Counsels are located at NASA field installations to provide technology-transfer access to industrial users. Inquiries can be made by writing to NASA field installations listed below.

Technology Utilization Officers and Patent Counsels

Ames Research Center
Technology Utilization Officer
Mail Code 223-3
Moffett Field, CA 94035

Patent Counsel
Mail Code 200-11
Moffett Field, CA 94035

Goddard Space Flight Center
Technology Utilization Officer
Mail Code 702-1
Greenbelt, MD 20771

Patent Counsel
Mail Code 204
Greenbelt, MD 20771

Lyndon B. Johnson Space Center
Technology Utilization Officer
Mail Code IC-4
Houston, TX 77058

Patent Counsel
Mail Code AL3
Houston, TX 77058

John F. Kennedy Space Center
Technology Utilization Officer
Mail Stop PT-PMO-A
Kennedy Space Center, FL 32899

Patent Counsel
Mail Code PT-PAT
Kennedy Space Center, FL 32899

Langley Research Center
Technology Utilization Officer
Mail Stop 143
Hampton, VA 23665

Patent Counsel
Mail Code 279
Hampton, VA 23665

Lewis Research Center
Technology Utilization Officer
Mail Stop 7-3
21000 Brookpark Road
Cleveland, OH 44135

Patent Counsel
Mail Code LE-LAW
21000 Brookpark Road
Cleveland, OH 44135

Jet Propulsion Laboratory
Technology Utilization Officer
Mail Stop 156-211
4800 Oak Grove Drive
Pasadena, CA 91109

NASA Resident Office-JPL
Technology Utilization Officer
Mail Stop 180-801
4800 Oak Grove Drive
Pasadena, CA 91109

Patent Counsel
Mail Code 180-801
4800 Oak Grove Drive
Pasadena, CA 91109

George C. Marshall Space Flight Center
Technology Utilization Officer
Code AT01
Marshall Space Flight Center, AL 35812

Patent Counsel
Mail Code CC01
Marshall Space Flight Center, AL 35812

John C. Stennis Space Center
Technology Utilization Officer
Code HA-30
Stennis Space Center, MS 39529

NASA Headquarters
Technology Utilization Officer
Code CU
Washington, DC 20546

Assistant General Counsel for Patent Matters
Code GP
Washington, DC 20546

Dryden Flight Research Center
Technology Utilization Officer
M/S D21-31
Bldg. 4832 Whse 7
Lilly Dr.
Edwards, CA 93523

NASA TechBriefs

National Aeronautics and
Space Administration

June 1997
97-06

5 Electronic Components and Circuits

11 Electronic Systems

17 Physical Sciences

29 Materials

35 Computer Programs

39 Mechanics

55 Machinery

61 Fabrication Technology

65 Mathematics and Information Sciences

This document was prepared under the sponsorship of the National Aeronautics and Space Administration. Neither the United States Government nor any person acting on behalf of the United States Government assumes any liability resulting from the use of the information contained in this document, or warrants that such use will be free from privately owned rights.

BLANK PAGE

Electronic Components and Circuits

Hardware, Techniques, and Processes

7 Planar Quad-Bridge-Diode Frequency Doubler
8 Multiloop Photonic/Electronic Frequency Synthesizers
9 Au/Ge/Au Contacts for Shallow-Junction InP Solar Cells
9 Ag/Zn Contacts on Shallow-Junction p-Doped InP Devices
10 Diffusion Barriers for GaAs and InP Devices

BLANK PAGE

Planar Quad-Bridge-Diode Frequency Doubler

Input and output circuits are isolated without complicated filter structures.

NASA's Jet Propulsion Laboratory, Pasadena, California

A quad-bridge varactor-diode 10-to-20-GHz frequency-doubling circuit features integrated planar construction on a quartz substrate, with quasi-optical input and output coupling via fully open antenna substructures. The design of this frequency doubler exploits electrical and geometrical symmetries to achieve a simple, compact overall structure with inherent isolation between input and output ports. This frequency doubler is a frequency-scaled prototype of proposed frequency multipliers that would operate at frequencies of the order of 1 THz and that would offer attractive alternatives to conventional waveguide-construction microwave and millimeter-wave frequency multipliers.

The quad-bridge circuit configuration (see Figure 1) results in balanced frequency-doubling action and provides frequency isolation between input and output ports, without need for complicated filter structures; this is because diodes in a quad-bridge configuration inherently reject even harmonics at the input port and reject odd harmonics at the output port. In comparison with the design of a single-diode frequency multiplier, the design of this multiplier maintains the same optimum conversion gain and optimum input and output load impedances but quadruples the power-handling capability.

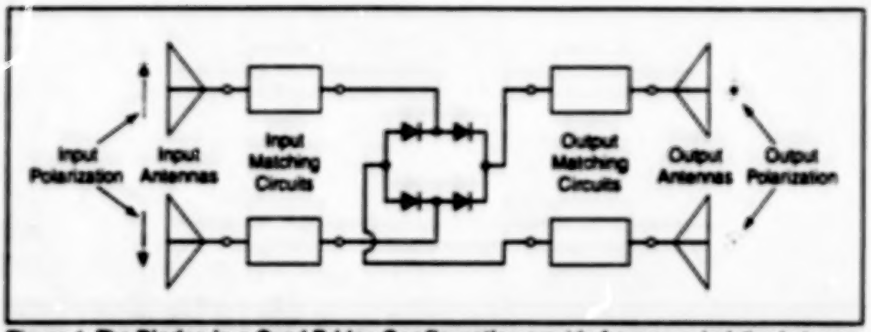

Figure 1. The Diodes in a Quad-Bridge Configuration provide frequency isolation between the input and output antennas.

Input and output couplings are implemented with two pairs of double-slot antennas that are polarized perpendicularly to each other (see Figure 2) to enhance input/output isolation. Compact coplanar transmission-line matching circuits are placed between the antennas and the diodes to maximize input coupling at the fundamental frequency and output coupling at the second harmonic, thus helping to maximize frequency-conversion efficiency. The circuit can be mounted on a dielectric lens or on the flat outer surface of a dielectric (quartz)-filled paraboloidal reflector to obtain the desired input/output radiation patterns.

This work was done by Moonil Kim, Jean Bruston, R. Peter Smith, Suzanne C. Martin, and Peter H. Siegel of Caltech for **NASA's Jet Propulsion Laboratory.** *Further information is contained in a TSP [see page 1].*

NPO-19724

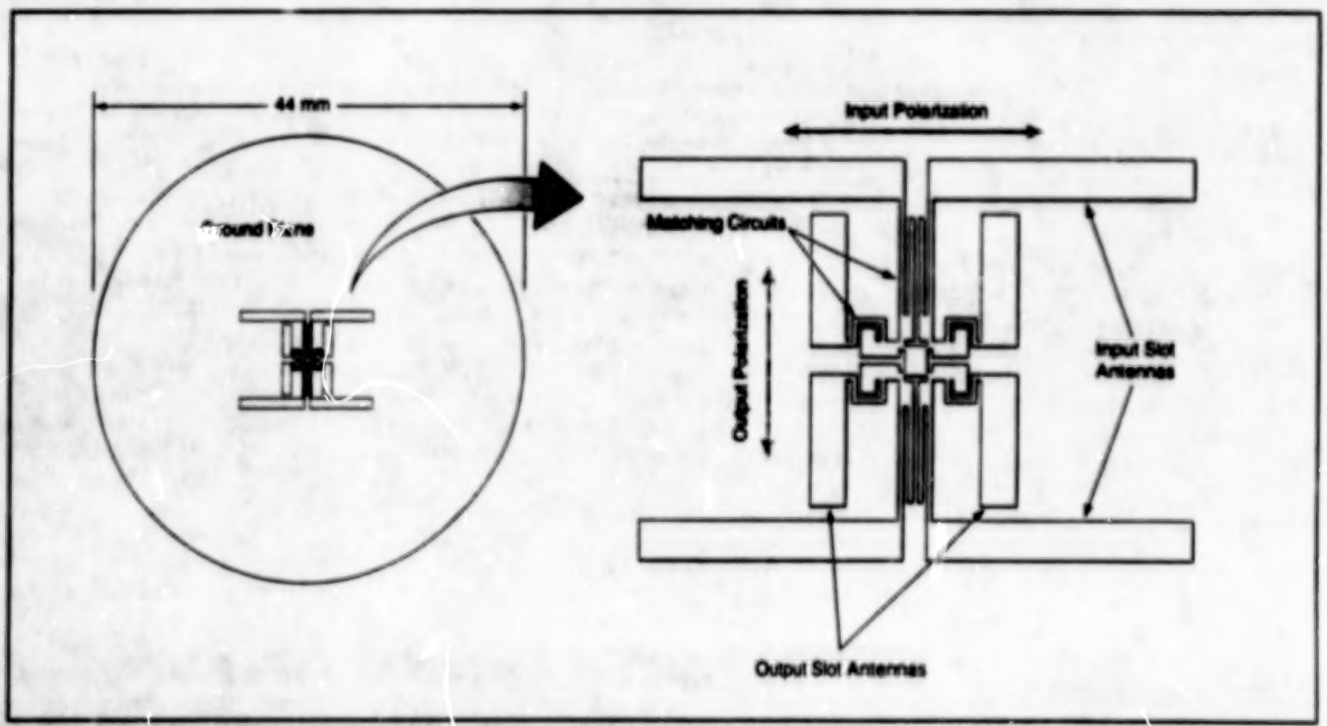

Figure 2. Orthogonal Input and Output Slot Antennas provide orthogonal input and output polarizations and thus polarization isolation between input and output antennas. A commercial quad-bridge diode chip is bonded to the center of the circuit.

Multiloop Photonic/Electronic Frequency Synthesizers

Advantages would include low phase noise, wide tuning range, and high frequency resolution.

NASA's Jet Propulsion Laboratory, Pasadena, California

Improved photonic/electronic oscillators with both optical and electrical outputs have been proposed in a continuing effort to develop frequency synthesizers with low phase noise, wide tuning range, and high resolution in frequency. A frequency synthesizer of this type would be an opto-electronic oscillator (OEO) with multiple parallel optical feedback loops and with a tunable radio-frequency (RF) filter.

OEOs were described (though not under the name "OEO") in three previous articles in *NASA Tech Briefs*, namely, "Light-Induced Microwave Oscillator" (NPO-19440), Vol. 20, No. 9 (September 1996), page 4a; "Electro-Optical Clock- and Carrier-Recovery Device" (NPO-19573), Vol. 20, No. 9 (September 1996), page 6a; and "Self-Injection-Locked Electro-Optical Microwave Oscillator" (NPO-19568), Vol. 20, No. 8 (August 1996), page 17a. These prior OEOs included single optical feedback loops. The use of multiple optical feedback loops in the proposed OEOs would be essential to their improved performance, as explained below.

In a basic OEO, a single optical feedback loop is concatenated with an electrical feedback loop. By including an RF filter with narrow pass band in the electrical feedback loop, one can allow oscillations to occur in one mode while suppressing oscillations in other modes. To reduce the phase noise of the OEO, the length of the optical feedback loop must be increased; this reduces the frequency interval between modes, necessitating a reduction in the bandwidth of the RF filter to ensure the selection of only the desired modal frequency. However, at a typical frequency that one seeks to generate (of the order of 10 GHz), it is difficult to make an RF filter with pass band narrow enough to discriminate between modes. In addition, the inclusion of a narrow-band RF filter sacrifices the tunability of the oscillator.

The proposed multiple-loop OEOs are intended to satisfy the need for both (1) longer optical feedback loops to reduce phase noise and (2) shorter optical feedback loops to facilitate discrimination against unwanted modes without narrow-band RF filters, while providing broad frequency tunability. The figure illustrates one of several dual-loop versions. This OEO would include a pump laser, a longer and a shorter fiber-optic delay line (longer and shorter optical feedback loops), a photodiode followed by an amplifier at the output end of each optical fiber, and a dual-drive electro-optical modulator driven by the outputs of the amplifiers.

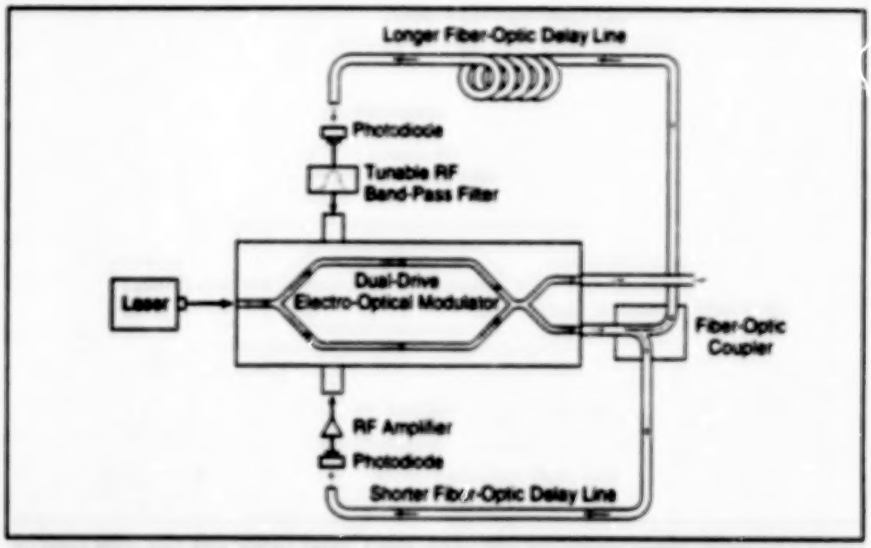

An OEO With Two Fiber-Optic Delay Lines would offer the greater phase stability of a longer feedback loop and the greater tuning range and frequency selectivity of a shorter feedback loop.

Suppose that the loop gains were adjusted to be more than 1/2 but less than 1 in each loop. Then oscillation could occur at and only at a radio frequency at which the signals arrive in phase at the output ends of both optical fibers; this would constrain the frequency interval between oscillation modes to be the larger interval of the shorter loop. Because of the relatively large frequency interval between oscillation modes, an RF filter with a relatively wide pass band would suffice to ensure single-mode operation. At the same time, the phase noise would be dictated by the longer loop and would thus be relatively low.

The tuning range of the OEO would be determined by the mode spacing of the shorter loop and the tuning resolution would be determined by mode spacing of the longer loop. For a larger tuning range, a tunable RF filter could be used. The combination of the twin loop OEO and a tunable RF filter would result in a novel frequency synthesizer with wide frequency tuning range, low phase noise, and high frequency resolution.

The frequency of oscillation (f) of a basic OEO can be changed by changing the effective length (L) of the feedback loop. The fractional change in frequency is given by $\Delta f/f = -\Delta L/L$. Because a given change in length constitutes a larger fraction of L in the shorter loop of a dual-loop OEO, such an OEO could be tuned through a wider range by adjusting the length of the shorter loop. The tuning range would be determined by the frequency interval between modes of the shorter loop, while the tuning resolution would be determined by the frequency interval between modes of the longer loop. For example, if the fiber-optic delay lines in a dual-loop OEO were made of typical materials and the lengths of the loops were 20 cm and 10 km, respectively, then the tuning range would be about 1 GHz and the tuning resolution would be about 20 kHz.

A tunable RF filter could be used to widen the tuning range. The tuning of the middle frequency of the pass band of the RF filter should be synchronized with the tuning of the length of the shorter optical fiber. The incorporation of the tunable RF filter in this way should result in a frequency synthesizer with a tuning range of tens of gigahertz, low phase noise, and high frequency resolution.

This work was done by Xiaotian Steve Yao of Caltech for **NASA's Jet Propulsion Laboratory**. *Further information is contained in a TSP [see page 1].*

In accordance with Public Law 96-517, the contractor has elected to retain title to this invention. Inquiries concerning rights for its commercial use should be addressed to

Larry Gilbert, Director
Technology Transfer
California Institute of Technology
Mail Code 315 - 6
Pasadena, CA 91125
(818) 395-3288

Refer to NPO-19825, volume and number of this NASA Tech Briefs *issue, and the page number.*

Au/Ge/Au Contacts for Shallow-Junction InP Solar Cells

These contacts exhibit low electrical resistivity and high thermal stability.

Lewis Research Center, Cleveland, Ohio

Au/Ge/Au contacts on InP semiconductor devices have been found to exhibit extremely low electrical resistivities. They have also been found to be highly thermally stable in the sense that the interdiffusion of metal and semiconductor materials during the sintering step of the fabrication process is retarded, relative to such interdiffusion that occurs during the sintering of devices made with other contact materials. The nature of this retardation of interdiffusion is such that sintering can be completed before the adverse effects of interdiffusion degrade the underlying semiconductor devices.

The development of Au/Ge/Au contacts is one achievement of a continuing program of research on fabricating electrical contacts for InP semiconductor devices, both with and without sintering. Some other achievements of this program were reported in previous articles in *NASA Tech Briefs*, namely: "Sinterless Fabrication of Contact Pads on InP Devices" (LEW-15863), Vol. 19, No. 10 (October 1995), page 90; "Sinterless Formation of Contacts on Indium Phosphide" (LEW-15814), Vol. 19, No. 10 (October 1995), page 45; "Sinterless Formation of Contacts on Indium Phosphide: Part 2 (LEW-15815), Vol. 21, No. 4 (April 1997), page 45; and "Ultra-Low-Resistance Metal Contacts on InP" (LEW-15816), Vol. 21, No. 4 (April 1997), page 45.

The need for sintering and the desire to avoid sintering if possible can be explained as follows: To make a low-resistance electrical contact to an InP semiconductor device according to the standard approach, one must deposit contact metal on the semiconductor, then sinter the contact metal at a suitably high temperature. Although sintering desirably reduces contact resistance, it also undesirably induces substantial interdiffusion between the metal and the underlying InP. Unless limited by imposition of one or more diffusion barrier(s) or by use of such techniques as rapid annealing, this interdiffusion can quickly degrade or destroy the device. Such shallow-junction devices as junction field-effect transistors and solar cells are particularly susceptible to damage during sintering to form contacts.

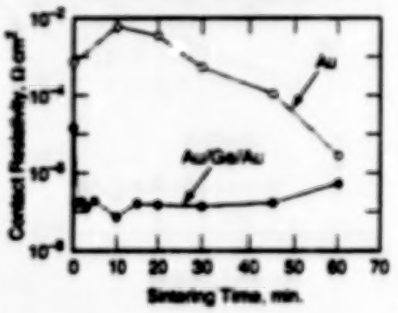

Figure 1. The Resistivities of Au/Ge/Au Contacts reached values much lower than those of Au (only) contacts after sintering for only 1 minute at 350 °C.

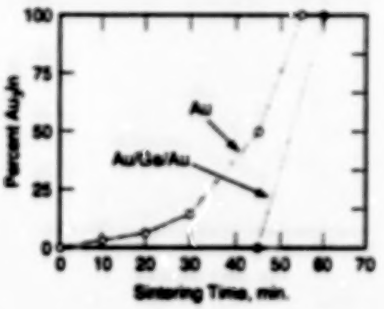

Figure 2. Conversion of Surface Au to Au_2In during sintering at 350 °C began immediately in Au (only) contacts but was delayed by 45 minutes in Au/Ge/Au contacts.

The desirable properties of Au/Ge/Au contacts were observed in experiments on InP n/p diodes with (100)-oriented substrates doped with Zn to a density of 8×10^{18} cm^{-3} and 2,000-Å-thick epitaxially deposited emitters doped with Si to a density of 1.7×10^{18} cm^{-3}. By use of electron-beam evaporation, contact layers were deposited on InP in the following sequence: Au 400 Å thick, Ge 200 Å thick, and Au 1,600 Å thick. After deposition of contacts, the devices were sintered in a nitrogen atmosphere at a temperature of 350 °C.

Figure 1 shows the evolution of contact resistivities of these devices and of similar devices with Au (only) contacts tested in previous experiments. Whereas the resistivity of the Au (only) contacts remained above 10^{-3} Ω·cm^2 for tens of minutes at the sintering temperature, only 1 minute at that temperature was necessary to bring the resistivity of the Au/Ge/Au contacts down to about 10^{-7} Ω·cm^2. The resistivities of these Au/Ge/Au contacts were among the lowest resistivities of any contacts on InP tested up to the time when these experiments were performed.

One measure of the interdiffusion of Au and InP is the fraction of outer-surface Au converted to Au_2In as a function of time during sintering at 350 °C. Using this measure, Figure 2 illustrates the retardation of interdiffusion in the Au/Ge/Au contacts as compared to the Au (only) contacts: whereas the formation of Au_2In was observed immediately on Au (only) contacts, it was not observed on Au/Ge/Au contacts until 45 minutes into the sintering process.

This work was done by V. G. Weizer of **Lewis Research Center**; *N. S. Fatemi of Sverdrup Technology, Inc.; and A. L. Korenyi-Both of Calspan Corp. Further information is contained in a TSP [see page 1].*

Inquiries concerning rights for the commercial use of this invention should be addressed to the Patent Counsel, Lewis Research Center [see page 1]. Refer to LEW-16280.

Ag/Zn Contacts on Shallow-Junction p-Doped InP Devices

Low-resistance contacts can be formed without substantial metal/semiconductor interdiffusion.

Lewis Research Center, Cleveland, Ohio

Ag/Zn contacts on p-doped InP semiconductor electronic devices have been found to exhibit electrical resistivities as low as 10^{-4} Ω·cm^2. The contacts are formed by deposition of a combination of Ag and Zn on the InP surfaces, then sintering. Unlike in the fabrication of contacts from some other materials, the sintering step in the fabrication of Ag/Zn contacts does not cause so much interdiffusion of metal and semiconductor materials as to

degrade or destroy the underlying devices.

The development of Ag/Zn contacts is one achievement of a continuing program of research on fabricating electrical contacts for InP semiconductor devices, as noted in the preceding article. The role of sintering in the fabrication of contacts is also discussed in the preceding article.

Zn apparently exerts two major effects in the fabrication of Ag/Zn contacts. One effect is substantial retardation of the interdiffusion of the metal contact and underlying semiconductor materials; the interdiffusion is suppressed to such an extent that contacts can be formed directly on very-shallow-junction devices without damaging them. The other major effect of Zn is a significant reduction in contact resistivity.

This work was done by Victor G. Weizer of **Lewis Research Center** *and Navid S. Fatemi of Essential Research, Inc. No further documentation is available.*

Inquiries concerning rights for the commercial use of this invention should be addressed to the Patent Counsel, Lewis Research Center [see page 1]. Refer to LEW-16037.

Diffusion Barriers for GaAs and InP Devices

Amorphous ternary alloys for gate metal and ohmic-contact diffusion barriers in GaAs and InP devices are proposed.

NASA's Jet Propulsion Laboratory, Pasadena, California

Thin films of ternary, amorphous refractory compounds have been proposed for use as gate metals and ohmic contact diffusion barriers to improve the reliability of GaAs- and InP-based devices. The proposed gate metals and diffusion barriers would be of general composition $M_xSi_yN_z$, where M denotes Ta, W, or Mo; such diffusion barriers have proven effective in Si-based devices, as described, for example, in "Amorphous Ta-Si-N thin film alloys as diffusion barriers in Al/Si metallizations," J. Vac. Sci. Technol. Vol. A8, No. 3, p 3006 (1990).

In GaAs- and InP-based electronic devices, diffusion of metal and semiconductor materials is especially problematic at the high processing temperatures encountered during fabrication, and in some cases can continue at significant rates during use of devices at lower temperatures. Such diffusion alters semiconductor channel thicknesses and other Schottky gate parameters and, in so doing, degrades performances and operational lifetimes. During operation of devices in atmospheres that contain hydrogen, diffusion of hydrogen can also degrade performances and lifetimes. This degradation has been associated with Pt and Pd, which are constituents of typical gate-metal alloys used heretofore. It has been hypothesized that the Pt or Pd in a metallic gate contact catalytically converts hydrogen molecules to hydrogen atoms, which then diffuse into the gate channel, where they compensate free charge carriers.

The proposed use of $M_xSi_yN_z$ layers offers several potential advantages over the use of conventional metal contacts without diffusion-barrier layers:

- Elimination of Pd and Pt from metal gate contacts would eliminate degradation by hydrogen.
- $M_xSi_yN_z$ alloys are thermodynamically stable with respect to GaAs; this characteristic would help prevent chemical reactions between the semiconductor and other layers.
- Because of the amorphous nature of the $M_xSi_yN_z$ layers, there would be no grain boundaries and thus no paths for rapid diffusion into or out of GaAs substrates.
- The crystallization temperatures of $M_xSi_yN_z$ are so high (800 to 1,000 °C) that during fabrication heat treatments, amorphous structures of diffusion-barrier layers would persist and microstructures of the gates would remain unchanged.
- Because of the amorphous nature of $M_xSi_yN_z$, it would be possible to deposit uniform, continuous layers with thicknesses as low as 10 nm.
- Contact electrical resistivities could be kept low and would remain stable over a wide range of temperatures.
- The range of processing temperatures that could be used in fabricating contacts would be relatively wide, so that temperature and time controls would not have to be as strict as they might otherwise be.
- Contact surfaces would be smoother.
- There would be greater flexibility in the choice of contact metals; for example, Au, Al, and/or Cu could be used.

This work was done by Elzbieta Kolawa, Sammy Kayali, and Marc A. Nicolet of Caltech for **NASA's Jet Propulsion Laboratory**. *Further information is contained in a TSP [see page 1].*

In accordance with Public Law 96-517, the contractor has elected to retain title to this invention. Inquiries concerning rights for its commercial use should be addressed to

Larry Gilbert, Director
Technology Transfer
California Institute of Technology
Mail Code 315-6
Pasadena, CA 91125
(818) 395-3288

Refer to NPO-19892, volume and number of this NASA Tech Briefs *issue, and the page number.*

Electronic Systems

Hardware, Techniques, and Processes

13 Concept for a Wide-Area Differential GPS Navigation System
14 Millennium Modem/Channelizer Special Test Equipment
15 Data Protocol for Optically Powered Sensors

BLANK PAGE

Concept for a Wide-Area Differential GPS Navigation System

Total user error would be reduced by an order of magnitude.

NASA's Jet Propulsion Laboratory, Pasadena, California

A proposed improved navigation system for civil aviation would exploit the signals broadcast by the Global Positioning System (GPS) and would incorporate a number of recent and anticipated advances in GPS technology to achieve decimeter real-time positioning accuracy. The underlying concept is that of a real-time wide-area differential (WAD) GPS navigation system that could be incorporated into the Federal Aviation Agency's Wide Area Augmentation System (WAAS). The proposed system is required to provide an increase, over prior GPS-based systems, in the accuracy with which a user's equipment can determine its real-time position ("user position accuracy," for short); this entails a requirement to (1) estimate GPS satellite orbits and clock offsets in real time with accuracies greater than those broadcast by the GPS itself and (2) estimate ionospheric GPS-signal-propagation delays with high accuracy to provide further corrections to improve user position accuracy.

The system would satisfy the accuracy requirements via a combination of (1) long-arc dynamic orbit estimation by means of a real-time Kalman filter, (2) rapid clock estimation, and (3) the use of the same Kalman filter in generating a dynamic global map of ionospheric delay (see Figure 1). This would be the first WAD GPS-based system to feature tuned dynamic (rather than geometric) determination of the GPS satellite orbits, enabling complete separation of orbit and clock corrections and reducing GPS orbit error (which is usually dominant) to insignificance. Moreover, the accuracies of the ionospheric-delay corrections in the proposed system would be at least 3 times those of the best known alternative system.

The system would utilize an extensively modified version of the GPS Inferred Positioning System/Orbit Analysis and Simulation Software (GIPSY/OASIS II), which was described briefly in "Software for Precise GPS Calculations" (NPO-19836), *NASA Tech Briefs*, Vol. 20, No. 12 (December 1996), page 84. To recapitulate: GIPSY/OASIS II accepts data collected by a permanent worldwide network of more than 60 Global Positioning System (GPS) reference receivers and continuously processes these data (see Figure 2), along with a network reference time, into precise three-dimensional position data on the orbits of GPS satellites, plus satellite

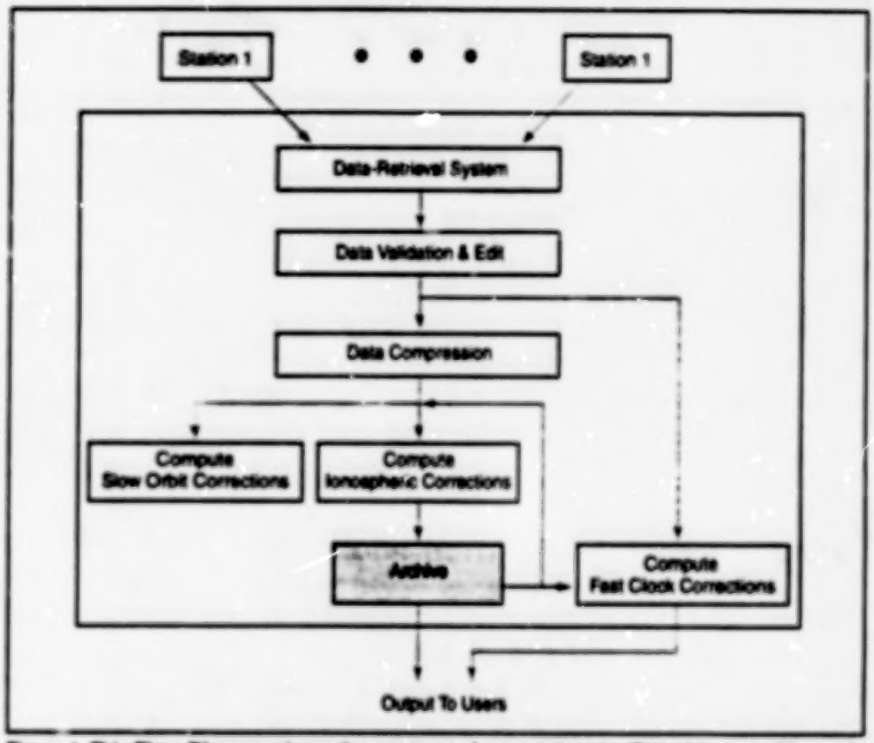

Figure 1. This **Flow Diagram** shows the sequence of computations in JPL's wide-area differential GPS navigation system.

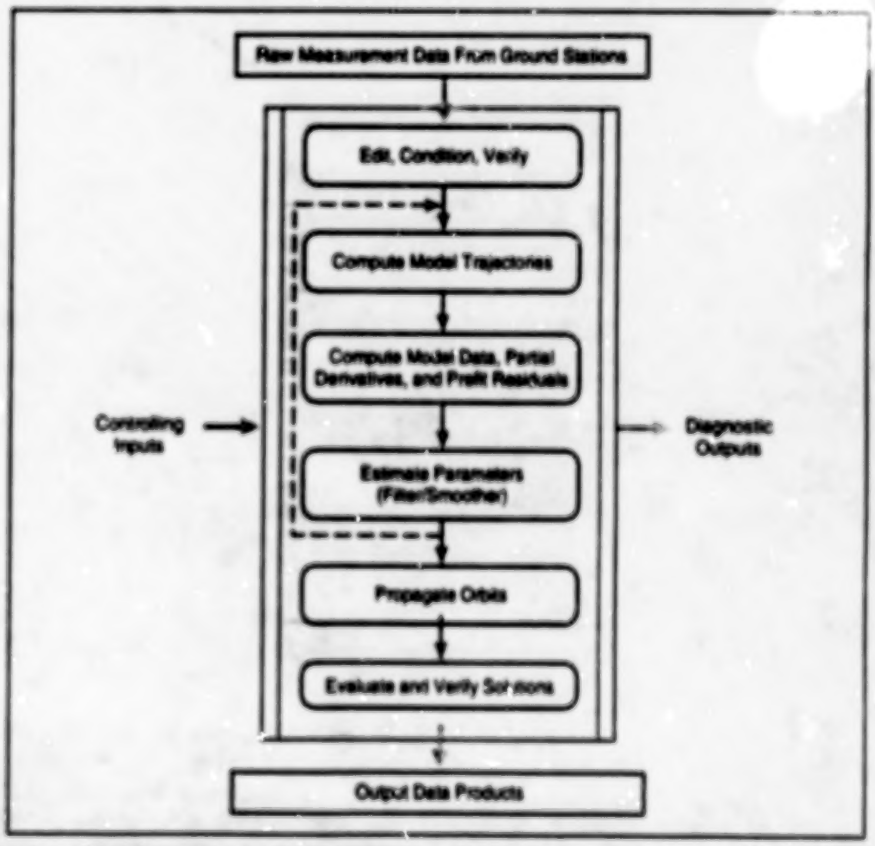

Figure 2. This **Flow Diagram** shows the sequence of computations effected by the GIPSY/OASIS II software.

and ground-station clock offsets. GIPSY/OASIS II incorporates the most precise available mathematical models of the dynamics of spacecraft, geophysical quantities, and propagation of radio signals and relativistic effects. The GIPSY estimator is formulated as a Kalman-type square-root information filter; this avoids matrix inversions and greatly enhances numerical stability. Any parameter estimated through the GIPSY Kalman filter/smoother can be modeled as a deterministic or stochastic process, or a combination of the two. The filter routinely solves simultaneously for thousands of parameters with data from dozens of receivers while maintaining sub-millimeter numerical precision globally.

GIPSY/OASIS II is highly modular in a way that makes it flexible and adaptable to almost any satellite-tracking estimation problem through simple modification of Unix script. In adapting GIPSY/OASIS II to the WAAS, different master-station functions to be performed by GIPSY could be performed in parallel, perhaps on several workstations, each directed by a different script designed to run the software optimally for its given task. These functions would include: (1) estimation of orbits and long-term satellite clock parameters, and computation of the associated slow corrections and their estimated errors; (2) computation of the predicted or a priori high-rate (1-second) GPS measurements in preparation for computing the fast corrections; (3) calculation of the fast clock corrections, together with their estimated errors, from the predicted and measured observables; (4) generation of ionospheric maps with high spatial and temporal resolution and computation of associated grid-point corrections; (5) computation of satellite integrity indicators; and (6) pre- and post-transmission independent validation of all data products. Each of these processes could be individually tuned for the job at hand without the need for a monolithic software package designed to perform all functions.

This work was done by Thomas P. Yunck, Willy I. Bertiger, Stephen M. Lichten, Anthony J. Mannucci, Ronald J. Muellerschoen, and Sien-Chong Wu of Caltech for ***NASA's Jet Propulsion Laboratory****. Further information is contained in a TSP [see page 1].*

This invention is owned by NASA, and a patent application has been filed. Inquiries concerning nonexclusive or exclusive license for its commercial development should be addressed to the Patent Counsel, NASA Resident Office–JPL [see page 1]. Refer to NPO-19625.

Millennium Modem/Channelizer Special Test Equipment

The equipment can be modified for testing different modems and multichannel

Lewis Research Center, Cleveland, Ohio

The Millennium modem/channelizer special test equipment ("test set" for short) is a fully programmable assembly of bit-error-rate electronic test equipment for broadband characterization of modems and of a multichannel demultiplexer/demodulator. The test set in its baseline configuration was designed for testing a specific wideband modem and channelizer that is capable of demultiplexing fifteen 80-MHz-wide channels stacked across the frequency band from 1.20 to 2.48 GHz. The test set is also designed to be readily modifiable for testing other modems and multichannel demultiplexer/demodulator systems. Developed for the Advanced Research Projects Agency, in a teaming effort with Honeywell, TRW, Raytheon, E-Systems, and Wright Patterson AFB, the test set is also available for use in industry.

The test set (see figure) contains three Broadband Integrated Services Digital Network (B-ISDN) modulators that generate octonary-phase-shift-keyed (8-PSK) data signals like those encountered in operation. These signals are mixed with local-oscillator signals for up-conversion and stacking in frequency in three adjacent channels in the set of communication channels to be passed through the multichannel demultiplexer/demodulator system to be tested. An attenuator is used to adjust the power of the signal in each channel. The test set then measures the bit-error rates of the signals put out by the modem, providing a characterization of both the demultiplexing and demodulation functions of the system.

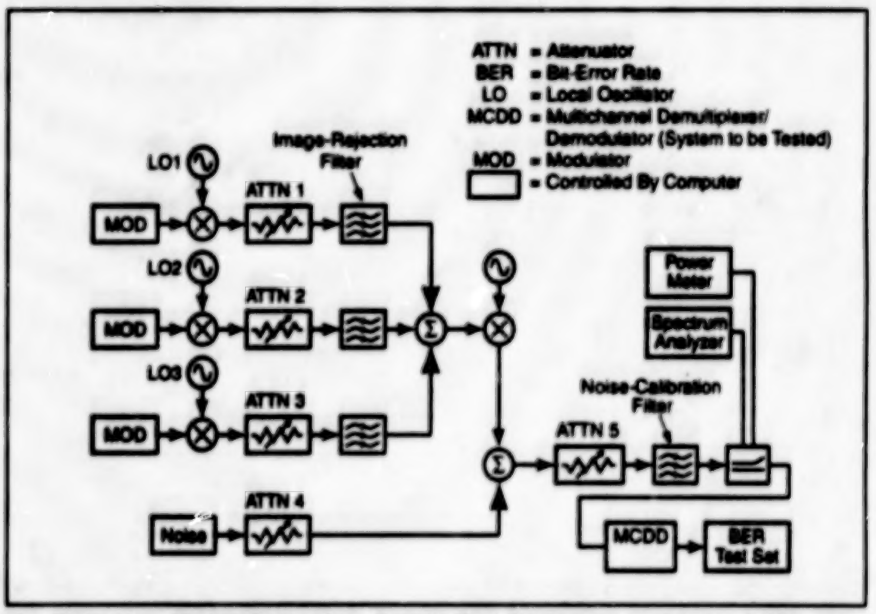

The Millennium Modem/Channelizer Special Test Equipment synthesizes 8-PSK data-communication signals for processing via the system under test, then measures the bit-error rates of the processed signals.

In addition to the requirement of reconfigurability for testing different systems, two important requirements in developing the test set were to keep the cost down and to complete the test set in a timely fashion. These requirements were satisfied by using, as much as possible, a combination of purchased off-the-shelf equipment and equipment already in NASA's possession.

The test set is automated to provide the capability for expedient, reliable, reproducible tests. All equipment is computer-controlled via a general-purpose interface bus (GPIB), a Versa Module Europa Bus Extensions for Instrumentation (VXI) bus, and RS-232 serial interfaces. Signals can be coupled off to a power meter and a spectrum analyzer for continuous monitor-

ing, without need to remove connections during calibration or debugging. All clock and local-oscillator signals are supplied by digitally synthesized signal generators. Attenuation and switching functions are provided via VXI circuit cards.

This work was done by William D. Ivancic of **Lewis Research Center**. *Further information is contained in a TSP [see page 1].*

Inquiries concerning rights for the commercial use of this invention should be addressed to NASA Lewis Research Center, Commercial Technology Office, Attn: Tech Brief Patent Status, Mail Stop 7–3, 21000 Brookpark Road, Cleveland, Ohio 44135. Refer to LEW-16428.

Data Protocol for Optically Powered Sensors

Data-transmission intervals would coincide with power-interception intervals.

NASA's Jet Propulsion Laboratory, Pasadena, California

A data-transmission protocol has been devised for proposed optoelectronic sensor units that would be strung in series along optical fibers and powered by pulses of light. More precisely, the sensor units would be connected in series along two optical fibers; one fiber for distribution of power from a master unit to the sensor units, and one fiber for transmission of sensor data from the sensor units back to the master unit (see figure).

The operation of the power-distribution subsystem was described in "Fiber-Optic Distribution of Pulsed Power to Multiple Sensors" (NPO-19420), *NASA Tech Briefs*, Vol. 20, No. 5 (May 1996), page 18a. To recapitulate: Pulses of laser light would be transmitted along an optical fiber from a power-supply unit. Each sensor unit would include an electronically controllable optical switch, which could be controlled to either (a) divert all of the optical power to a photovoltaic cell and power-conditioning circuitry to charge an energy-storage device in the sensor unit or else (b) allow the light to continue traveling along the power-distribution optical fiber to other sensor units downstream. Each sensor unit, beginning with the one nearest the laser source, would take all the optical power in the fiber for a fraction of each pulse period, and then would once again allow light to pass through to the next sensor. Thus, each sensor in turn would consume all the power for some fraction of the time of the pulse that remained after partial consumption by the preceding sensors.

The data-transmission protocol would be based on the power-distribution protocol and would be implemented with the help of a second electronically controlled optical switch in each unit. Success in building systems according to this concept would depend on the anticipated development of such optical switches with low insertion losses and the ability to operate on low control power. The data-transmission switch in each unit would be set in the pass-through state during the power-pass-through portion of the operating cycle. However, during the power-interception portion of the operating cycle, the data-transmission switch would be set to couple an optical data signal from the sensor unit into the fiber, propagating toward the master unit. This optical signal would bear sensory data stored since the previous transmission period. By relying on the power-transmission protocol for timing, one could ensure that each sensor unit, in turn, could have a clear optical channel to the master unit for optical transmission of data without interference from the other units.

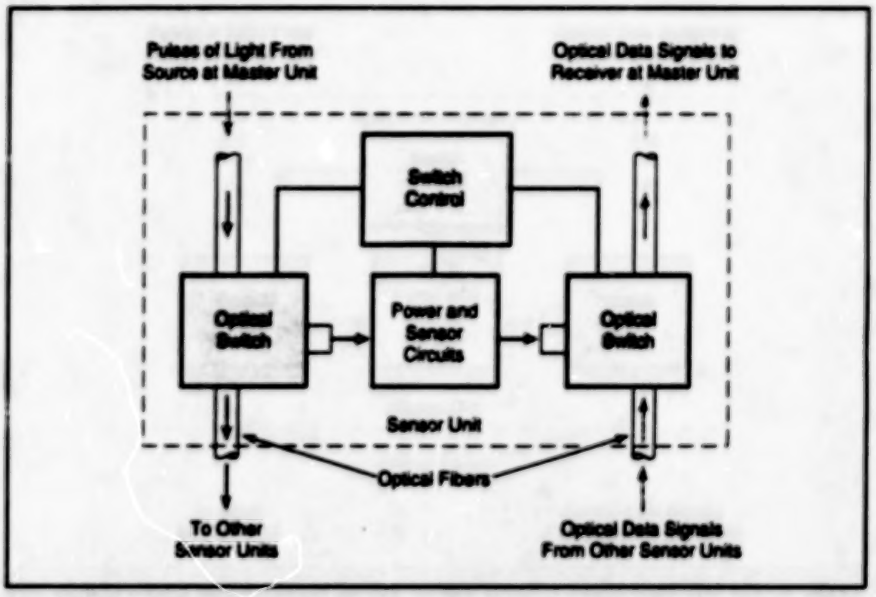
Pulses of Light From Source at Master Unit
Optical Data Signals to Receiver at Master Unit
Switch Control
Optical Switch
Power and Sensor Circuits
Optical Switch
Sensor Unit
Optical Fibers
To Other Sensor Units
Optical Data Signals From Other Sensor Units

Two Optical Fibers would connect all units, as in a string of beads. Each unit, in turn, would extract power from the left optical fiber and transmit data to the master unit along the right optical fiber during part of the operating cycle.

This work was done by Harold Kirkham of Caltech for **NASA's Jet Propulsion Laboratory**. *Further information is contained in a TSP [see page 1].*

NPO-19421

BLANK PAGE

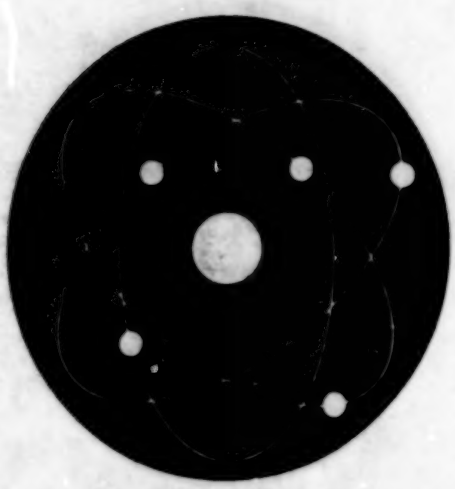

Physical Sciences

Hardware, Techniques, and Processes

19 Digitized X-Radiographs Indicate Densities in Ice Samples
20 Window Units for Solar-Assisted Heating and Cooling
21 Electrokinetic Evaluation of Surface Coatings
22 Joint-Transform Optical Correlator With Holographic Memory
24 Portable FTIR Scatterometer Measures Surface Contaminants
25 Dropped Devices Would Penetrate Ground to Regulated Depths
26 Full-Flow-Field-Tracking Particle-Image Velocimetry
27 Apparatus Measures Directional Reflectance Properties
28 Improved Data-Reduction Algorithm for Doppler Radar Wind Profilers
28 Using Langmuir-Blodgett Coatings To Calibrate Mass Microbalances

BLANK PAGE

Digitized X-Radiographs Indicate Densities in Ice Samples

Modern image-processing techniques are used.

Lewis Research Center, Cleveland, Ohio

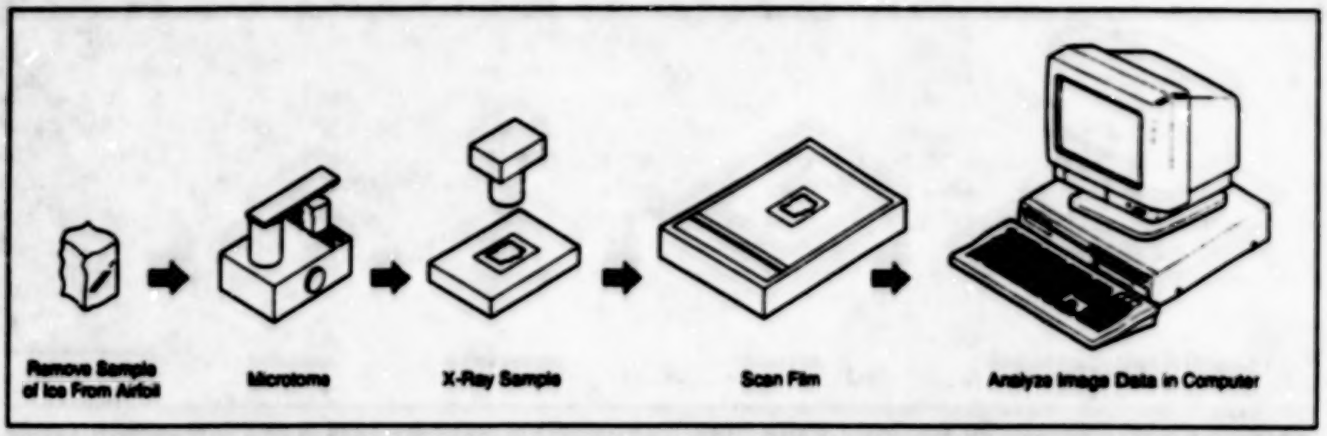

Figure 1. A Sample of Ice From an Airfoil is sliced thin on a microtome and used to make an x-radiograph. The radiographic image is digitized and processed to determine the local density of ice throughout the sample.

An improved method for measuring the local and total densities of ice accreted on airfoils incorporates contact x-radiography, along with modern image-acquisition and image-processing techniques (see Figure 1). The method was developed to facilitate a more detailed study of internal characteristics of ice formed on airfoils in wind-tunnel experiments under conditions that resemble those encountered in flight. Measurements of density, like those provided by this method, are needed to study the structure and formation of ice and to improve density values employed in computer programs that mathematically model the accretion of ice.

The improved method was derived partly by extending an older contact-x-radiographic technique for measuring the densities of ice in hailstones. In the improved method, the first step is to remove samples of accreted ice from a test airfoil and store them in a freezer. Next, while maintaining a temperature of 0 °F (–18 °C), the samples are sliced on a band saw to a thickness of about 10 mm, then further cut on a microtome to obtain samples with parallel sides and with a thickness of 3 mm. Each sample is placed on polyethylene terephthalate film on top of a sealed packet of x-ray film. Also placed on the film is a 3-mm-thick reference sample of clear ice. The samples and film are then exposed to x rays. Typical exposure conditions are a source potential of 25 kV, source current of 1 mA, and exposure time of 30 seconds.

To extract fine detail, the radiographs are scanned by a high-resolution film scanner with a resolution of 1,100 pixels per inch (433 pixels per centimeter). Then the digitized image data is processed to

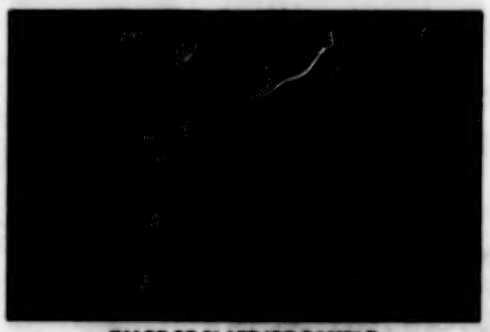

IMAGE OF GLAZE ICE SAMPLE

THRESHOLDED IMAGE OF GLAZE ICE SAMPLE SHOWING AIR POCKETS

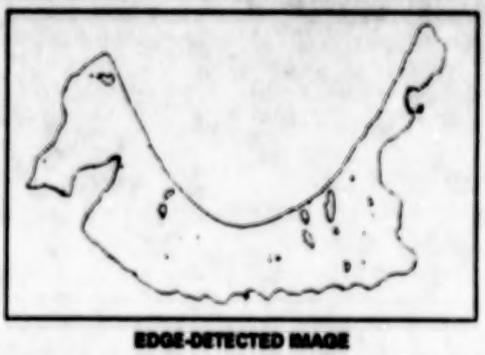

EDGE-DETECTED IMAGE

Figure 2. These Images Were Obtained by Digital Processing of an x-radiograph of a sample of glaze ice. Note how thresholding of density levels and the application of an edge-detection algorithm reveal different aspects of pockets of air trapped in the ice.

convert local image-intensity values into local ice-density values, using the image intensities and the known density of the reference samples as calibration data.

This method affords several advantages. The radiographs reveal interior density variations that would ordinarily be concealed from the naked eye. Digitization of the images makes it possible to use image-processing techniques to determine the positions of image features with high repeatability and accuracy. Image-processing techniques can be used to evaluate ice formation and morphological anomalies or to reveal features (see Figure 2) or characteristics that might otherwise go unnoticed. Digitization also makes it convenient to store and retrieve image data, and eliminates the need to handle original radiographs for each analysis.

Variability in the results obtained by this method can be attributed to two sources: (1) quantization error and (2) nonuniformity in the thicknesses of ice samples. Quantization error can be reduced by digitizing the images to greater numbers of bits. Thicknesses of samples can be made more nearly uniform by taking smaller slices to reduce flexing of the microtome blade.

This work was done by Mario Vargas of **Lewis Research Center** *and Howard Broughton and James Sims of Cortez III Service Corp. Further information is contained in a TSP [see page 1].*

Inquiries concerning rights for the commercial use of this invention should be addressed to NASA Lewis Research Center, Commercial Technology Office, Attn: Tech Brief Patent Status, Mail Stop 7–3, 21000 Brookpark Road, Cleveland, Ohio 44135. Refer to LEW-10630.

Window Units for Solar-Assisted Heating and Cooling

Spaces between inner and outer panes would be connected to inside or outside circulation paths.

Marshall Space Flight Center, Alabama

Window units containing inner and outer (storm) windows plus solar screens and mechanisms to control the circulation of air have been proposed. In the presence of sunlight, these window units would contribute some solar assistance for heating and cooling. At night or in cloudy weather, these units would act like ordinary inner-window/storm-window assemblies, suppressing the conduction and radiation of heat between the inside and outside to minimize undesired heating in hot weather or cooling in cold weather.

A typical proposed unit (see Figure 1) would include two window assemblies separated by a bay. Inlets and outlets through which air could enter and leave the space between the window panes would be located at the bottom and top, respectively, on both the outside and the inside. The bay would contain part of a mechanism that would open and close the inlets and outlets to control the circulation of air in the space between the window panes.

Each window assembly would contain a removable solar screen stretched across the space between the panes. In a conventional window equipped with a solar screen, the radiant solar energy intercepted by the screen heats the air trapped between the panes. In cold weather, this trapped hot air is wasted, though it could potentially be used for heating. In hot weather, some of the heat in the trapped air inevitably leaks into the building by conduction through the inner pane. The proposed window unit would utilize the trapped solar-heated air for heating the building in cold weather, and it would suppress leakage of solar heat into the building during hot weather. This would be accomplished by use of dampers at the top and bottom to control the flow of air through the inlets and outlets (see Figure 2), in response to the temperatures of the outside air and the air between the panes.

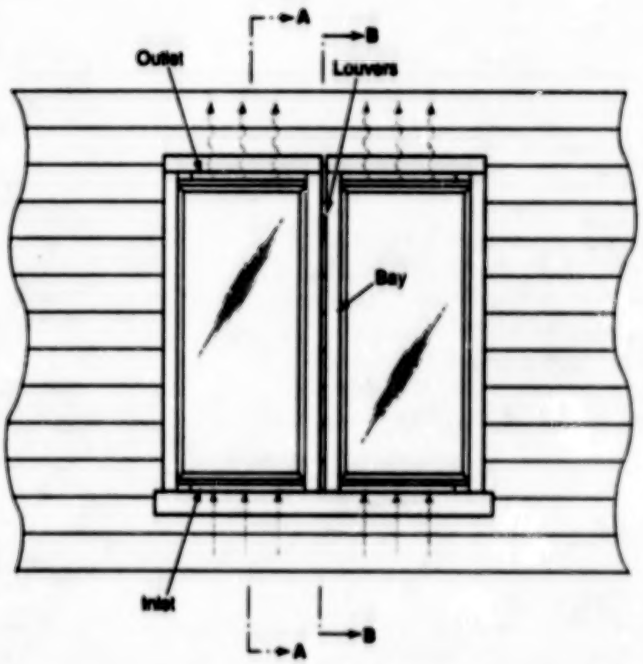

Figure 1. A Thermally Efficient Window Unit of the type described in the text would superficially resemble an ordinary window assembly in most respects, except that inlets, outlets, and louvers would be visible on closer inspection.

The mechanism for controlling the dampers would include levers and cams actuated by two hydraulic cylinders filled with temperature-sensitive material and opposed by springs. One of the hydraulic cylinders would be exposed to the outside air through louvers in the outer wall of the bay. The other cylinder would be exposed to the air between the panes through a hole between this space and the interior of the bay.

In the absence of appreciable solar heating (at night or in cloudy weather), the dampers would be positioned to close all inlets and outlets, so that the air between the panes would remain trapped as in an ordinary window assembly. In the presence of solar heating and cold outside air, the outside inlets and outlets would be closed, while the inside inlets and outlets would be opened to allow the solar-heated air to circulate from the window to the inside of the building. In the presence of solar heating

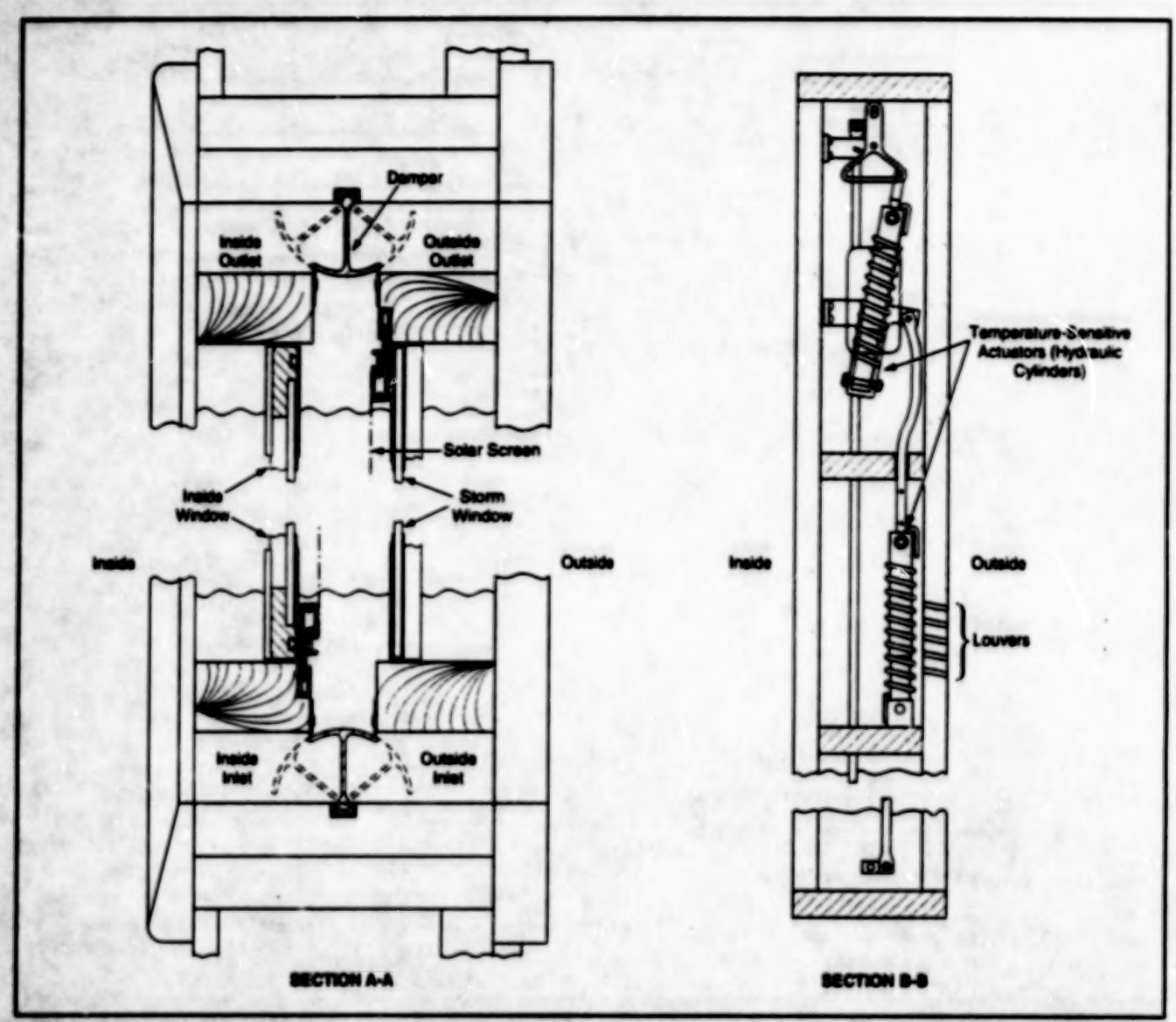

Figure 2. These Enlarged Views of the Cross Sections indicated in Figure 1 illustrate the major components of the air-circulation-control mechanisms of the window units.

and hot outside air, the inside outlets would be closed and the outside outlets would be opened, so that circulation of the solar-heated air to the outside would dissipate most of the solar heat from the window, reducing leakage of heat into the building.

This work was done by W. Neill Myers of **Marshall Space Flight Center.**

Further information is contained in a TSP [see page 1].
MFS-31088

Electrokinetic Evaluation of Surface Coatings

Measurements yield data on surface chemistries.

Marshall Space Flight Center, Alabama

An improved method has been devised for electrokinetic evaluation of surface chemistries of polymeric and other coating materials that are typically biocompatible and intended for use in suppressing, enhancing, and/or utilizing a variety of phenomena that could include wetting, adsorption of proteins, and/or electrophoresis. The method overcomes some of the limitations of conventional electrokinetic evaluation in terms of the zeta potential (the electric potential across the interface between a solid and a liquid).

Because the zeta potential of a chemical system can be related to a number of other properties of the system (e.g., agglutination, electrophoretic mobility, and surface charge density), it is widely used in industry and medicine to characterize particles in suspension and the surfaces of fixed apparatuses. However, it has been very difficult to use the zeta potential to derive such useful information as the densities of surface chemical groups, whether those groups are reactive, whether they have reacted with a coating polymer, and how long the coating has stayed attached. The improved method makes it possible to obtain such information.

The method involves measurements of the pH dependence of electroosmotic flow in an electrophoresis chamber in which the flow channel is typically a

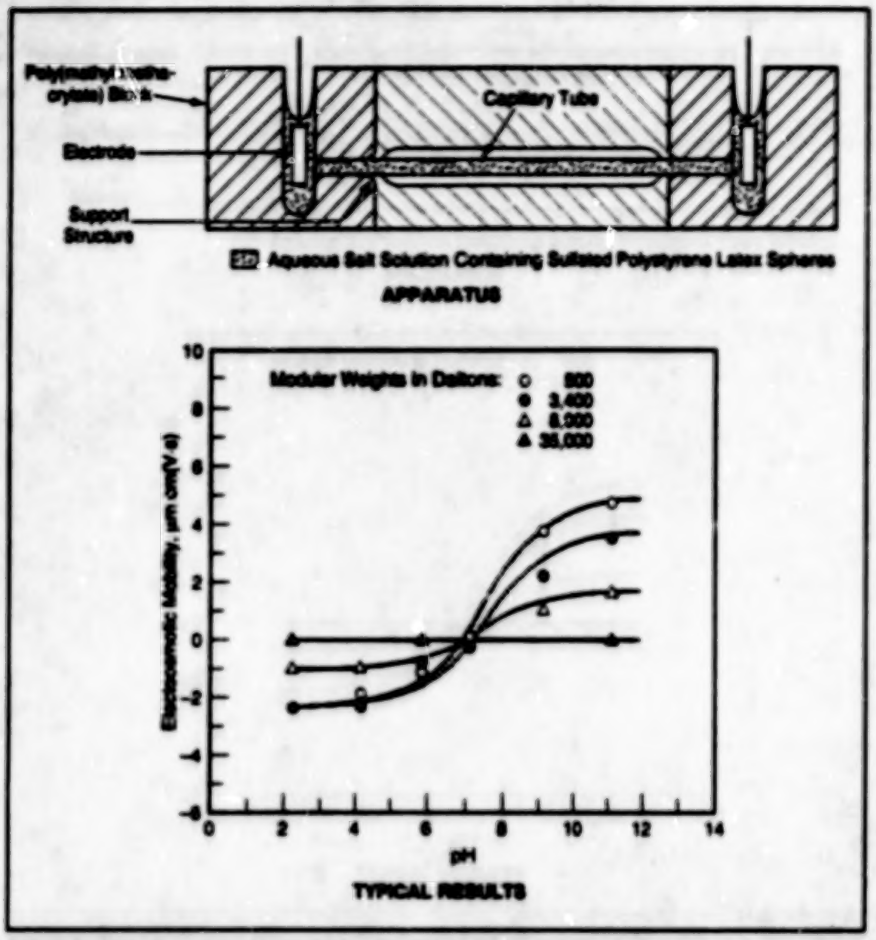

Electroosmotic Flow Was Measured in a modified microelectrophoresis apparatus. The curves were computed from measurements taken with capillary tubes coated with PEG of various molecular weights.

quartz capillary tube coated with a suitable polymeric material, which could be, for example, poly(ethylene glycol) (PEG). The measurement data are analyzed via a site-dissociation mathematical model of pH-dependent electroosmotic flow: the model, adopted from the classical theory of electrokinetics, is used to relate electroosmosis to surface chemistry. In the model, surface charge is represented in terms of acid/base site dissociation of ionizable surface groups. The distribution of electrostatic potential at the liquid/solid interface is related to surface charge by use of the Gouy-Chapman theory of the electrical double layer, plus exact solutions of the Poisson-Boltzmann equation. Electroosmotic mobility is related to zeta potential via the Smoluchowski equation.

In preparation for initial experiments according to this method, terminally activated derivatives of PEG were grafted onto the inner surfaces of quartz capillary tubes that had been functionally activated, variously, with 3-aminopropyltriethoxysilane, 3-mercaptopropyltrimethoxysilane, or poly(ethylene imine). For each experiment, the capillary tube was inserted in a modified microelectrophoresis apparatus and the electrophoresis chamber (including the tube) was filled with an aqueous solution of 7.5 mM NaCl. To make the electroosmotic flow visible, the solution was formulated with a suspension of 1.02-μm-diameter sulfated polystyrene latex spheres at a concentration of < 0.01 percent solids. In the experiments, grafts and activated surfaces were electrokinetically characterized by measuring the pH dependence of induced electroosmotic flow. The figure illustrates the apparatus and the results of some of the measurements.

The mathematical model in this method provides means for quantitative determination of the densities of ionogenic surface molecular groups and of acidity and/or basicity in the near-surface environment. The model can also provide information on the effective coating thicknesses of adsorbed neutral polymers and, for some polymers, the relative graft densities. This information can be useful in interpreting complex chemical phenomena involved in applications of such PEG coatings as those used in preparation of nonfouling surfaces. In addition, electrokinetic characterization can provide information regarding stability of coatings, control of electroosmotic flow in analytical instrumentation, and the influences of adsorbed polymers on regulation of electric charges at aqueous/solid interfaces.

This work was done by J. M. Van Alstine, J. M. Harris, and N. L. Burns of the University of Alabama in Huntsville for Marshall Space Flight Center. Further information is contained in a TSP [see page 1].

Inquiries concerning rights for the commercial use of this invention should be addressed to the Patent Counsel, Marshall Space Flight Center [see page 1]. Refer to MFS-26360.

Joint-Transform Optical Correlator With Holographic Memory

Many correlations could be made quickly, without a large computer memory or extensive computation.

NASA's Jet Propulsion Laboratory, Pasadena, California

A joint-transform optical correlator has been demonstrated as a prototype of a class of real-time and nearly-real-time pattern-recognition systems. Like other optical correlators, its overall function is to make a correlation image, which indicates, in effect, the closeness of match between an input image and a known stored image. One of the outstanding features of this apparatus is a memory device in the form of a photorefractive crystal that stores holograms of as many as 5,000 known reference images. This optical memory device eliminates the need for a large digital

computer memory to store the data on the reference images. The input image can be correlated quickly with all of the reference images by mostly optical and some relatively simple electronic means, without need for time-consuming digital computation. This joint-transform optical correlator is also shift-invariant, so that it can also track the input image. Systems of this type could be useful in such diverse applications as recognition of military targets, identification of fingerprints, and robotic navigation.

The left side of Figure 1 illustrates schematically the recording and readout of reference-image holograms in the photorefractive crystal. A reference image to be recorded is illuminated by a plane-wave laser beam (denoted the input beam) that is projected at an angle into the photorefractive crystal. Another plane-wave laser beam (denoted the reference beam) is projected into the crystal at another angle and the hologram formed by the two beams is recorded by an appropriate exposure.

There are two methods of recording multiple reference images in the same crystal. The first method requires a tunable laser, which is set to different wavelengths to record different images. In the second method, the reference beam is made incident at different angles to record different images. These methods can be combined in a wavelength- and angle-multiplexing scheme to enable the recording of thousands of reference images in a photorefractive crystal as small as a 1-cm cube. As shown on the right side of Figure 1, readout of the image previously recorded at a given angle and wavelength is effected by use of a readout laser beam that is conjugate to the reference beam used during recording; that is, a beam of the same wavelength and traveling along the same path but in the reverse direction. Thus, multiple recorded images could be addressed by varying the angle and wavelength of the readout laser beam.

Figure 2 is a schematic diagram of the joint-transform optical correlator. The beam from a tunable laser is split into two parts, one part being used to read out one of the reference images from the photorefractive crystal by the method described above. The other part of the laser beam is used to read out the real-time input image from an input spatial light modulator (SLM); this input image is fed to the input SLM from a charge-coupled-device (CCD) camera aimed at the scene or object that one seeks to recognize. The input SLM is placed alongside the reference image, in the same plane as that of the reference image.

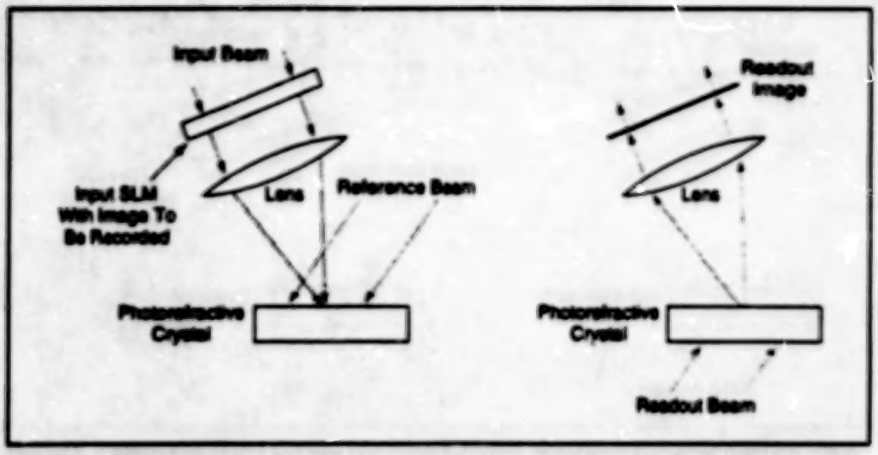

Figure 1. A Photorefractive Crystal can record multiple holograms formed at different wavelengths and different angles of incidence of the reference beam.

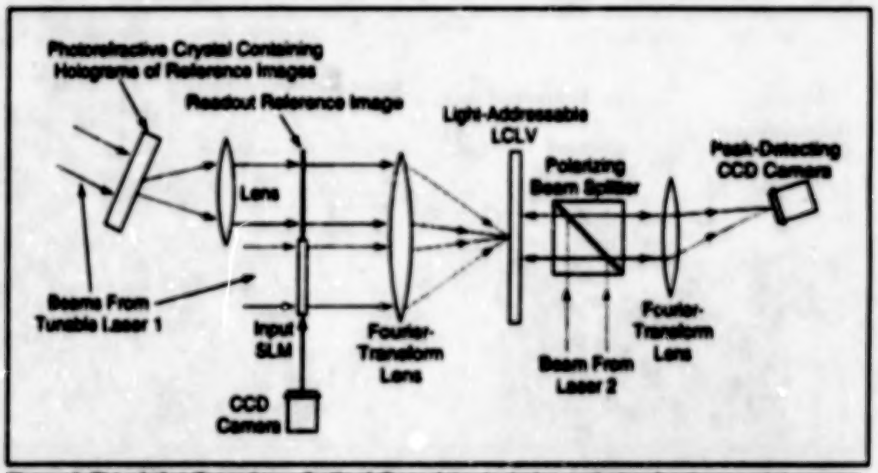

Figure 2. This Joint-Transform Optical Correlator includes a photorefractive-crystal memory device like that of Figure 1, containing thousands of reference images. The input image can be correlated with the reference images in rapid succession by varying the wavelength of the tunable laser and the angle of the laser beam incident on the photorefractive crystal.

The optical paths from the laser to the input and reference images are aligned to be within the coherence length of the laser, so that a hologram can be formed in the plane of a Fourier transform of the two images. By use of a lens, the two images are jointly Fourier-transformed, and they form an interference pattern on the Fourier-transform plane.

The input surface of a light-addressable liquid-crystal light valve (LCLV) is placed in the Fourier-transform plane. The output surface of the LCLV is illuminated with a collimated laser beam through a polarizing beam splitter. The reflected beam containing the Fourier-transform interference pattern travels through the beam splitter and through a lens, which forms the inverse Fourier transform on the focal plane of a peak-detecting CCD camera. If the input image matches the reference image, a pair of symmetric first-order correlation spots appears on the focal plane. The intensity of the correlation spots is proportional to the similarity between the images. The input image could be compared with multiple reference images in rapid succession by varying the wavelength and/or angle of the readout beam incident on the photorefractive crystal.

This work was done by Tien-Hsin Chao and Francis Yu of Caltech for **NASA's Jet Propulsion Laboratory**. *Further information is contained in a TSP [see page 1].*
NPO-19139

Portable FTIR Scatterometer Measures Surface Contaminants

Nondestructive measurements can be performed in the field.

Marshall Space Flight Center, Alabama

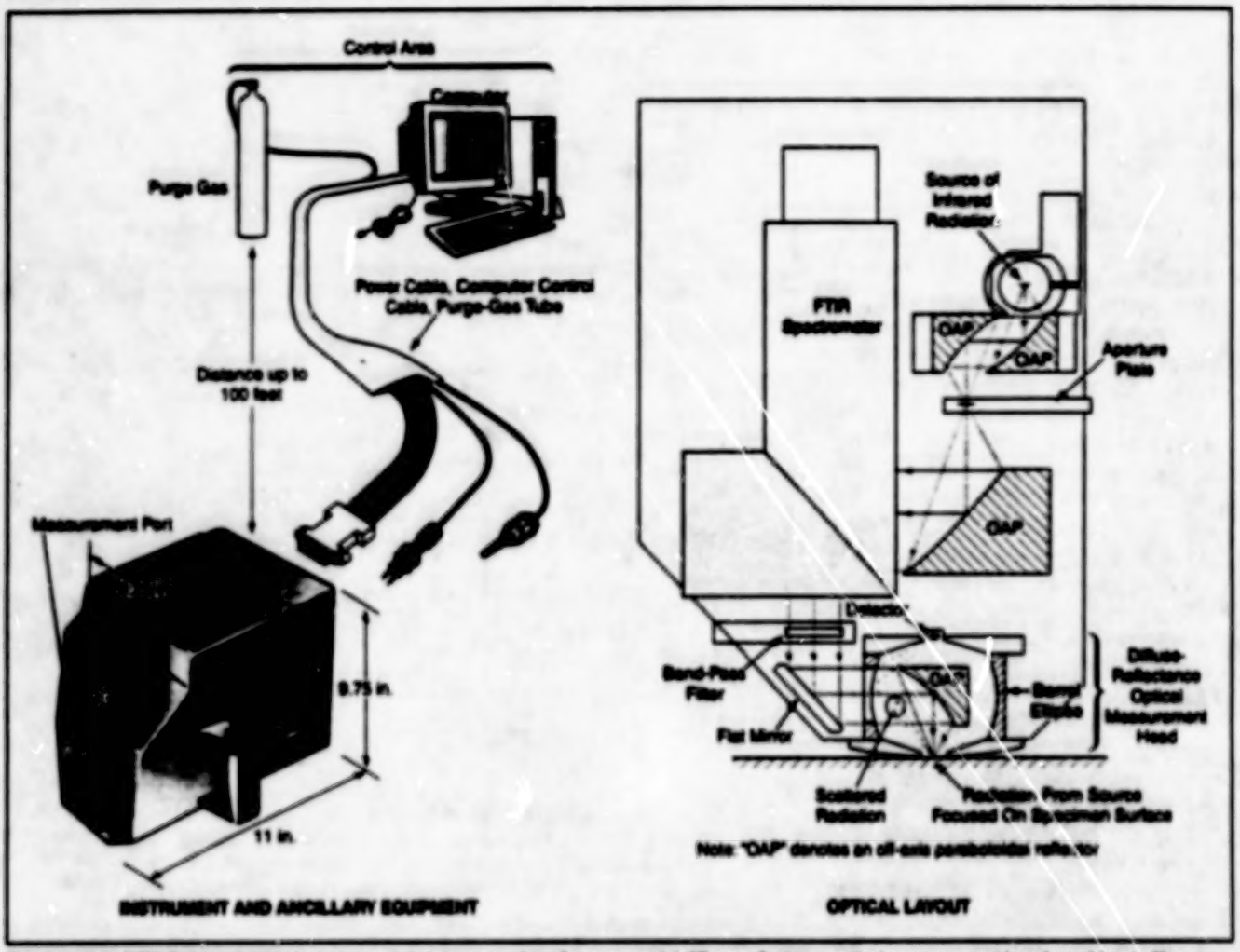

The Portable FTIR Scatterometer includes a scaled-down version of a commercial diffuse-reflectance optical measurement head combined with a commercial FTIR spectrometer in a compact, lightweight package. The instrument operates under computer control, is nondestructive, and can be used in any orientation.

A rugged, portable Fourier-transform infrared (FTIR) scatterometer has been developed for use in rapidly and nondestructively identifying and measuring quantities of greasy and oily contaminants on solid surfaces. This instrument is meant to be used in conjunction with other contamination-measuring instruments to ensure that inspected surfaces are clean enough for subsequent coating and/or adhesive-bonding treatments.

Typical contaminants include fluorocarbons, silicones, hydrocarbons, and other organic compounds. Commercial laboratory FTIR spectrometers can be used to identify and measure such contaminants, but are too large and delicate to be carried into the field to inspect surfaces at all orientations in situ; thus, it is necessary to engage in destructive inspection procedures wherein one cuts small coupons out of inspected surfaces and brings them to the laboratory instruments.

FTIR spectroscopy is a powerful tool for chemical analysis and is a mature discipline that has made excellent use of recent progress in computer hardware and software. In a typical FTIR spectrometer, a collimated beam of infrared light in the wavelength range of 2 to 25 μm (the predominant wavelength range of blackbody radiation at a temperature of about 1,600 K) is modulated by a Michelson interferometer, focused onto or through a specimen, and refocused onto a detector. The detector outputs are digitized and the resulting data are Fast-Fourier-transformed into a spectrum of beam intensity, in arbitrary units, as a function of wavelength or wave number (reciprocal of wavelength). The spectrum gives data on the identities and amounts of chemical functional groups.

In a given application, FTIR spectroscopy involves measurement of either transmittance, diffuse reflectance, or specular reflectance. Each of the three types of measurement is advantageous for some kinds of specimens. The present instrument utilizes diffuse reflectance, which is preferable for measurements on rough and/or curved surfaces (e.g., flat or curved surfaces that have been sandblasted).

The present instrument (see figure) is an automated, computer-controlled, high-performance FTIR spectrometer with an integral measurement head that includes a diffuse-reflectance optical measurement head, all in a compact, lightweight package that features rugged

construction for use in the field. The FTIR spectrometer is a commercially available unit adapted to fit into the package. The diffuse-reflectance optical measurement head is a half-scale version of a commercial unit that contains ellipsoidal ("barrel ellipse") and off-axis paraboloidal reflectors; the barrel-ellipse design provides for collection of scattered radiation and excludes specularly reflected radiation. The instrument weighs less than 13 lb (6 kg). The computer can be programmed to provide spectral matched filtering, enabling automated identification of spectral features.

This work was done by Bill H. Nerren of **Marshall Space Flight Center**, *G. Louis Powell of Martin Marietta Energy Systems, Inc., and John T. Neu and R. Samuel Dummer of Surface Optics Corp. Further information is contained in a TSP [see page 1].*

Inquiries concerning rights for the commercial use of this invension should be addressed to the Patent Counsel, Marshall Space Flight Center [see page 1]. Refer to MFS-26421.

Dropped Devices Would Penetrate Ground to Regulated Depths

Instruments would be set up at prescribed heights in inaccessible locations.

NASA's Jet Propulsion Laboratory, Pasadena, California

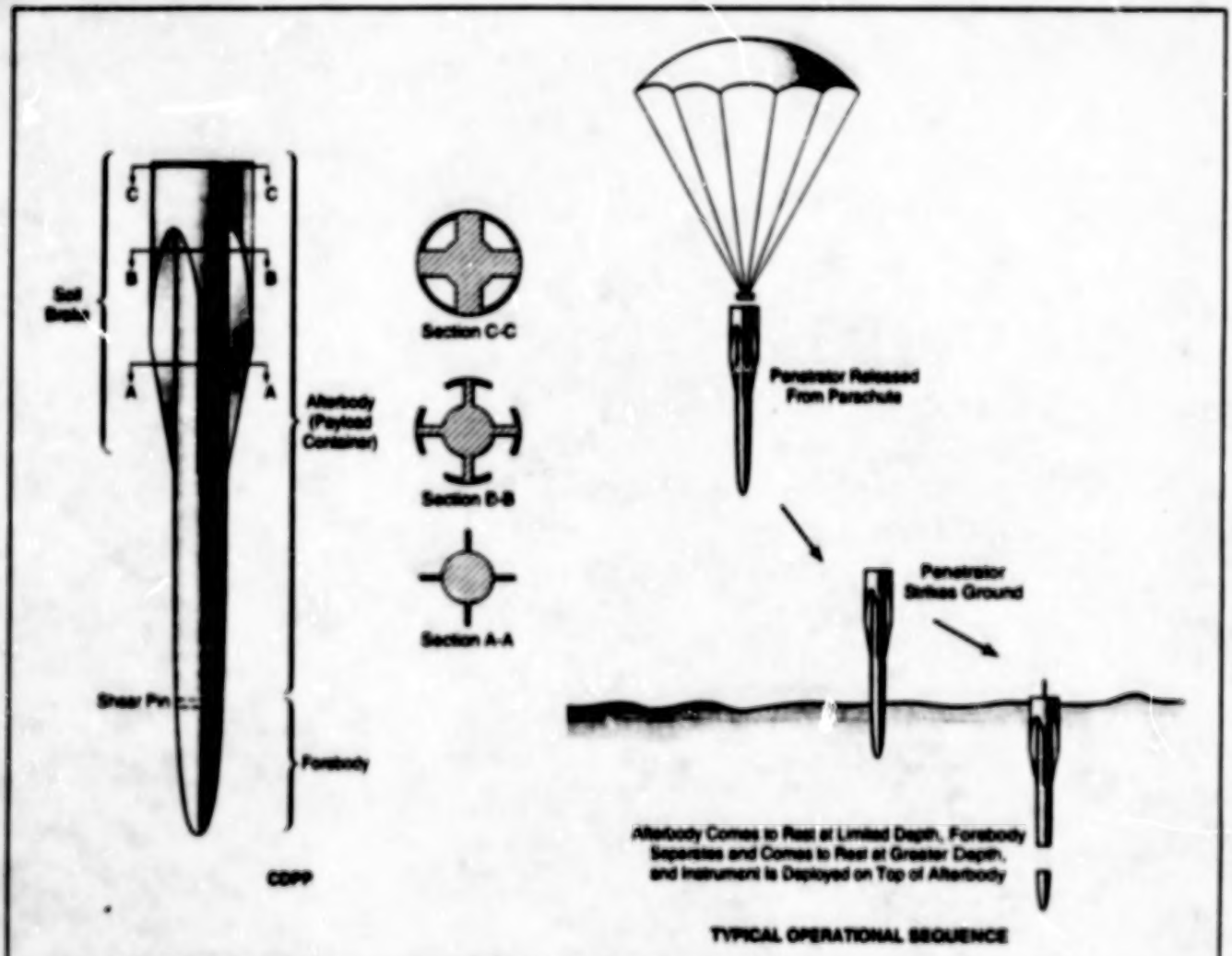

The Forebody and Afterbody would separate after impact, after the relatively heavy forebody had dragged the relatively lightweight afterbody to a prescribed limited depth.

Devices that would penetrate the ground to regulated depths after being dropped from heights are undergoing development. These devices — known as controlled-depth-of-penetration penetrators (CDPPs) — would be used to carry cameras and/or other instruments, which, after impact, would be deployed at predetermined heights above the ground. CDPPs could be dropped from aircraft or balloons, for example, to install instruments in locations not readily accessible by travel along the ground. CDPPs would minimize impact forces so that high-resolution optical components, scanning mechanisms, and other delicate instrument components would not be damaged. CDPPs would function in soils of various types and over a wide range of impact velocities.

Each CDPP would comprise two sections: a heavy ogive forebody and a relatively light afterbody, which would be a payload container with exterior fins

shaped to act as a soil brake (see figure). The forebody would have the shape and mass needed to penetrate the soil to an acceptable depth. The soil brake would be designed to decelerate the payload at a rate small enough to prevent damage to the instrumentation, yet large enough to limit penetration to no more than a prescribed depth. The forebody and afterbody would be connected by a shear pin.

Upon impact, the forebody would penetrate the soil, carrying the payload with it until the drag of the soil brake exceeded the design strength of the shear pin. The shear pin would then break, releasing the forebody from the payload. The forebody would continue into the ground until its kinetic energy was spent, while the soil brake would cause the afterbody to come to rest at no more than the prescribed depth, with its upper end at approximately the prescribed height above the surface. The instrument(s) would then be deployed.

This work was done by David W. Juergens of Caltech for **NASA's Jet Propulsion Laboratory**. *Further information is contained in a TSP [see page 1].*
NPO-19646

Full-Flow-Field-Tracking Particle-Image Velocimetry

Velocities and accelerations can be determined over entire flow fields.

Lewis Research Center, Cleveland, Ohio

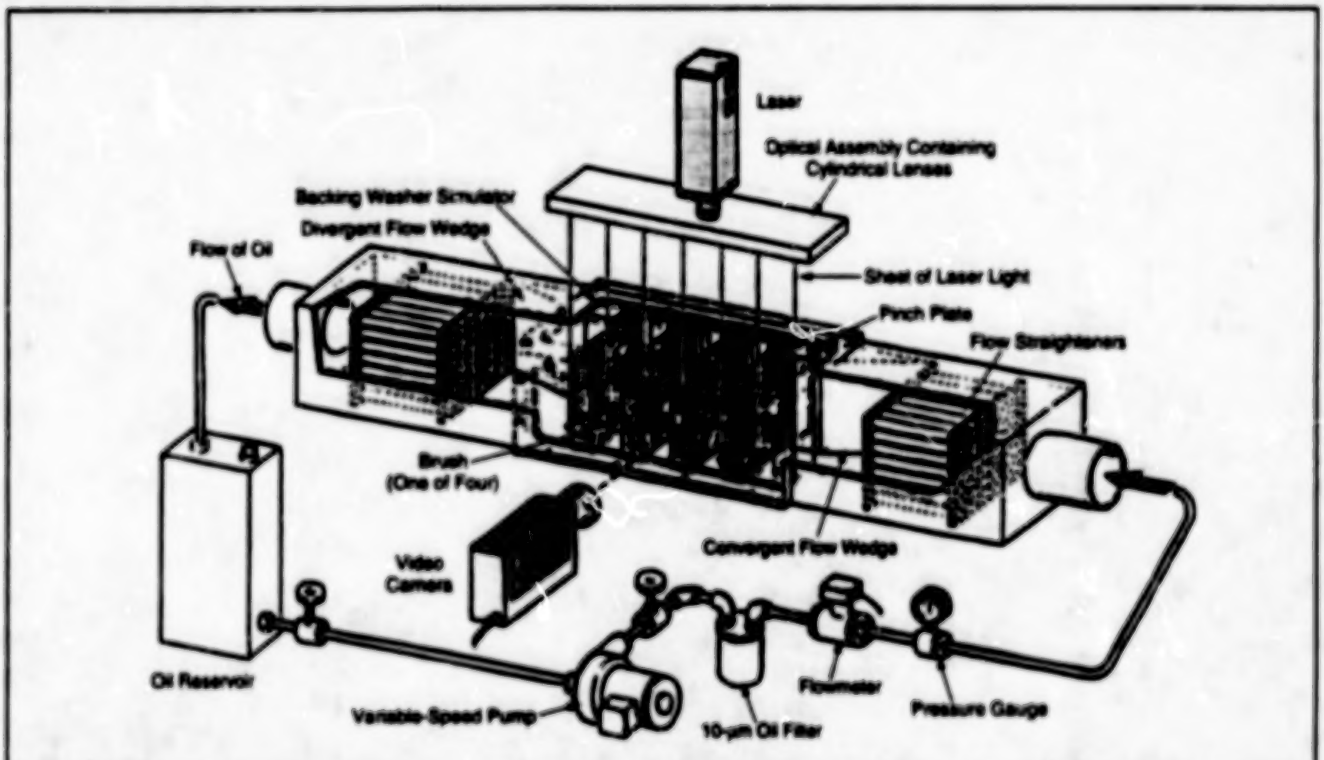

An Oil Tunnel Is Instrumented with an FFFT PIV apparatus to study flows through brushes that represent brush seals in turbomachines. The FFFT PIV apparatus has also been used to study flows of water past cylinders, airfoils, and other objects, and flows of air past an array of pins in staggered rows.

Full-flow-field-tracking (FFFT) particle-image velocimetry (PIV) is a technique for obtaining quantitative and qualitative data on flows from sequences of images of small seed particles entrained in the flows. FFFT PIV is closely related to other velocimetric methods, described in several previous articles in *NASA Tech Briefs*, that are also denoted by "PIV" and by similar names like "particle-tracking velocimetry" (PTV) and "particle-displacement tracking" (PDT).

The figure schematically illustrates a flow experiment conducted with a FFFT PIV apparatus, which is similar to the apparatuses used in the other techniques mentioned above. Illumination is supplied by a continuous-wave argon-ion laser with a power of 8 W. An assembly of cylindrical lenses forms the laser beam into a sheet of light to illuminate a plane of interest in the test section of a wind tunnel, water tunnel, oil tunnel, or other flow apparatus.

The flow is seeded with highly reflective particles with sizes up to about 10 μm. For studying flows of water or oil, a suitable particle material is MgO_2, which is nearly neutrally buoyant in those liquids. For studying flows of air, the selection of particle materials is more problematic; care must be taken to eliminate spurious particle motions (e.g., bouncing off surfaces of objects) in specific experimental regimes.

A low-luminosity charge-coupled-device video camera with a resolution of 756 horizontal pixels by 581 vertical pixels is focused on the illuminated plane. The camera is equipped with long-distance-microscope optics that can magnify a selected portion of the plane by a factor as large as 100 to reveal details of the flow field. The output of the camera can be either digitized and stored directly in a computer memory or else recorded on video tape and subsequently digitized for processing by the computer.

The camera operates at a frame rate of 30 Hz; this frame rate is adequate as long as the flow under observation is not so fast that images of particles become continuous streaks across the field of view. To pro-

vide stroboscopy for viewing such rapid flows, the optical system includes a rotating laser-beam-chopping disk. The speed of rotation can be chosen to obtain strobing frequencies at integer multiples of 30 Hz, up to a maximum of several kilohertz.

Sequences of images are processed by a computer integrated image-quantification (CIIQ) method, which is a partly manual, partly automated method for identifying images of individual particles and tracing their motions across the flow field during a chosen observation interval. The CIIQ method involves three computer programs called "FACT," "SNAP," and "VADT." Using calibration images obtained by focusing the video camera on graph paper, FACT generates magnification factors for the recorded images. Then by use of a digitizing puck (similar to a mouse) and pad along with SNAP, a technician visually identifies and digitizes the position of each particle of interest in the succession of strobe or frame intervals that, collectively, constitute the observation interval. The technician continues this process until the digitized particle trajectories are sufficiently numerous to represent the flow field to the desired level of detail.

The digitized trajectory data are fed to VADT, which fits the sequence of positions of each particle to a polynomial (up to ninth order) function of time. Velocities and accelerations are computed as the first and second derivatives, respectively, of the polynomials. The resulting velocity and acceleration data from the magnified small areas of the plane of interest are then computationally assembled to obtain a representation of the flow field throughout the plane.

This work was done by Victor A. Canacci and M. Jack Braun of the University of Akron for **Lewis Research Center**. *Further information is contained in a TSP [see page 1].*

Inquiries concerning rights for the commercial use of this invention should be addressed to the Patent Counsel, Lewis Research Center [see page 1]. Refer to LEW-16309.

Apparatus Measures Directional Reflectance Properties

Advantages include precision and automation.

NASA's Jet Propulsion Laboratory, Pasadena, California

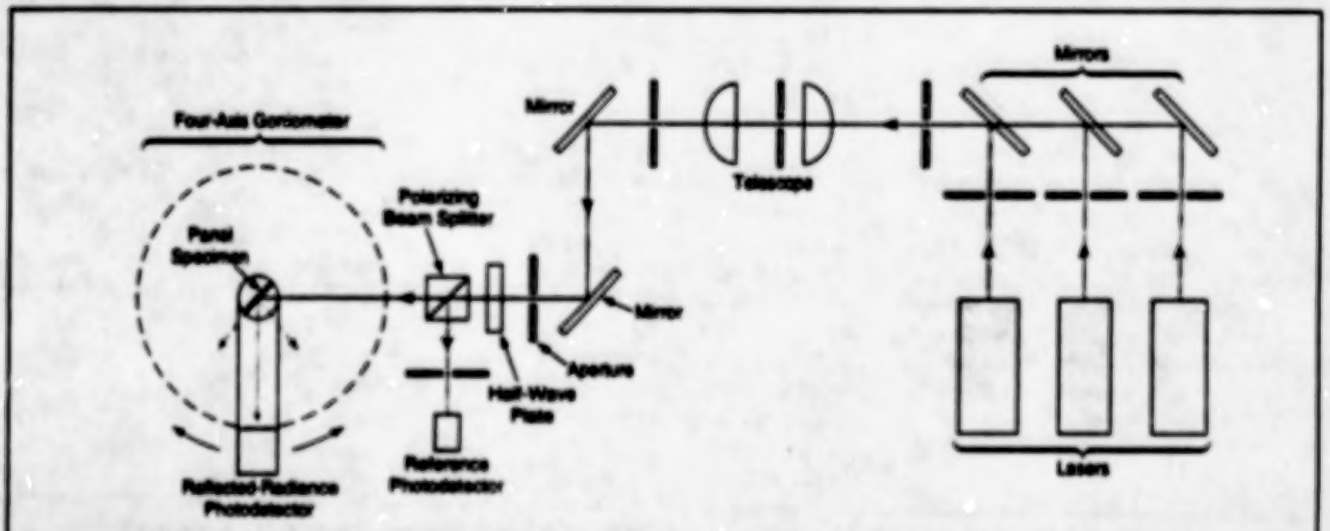

The Panel Specimen Is Illuminated at a selected one of three wavelengths and at a specified angle of incidence, and the light reflected at a specified other angle is measured. All angular settings, acquisition and processing of photodetector readings, and other functions are performed under computer control.

A computer-controlled, semiautomated apparatus measures the bidirectional reflectance distribution functions (BRDFs) of panel specimens of materials at three wavelengths. Other visible and near-infrared wavelengths can be conveniently added. Designed originally for characterizing nearly Lambertian panels that will serve as internal diffuse-reflection calibration standards for a spaceborne imaging radiometer, the apparatus can also be used to characterize other diffusely reflective panels. In comparison with other apparatuses that also measure BRDFs, this apparatus offers advantages of a four-axis angular-positioning capability that facilitates characterization of anisotropic specimens, greater measurement precision, and computer control of the acquisition and processing of data.

The apparatus (see figure) includes a helium/cadmium laser with a wavelength of 442 nm, a helium/neon laser with a wavelength of 632.8 nm, and a gallium aluminum arsenide semiconductor diode laser with a wavelength of 859.9 nm. The laser output is directed sequentially through a beam-expanding telescope to produce a magnified collimated beam. This beam is then reflected through a linear polarizer, which separates the beam into a reference beam and a signal beam that are decoupled from each other. The reference beam goes directly to a silicon photodetector (the reference photodetector), which thus provides a measure of the intensity of the signal beam. The signal beam strikes the panel specimen, and the portion of light reflected from the specimen in a given direction is measured by another photodetector (the reflected-radiance detector) that is positioned and oriented to receive light in that direction. By using the ratio between the output of the reflected-radiance detector and the reference detector as the raw reflectance signal, this apparatus inherently minimizes the effects of any amplitude instability in the selected laser.

The panel specimen is centered on the optical axis of the signal beam, and the reflected-radiance photodetector is

mounted on a 30-cm-long boom that extends radially outward from the center of the panel. The panel specimen and the boom are mounted on a four-axis goniometer that includes rotary stages driven by high-torque dc motors and monitored by shaft-angle encoders. Under computer control, the rotary stages can reproducibly orient the specimen panel and the reflected-radiance photodetector at various angles to obtain BRDFs over wide ranges of angles. The level of repeatability and resolution of angular positioning is 0.01°. The overall precision with which the apparatus can determine the BRF of a specimen is represented by a standard deviation of a factor of 0.002.

This work was done by Brendan T. McGuckin, David A. Haner, Robert T. Menzies, Carlos Esproles, and Alan M. Brothers of Caltech for **NASA's Jet Propulsion Laboratory**. *Further information is contained in a TSP [see page 1].*
NPC-19806

Improved Data-Reduction Algorithm for Doppler Radar Wind Profilers

Wind profiles are generated more frequently.

John F. Kennedy Space Center, Florida

An improved data-reduction algorithm has been developed to enhance the availability, accuracy, and reliability of wind data extracted from outputs of Doppler radar wind profilers. The reduction of data from Doppler wind measurements includes, among other things, the extraction of weak wind-related spectral signatures from noisy signals that are contaminated with side lobes. The noise and side lobes contribute to errors and unreliability of wind data.

The original application for the present algorithm is in a 50-MHz Doppler radar wind profiler at Kennedy Space Center. Previously, a "consensus" algorithm was used to separate wind spectral signatures from noise and side lobes. The consensus algorithm involved extensive averaging, which took excessive time; only two wind profiles could be generated in an hour. Moreover, the averaging did not adequately suppress errors in that frequently, the consensus algorithm locked onto side lobes.

The present algorithm looks for the wind spectral signature within a "first-guess" spectral window based on previous valid data. Within the first-guess window, a median-filter technique is used to extract the current wind spectral signature for processing. Side lobes are usually rejected because they tend to fall outside the first-guess window. The median-filter technique takes much less computation time than does averaging in the consensus algorithm.

The major conceptual problems encountered in developing the present algorithm were selecting the width of the first-guess window and the parameters of the median filter to maximize the rejection of side lobes and noise while ensuring detection of the correct signal. In tests, the algorithm performed reliably and accurately, and was found to be capable of generating twelve wind profiles per hour. The root-mean-square wind-speed error of the present algorithm is of the same order of magnitude (1 m/s) as that of the consensus algorithm. Also in comparison with the consensus algorithm, the present algorithm produces large (> 5 m/s) wind-speed errors less frequently, and produces wind data that are more reliable in the sense that they are valid a greater fraction of the time. The major weakness of the present algorithm is that the first-guess window occasionally fails to eliminate strong side lobe signals that are close to the true wind signal, and manual intervention is required to recognize and correct the situation.

This work was done by Robin Schumann of ENSCO, Inc., Timothy Wilfong of the University Space Research Association, and Steve Smith of Marshall Space Flight Center for **Kennedy Space Center**. *Further information is contained in a TSP [see page 1].*

Inquiries concerning rights for the commercial use of this invention should be addressed to the Patent Counsel, Kennedy Space Center [see page 1]. Refer to KSC-11860.

Using Langmuir-Blodgett Coatings To Calibrate Mass Microbalances

Langmuir-Blodgett coatings can be used to calibrate mass microbalances like quartz-crystal microbalances and surface-acoustic-wave sensors. Microbalances are used to measure small quantities of solids or liquids deposited on surfaces. Calibration of a microbalance involves measurement of the response of the microbalance to a deposited surface film of known mass density. In comparison with other techniques for depositing a calibration film, the Langmuir-Blodgett coating technique offers advantages of less difficulty and repeatability without the use of an expensive surface tensiometer. In this technique, one prepares a monolayer of a suitable coating material in a Langmuir-Blodgett trough, then dips the microbalance in the trough to coat its sensory surface with the monolayer film. If necessary, the process can be repeated with different coating materials for a series of calibration measurements to determine the linearity of the response of the microbalance. The only major limitation on this technique is that one must select coating materials that do not chemically attack any part of the microbalance.

This work was done by Paul A. Mogan of **Kennedy Space Center** *and Lee Chow and Isaish O. Oladeji of the University of Central Florida. Further information is contained in a TSP [see page 1].*

Inquiries concerning rights for the commercial use of this invention should be addressed to the Patent Counsel, Kennedy Space Center [see page 1]. Refer to KSC-11863.

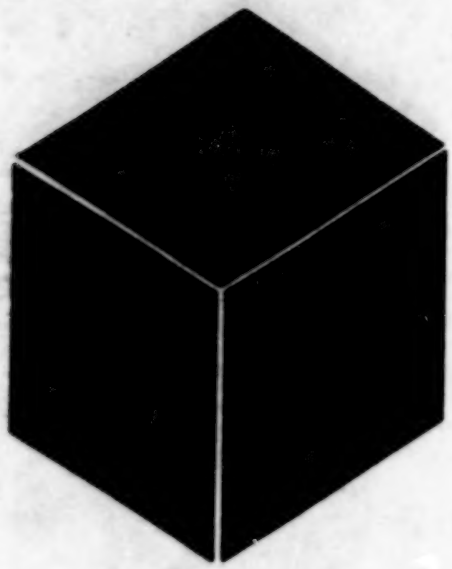

Materials

Hardware, Techniques, and Processes

31 Adherent and Stable Metallization of CVD Diamond
32 Reinforced, Stretchable Elastomer for Use at Low Temperature
32 Testing and Analysis of Clothlike Structural Components
33 Water/Surfactant Solution as a Substitute for CCl_2F-$CClF_2$

BLANK PAGE

Adherent and Stable Metallization of CVD Diamond

The choice of adhesion and diffusion-barrier materials is critical.

NASA's Jet Propulsion Laboratory, Pasadena, California

Experiments have shown that with the proper choice of materials, adherent and metallurgically stable metal contacts can be formed on chemical-vapor-deposited (CVD) diamond. Such contacts are needed for efficient thermal conduction and structural integrity in electronic devices designed for operation over a wide range of temperatures — especially in high-temperature electronic devices that exploit the electrically insulating and highly thermally conducting nature of diamond.

A metal contact on diamond is generally required to be both strongly adherent and stable at high temperature. The figure illustrates the material layers that are deposited in metallization of diamond, both (1) as practiced heretofore and (2) according to the present scheme for achieving adherence and metallurgical stability. To obtain strong adhesion, it is necessary to deposit a first layer of metal (the adhesion layer) that reacts chemically with diamond; to obtain high-temperature stability, it is necessary to deposit an overlayer.

Heretofore, adhesion layers have been made, variously, of Cr or Ti, while overlayers have been made, variously, of Au or Au/Sn alloy. Unfortunately, at high temperatures, Cr and Ti are soluble in Au and therefore diffuse from the adhesion layers into the overlayers, with resultant degradation of diamond/metal bonds and thus loss of adhesion. Typically, the maximum operating temperature at which minimum acceptable adhesion can be maintained is < 450 °C.

In the scheme for adherent and stable metallization of diamond, the adhesion layers and overlayers are made of the same materials as before, but in each case there are two adhesion layers separated by a diffusion-barrier layer. In this material system, a suitable diffusion-barrier layer is a film of amorphous Ti+Si+N that is reactively sputter deposited on the first adhesion layer, before depositing the overlayer. [Amorphous Ti+Si+N was previously developed for diffusion barriers between Si substrates and Cu overlayers.]

In the experiments, some CVD diamond specimens metallized variously as described above and illustrated in the figure were annealed for 30 minutes at each of a sequence of temperatures at intervals of 100 °C up to 900 °C. Each annealed specimen was subjected to 3.2-MeV-α-particle-backscattering spectroscopy to measure interdiffusion of metal, and to a tape-pull adhesion test. In the specimen with a Cr adhesion layer but no diffusion barrier, substantial interdiffusion and delamination was observed after annealing at 300 °C. In the specimen with Cr adhesion layers and a diffusion barrier, some interdiffusion was observed above the diffusion barrier, but the Cr adhesion layer below the diffusion barrier remained unchanged, and there was no delamination, even after annealing at 600 °C. In the specimen with Ti adhesion layer and no diffusion barrier, substantial interdiffusion was observed after annealing at 500 °C. The specimen with a Ti adhesion layer and a diffusion barrier performed the best of all: it exhibited no interdiffusion or delamination after annealing at 900 °C. In an additional test, this specimen also exhibited neither diffusion nor delamination after annealing for 100 hours at 400 °C.

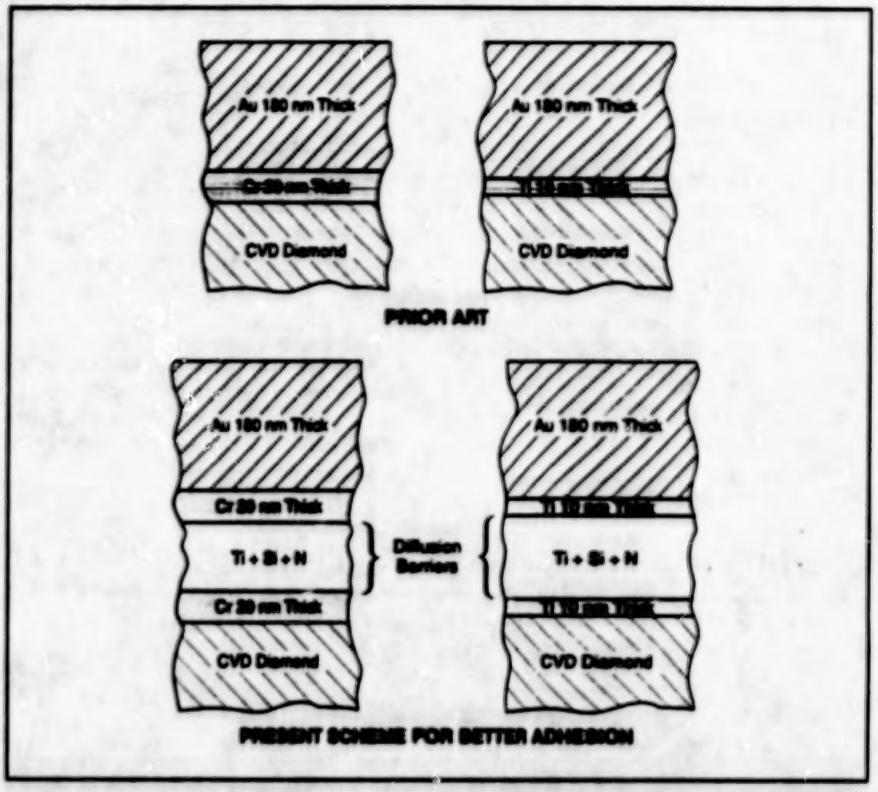

Layers of Amorphous Ti+Si+N help to preserve adhesion at high temperatures by preventing diffusion of metal from the adhesion layers to the gold overlayers.

This work was done by Andreas Bachli, Marc Nicolet, Elzbieta Kolawa, and Jan Vandersande of Caltech for **NASA's Jet Propulsion Laboratory**. *Further information is contained in a TSP [see page 1].*

In accordance with Public Law 96-517, the contractor has elected to retain title to this invention. Inquiries concerning rights for its commercial use should be addressed to

Larry Gilbert, Director
Technology Transfer
California Institute of Technology
Mail Code 315 - 6
Pasadena, CA 91125
(818) 395-3288

Refer to NPO-19672, volume and number of this NASA Tech Briefs *issue, and the page number.*

Reinforced, Stretchable Elastomer for Use at Low Temperature

Knit fabric reinforcement prevents tears.

Lyndon B. Johnson Space Center, Houston, Texas

An elastomer reinforced with a knit fabric has been developed to satisfy the need for a material that remains flexible at temperatures down to –60 °F (–68 °C), can be stretched somewhat, and resists tearing. The material can be used in such diverse applications as lip seals, stretchable covers for machines, and Arctic structures.

The elastomeric matrix of this material is RTV 560 (or equivalent) silicone rubber, which remains flexible in the required temperature range, wherein most other elastomers become stiff or even brittle. However, this elastomer exhibits poor resistance to tearing. Accordingly, it is reinforced against tearing by incorporation of a knit polyester fabric (see figure).

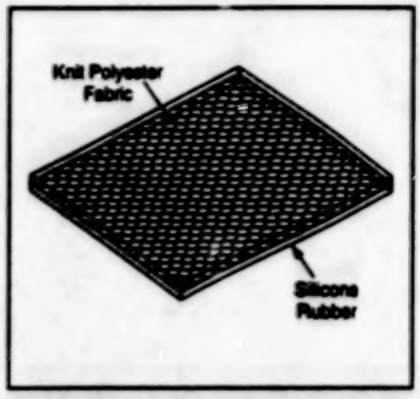

Knit Polyester Fabric reinforces silicone rubber, affording a somewhat stretchable material that resists tearing and remains flexible in extreme cold.

The fabric stretches with the silicone rubber, but reaches a limit of stretchability below that of the rubber. The fabric thus stops the stretching at a predetermined tension, preventing tearing of the rubber. A knit (as distinguished from woven) reinforcing fabric was chosen because it stretches readily in any direction. A woven fabric, in contrast, stretches only on the bias and its fibers could slide relative to each other, allowing the rubber to tear.

This work was done by Scott A. Swan, Frederic Dawn, and Ernest Murry of **Johnson Space Center**. *No further documentation is available.*
MSC-22445

Testing and Analysis of Clothlike Structural Components

Nonlinear properties are characterized by a combination of experimental and theoretical techniques.

Marshall Space Flight Center, Alabama

A method of testing and analysis has been developed to enable characterization of the nonlinear mechanical properties of three-dimensional structural components made of cloth and clothlike materials. This development was prompted by the need to understand the properties of proposed spacecraft aerobrakes that would be made of tailorable advanced blanket insulation (TABI) (see Figure 1). The method is also applicable to the analysis of textile structural components for terrestrial use.

An essential part of the method is a series of tests to determine some basic in-plane mechanical properties of the material or structural component of interest. Testing is necessary because manufacturers' data on the properties of individual filaments and yarns do not include the effects of slippage between filaments and yarns woven into fabrics, nor do they account for the weakening effects of contact stresses and residual stresses generated in the weaving process. The tests include tensile stress-vs.-strain measurements to obtain data on moduli of elasticity and strengths in the warp and fill directions, measurements of damping of free and forced vibrations under tension, and measurements of hysteresis curves under oscillating tension to obtain more complete information on the amount and type of damping. The results of initial tests of this type on TABI show that it stiffens as the applied load increases (see

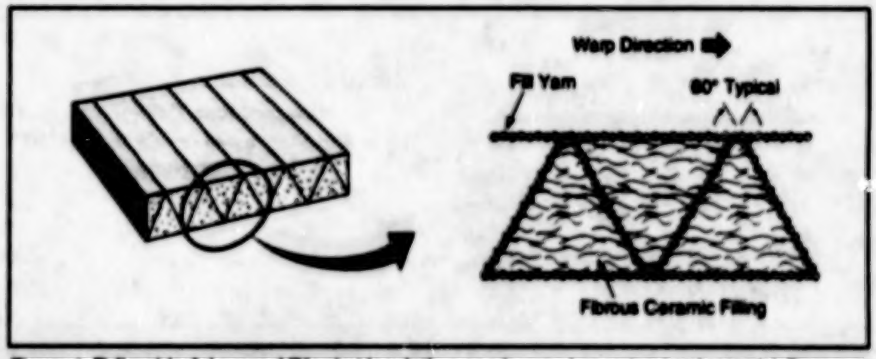

Figure 1. Tailorable Advanced Blanket Insulation can be used as a structural material. Because it has a three-dimensional configuration and complex mechanical properties, it must be analyzed by the method described in the text. Note that the fill direction is perpendicular to the page.

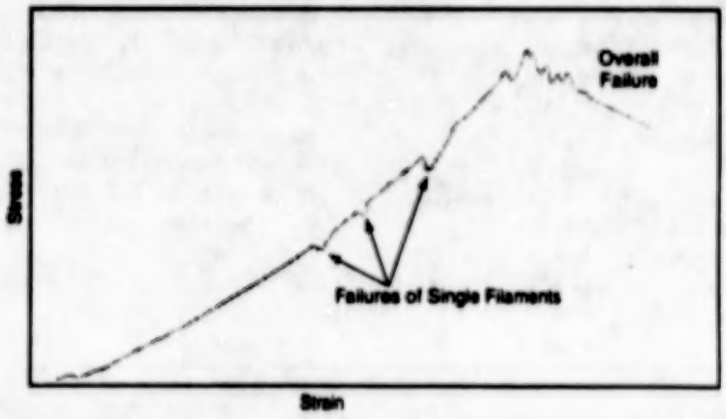

Figure 2. This Experimental Stress-vs.-Strain Curve shows the increase in stiffness with applied stress. It also shows that failure of the specimen occurred as a propagation of breakages of individual filaments rather than sudden failure of the entire specimen.

Figure 2) and that its in-plane damping behavior is consistent with that of a basic viscous damping mechanism for small vibration amplitudes.

Another essential part of the method is prediction of the out-of-plane dynamic behavior of a clothlike structure from the in-plane data derived from tests and/or from mathematical models that incorporate these data. This is accomplished by use of a finite-difference mathematical model of the structure and the applicable differential equations of motion.

This work was done by Michael L. Tinker of **Marshall Space Flight Center** *and Joseph P. Clayton of Remtech, Inc.*

Further information is contained in a TSP [see page 1].

Inquiries concerning rights for the commercial use of this invention should be addressed to the Patent Counsel, Marshall Space Flight Center [see page 1]. Refer to MFS-26357.

Water/Surfactant Solution as a Substitute for CCl_2F-$CClF_2$

Commercial surfactants were tested to substitute for trichlorotrifluoroethane (CCl_2F-$CClF_2$) in special applications in which there is a need for solvent rinses to detect particulate contamination of workpieces. Deionized water without any additives has been found to dislodge fewer particles than does CCl_2F-$CClF_2$ because, it has been hypothesized, the high surface tension of pure water keeps the water from penetrating narrow passages, so that the water does not make contact with the entire surfaces of workpieces. In an experiment, water containing 25 parts per million of the commercial surfactant Zonyl FSN reduced the surface tension of the water from 72.8 dynes/cm to about 36 dynes/cm, and the water containing the surfactant was found to dislodge nearly the same amount of particulate matter as did CCl_2F-$CClF_2$. Unlike CCl_2F-$CClF_2$, the surfactant-treated water is nonpolluting and nontoxic. Moreover, in comparison with CCl_2F-$CClF_2$ the surfactant is inexpensive.

This work was done by Christian A. Clausen III of the University of Central Florida for **Kennedy Space Center.** *Further information is contained in a TSP [see page 1].*

Inquiries concerning rights for the commercial use of this invention should be addressed to the Patent Counsel, Kennedy Space Center [see page 1]. Refer to KSC-11906.

BLANK PAGE

Computer Programs

Physical Sciences

37 Software for Internet Distribution of Oceanographic Data

Mathematics and Information Sciences

37 MOO Web Core
37 Software for Evaluation of Data-Compression Algorithms
37 Algorithms for Selection of Scheduling Heuristics
38 Software for Managing SAR Systems

BLANK PAGE

These programs may be obtained from COSMIC. Please contact

COSMIC®
Computer Services Annex
University of Georgia
Athens, GA 30602
Telephone No. (404) 542-3265.

Physical Sciences

Software for Internet Distribution of Oceanographic Data

The DODS HDF Data Server and Client Library computer program facilitates distribution, via the Internet, of oceanographic data that reside on servers in the Distributed Ocean Data System (DODS). This software extends the suite of DODS data formats to include Hierarchical Data Format (HDF), which is the primary format for dissemination of data from NASA's Earth Observing System (EOS). With the help of this software, an application program that utilizes the HDF application programmer interface (API) can gain direct access to data on a remote DODS server; the access and the concomitant translation of data between formats are both automatic and transparent to the application program. Users can develop programs that perform such operations as extracting subsets and conducting searches as though the data to be examined resided in their own local computer files. The DODS and this software work under UNIX. At the time of receipt of information for this article, the server component of the software was undergoing beta testing, and the client component was still undergoing development. It is planned to release the client and server components together in a single package. This work was sponsored by NASA's Earth Science Data and Information System (ESDIS) Prototyping effort. It is intended that this software will be incorporated into the EOSDIS (EOS Data and Information System) core system to provide remote access to EOS data sets.

This program was written by Todd Karakashian of Caltech for **NASA's Jet Propulsion Laboratory**. *Further information is contained in a TSP (see page 1).*
NPO-20020

Mathematics and Information Sciences

MOO Web Core

The MOO Web Core computer program implements an interface between the MOO multiple-user database computer system and the World Wide Web, enabling any Web user to obtain information from a MOO server. At the time of reporting information for this article, there were about 100 MOO servers at industrial, university, and government sites, and the number of them is expected to grow. The nature of the MOO system and its software can be understood partly in terms of the history of its name: "MOO" stands for "MUD, Object Oriented", while "MUD" originally stood for "Multi-User Dungeon," (an Internet adventure game with a large number of simultaneous players), which then evolved into self-explanatorily-named software called "Multi-User Data base." MOO has evolved in conjunction with a collaborative project called "AstroVR," wherein MOO and MOO Web Core have been used to make images of celestial objects available on the Internet. MOO Web Core creates a set of MOO objects designed to provide an http interface to a MOO server running a LambdaCore-derived data base. By use of MOO Web Core, any standard World Wide Web client can connect to a MOO server and request data. MOO Web Core implements the http "GET" and "POST" commands, supporting html document delivery, search services, and fill-in form queries. MOO Web Core is designed to fit into any LambdaCore-based MOO data base.

This work was done by David Van Buren of Caltech for **NASA's Jet Propulsion Laboratory**. *Further information is contained in a TSP (see page 1).*
NPO-19642

Software for Evaluation of Data-Compression Algorithms

The Advanced End-to-end Simulation for On-board Processing (AESOP) program facilitates computational simulations of the performances of data-compression and -decompression algorithms in the presence of noise. AESOP satisfies a need for a single program that can be used to evaluate, compare, and build on data-compression algorithms developed by different scientists and engineers. AESOP provides a graphical interface to an extensible set of data-compression algorithms, interfacing with both compiled code and stand-alone programs. Most interactions between AESOP and the user take place via a mouse. Once compressed, data can be fed through simulated transmission and decompression to evaluate the effects of compression parameters, noise, and error-correction subalgorithms. The user can predict the ultimate data quality attainable via different compression methods and compression ratios, and evaluate data compression in the larger context of packeting and noisy transmission. Written in C and C++, AESOP currently runs on Sun SPARCstation computers using SunOS 4.1.3 and Motif. Operating-system dependences are minimal.

This work was done by Alan Mazer, Roberto Mendoza, and Andy Boden of Caltech for **NASA's Jet Propulsion Laboratory**. *Further information is contained in a TSP (see page 1).*

In accordance with Public Law 96-517, the contractor has elected to retain title to this invention. Inquiries concerning rights for its commercial use should be addressed to

Larry Gilbert, Director
Technology Transfer
California Institute of Technology
Mail Code 315 - 6
Pasadena, CA 91125
(818) 395-3288

Refer to NPO-19673, volume and number of this NASA Tech Briefs *issue, and the page number.*

Algorithms for Selection of Scheduling Heuristics

A computer program incorporates the STOP1, STOP2, EL1, and EL2 algorithms, which implement different versions of a statistical approach to choosing one out of a number of alternative heuristic strategies for scheduling. The basic rules for making this choice are that (a) the chosen scheduling strategy should be the one that allo-

cates resources most efficiently, (b) the choice must be made on the basis of incomplete information, and (c) excessive information-gathering cost must not be incurred in making this choice. Each algorithm tests the performance of each strategy on a randomly selected sample of scheduling problems, then uses parameter-estimation techniques to infer statistical models of performance on the general population of scheduling problems. These models are then used to estimate (a) the utility and cost of acquiring additional information and (b) the desirability of selecting a particular strategy. Each algorithm implements a different method of balancing the expected utility of additional information against the cost of acquiring that information. The program can be executed on Sun Spacestations running common LISP. In computational experiments on representative sets of scheduling data, all four algorithms were found to outperform both the benchmark COMPOSER algorithm and the traditional manual selection procedure.

This work was done by Steven A. Chien and Jonathan Gratch of Caltech for **NASA's Jet Propulsion Laboratory.** *Further information is contained in a TSP [see page 1].*
NPO-19766

Software for Managing SAR Systems

The Data Acquisition and Production Planning System (DAPPS) computer program assists in the management of synthetic-aperture-radar (SAR) equipment and data. DAPPS incorporates three subsystems: the Flight Agency Interface Subsystem (FAIF), the Acquisition Planning Subsystem (APS), and the Production Planning Subsystem (PPS). The FAIF manages interfaces with the Canadian, European, and Japanese space agencies. Satellite planning and scheduling files received from the various flight agencies are used to plan the acquisition of raw signal data transmitted from the satellites to the McMurdo (in Antarctica) and Alaska SAR Facility (ASF) ground stations. Users can submit data-acquisition requests. The APS uses the satellite planning and scheduling files to incorporate data-acquisition requests into satellite schedules. When final flight-agency schedules are received, the APS generates an antenna schedule file for the appropriate antenna at ASF or McMurdo. The PPS manages the production of SAR imagery and other data products; in so doing, it also provides an interface for operators to queue various product requests, modify their priorities, and provide a central control mechanism for the generation of SAR data products at ASF. DAPPS runs on two SUN SPARCstation 20/71 computers with 96 MB of memory and 9 GB of disk space. Each computer includes two Ethernet connection cards.

This work was done by Navid Dehghani, Quentin Sun, Sally Chou, Richard Norman, Philip Yurchuk, Rodney Hoffman, Miguel Siu, Teresa McKillop and Larry Stevens of Caltech for **NASA's Jet Propulsion Laboratory.** *Further information is contained in a TSP [see page 1].*
NPO-19995

Mechanics

Hardware, Techniques, and Processes

41 Fluid Reservoir Maintains Constant Back-Pressure During Addition and Removal of Liquid
41 Low-Differential-Pressure Test Apparatus
42 Procedure for Quick Calculations of Hydroelastic Loads
43 Mechanisms for Fine Adjustment of Radio-Frequency Reflectors
44 Active Suppression of Vibrations in Automobile Drive Trains
45 Fixture Holds Flexible Waveguide Rigidly After Installation
46 Self-Cleaning Spool Valve
46 Air-Slide Powder Preblender and Gas Seal
48 Discharge Valve for Gravimetric Feeder
49 Preventing Fouling of Feeder Mechanisms by Aluminum Powder
49 Inlet Gas Distributor for Pneumatic Powder-Conveying Vessel
50 Liners for Inlet Bellows of Gravimetric Feeders
51 Deflectors for Outlet Bellows of Gravimetric Feeders
52 Discharge Knife for a Gravimetric Feeder
53 Deployable Rigid Wheel
54 Turbine-Blade Radial Damper With Offset Center of Gravity

Books and Reports

54 Crack-Propagation Studies of Failure Modes in Thin-Rim Gears

BLANK PAGE

Fluid Reservoir Maintains Constant Back-Pressure During Addition and Removal of Liquid

A piston moves to accommodate addition or removal of liquid from a completely filled reservoir.

Marshall Space Flight Center, Alabama

The figure shows a chamber completely filled with liquid. The chamber is equipped with a mechanism, a free-floating piston at one end, that can be attached to a spring-driven lever arm of variable mechanical advantage, to help prevent the introduction of bubbles of gas during liquid addition or removal. Originally developed for use in the microgravity environment of space, where lack of hydrostatic pressure and buoyancy can cause problems with unwanted bubbles during liquid-filling, this apparatus can also be used on Earth in any situation in which a constant back-pressure would be desirable. A syringe needle is inserted into the reservoir through a septum port on the end opposite to the piston for liquid transfer, and a pressure transducer is mounted within the reservoir to allow pressure monitoring during liquid transfer.

The overall function of the apparatus is to maintain a nearly constant back-pressure (including zero pressure) on the liquid in the reservoir while providing a storage volume that can expand or contract just enough to match the volume of additional liquid being injected or withdrawn from the reservoir, thereby minimizing bubble formation. This apparatus has been tested aboard the NASA KC-135 low-gravity aircraft to test liquid handling during low gravity, for applications such as solution crystal growth and cavitation tests.

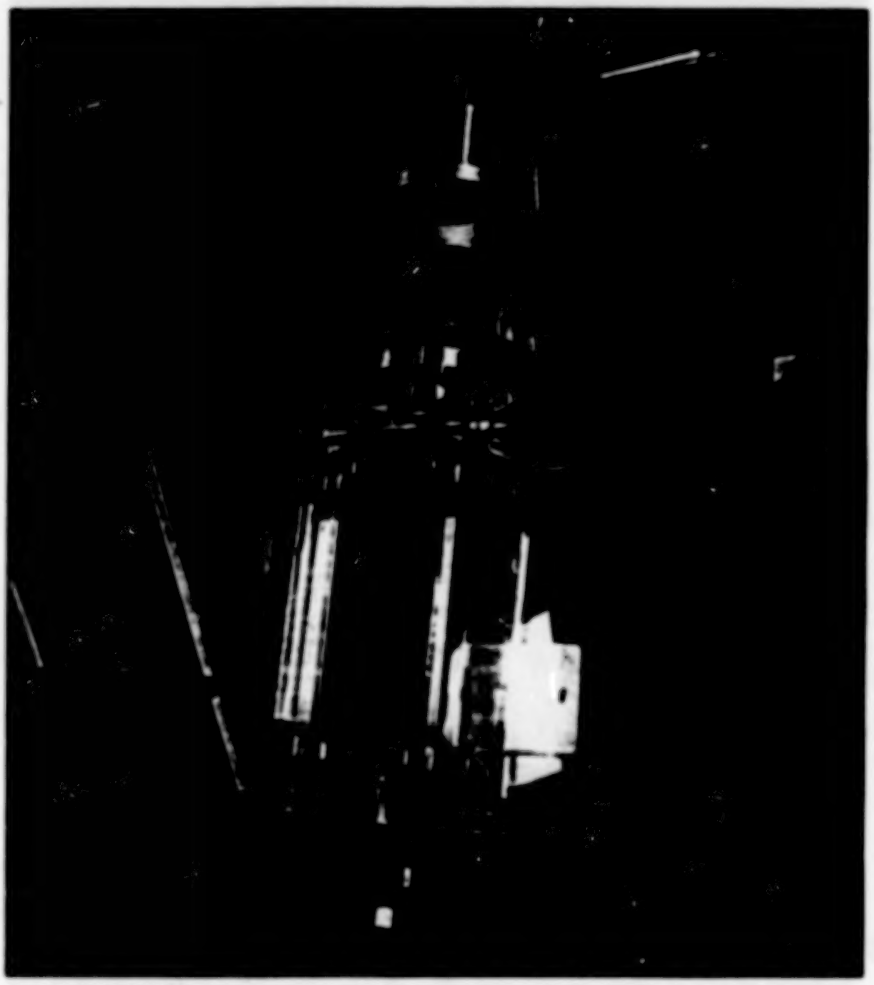

The Cylindrical Mechanism attached to the rectangular chamber serves as a pressure-regulating reservoir to help suppress bubbles.

The apparatus includes a piston-cylinder assembly attached to one end of the reservoir. The piston is held centered in the cylinder and guided by a linear ball bushing to minimize pressure error due to friction. Instead of piston rings, sealing between the cylinder wall and piston is accomplished by a very thin flexible latex rubber bladder which unrolls from the cylinder wall as the piston moves outward, to provide additional liquid volume. Pressure is applied to the back of the piston through a linkage mechanism by a constant-force spring motor — that is, a spring which does not change force as it winds or unwinds. This spring motor maintains a constant force on the piston as the piston moves in or out to accommodate changes in the volume of the liquid, and this force may be set to any desired level by changing the mechanical advantage lever in the linkage mechanism.

This work was done by Dale M. Kornfeld of **Marshall Space Flight Center** *and Raymond H. Moore, Mark Wells, and Byron Burden of Teledyne Brown Engineering. Further information is contained in a TSP [see page 1].*
MFS-31081

Low-Differential-Pressure Test Apparatus

Differential-pressure transducers can be tested and calibrated more easily and cheaply.

John F. Kennedy Space Center, Florida

An apparatus for testing and calibrating low-differential-pressure transducers can be used under various conditions in the laboratory or in the field. The apparatus is designed especially for use on clean-room-air-conditioner differential-pressure transducers with typical full-scale ranges of about 0.1 in. of water (about 25 Pa).

Previously, it was necessary to test and calibrate such transducers in the laboratory by use of expensive and cumbersome dead-weight testers, with strict control of

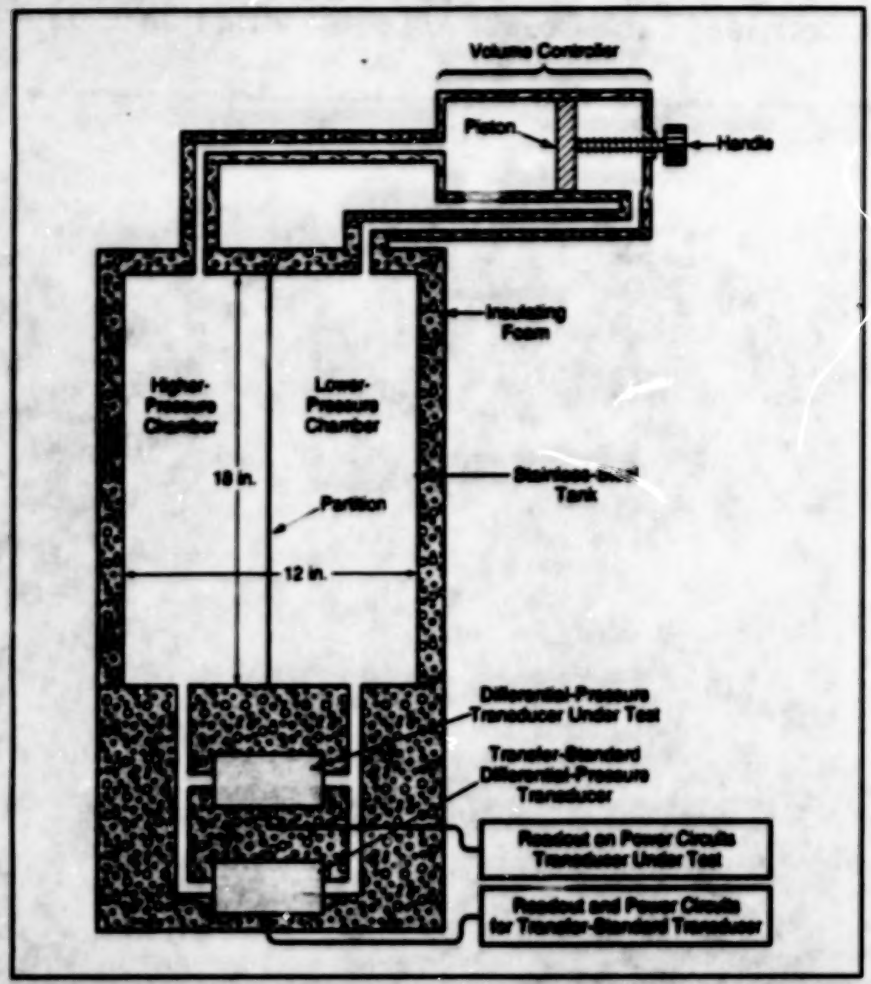

Pressures of Gas in the Two Chambers can be made to differ slightly by use of the volume controller, which contains a manually adjustable piston that increases the volume of the gas on one side while decreasing the volume of gas on the other side by an equal amount.

room temperatures and long waiting times for equalization of temperatures. The present apparatus costs about one-third as much as a dead-weight tester does, is portable, does not depend on strict control of room temperature, and can be operated easily by a technician with minimal training.

The apparatus (see figure) comprises a differential-pressure generator, a standard differential-pressure gauge with electronic output that can be displayed and recorded by a computer, and associated plumbing. The differential-pressure generator includes a stainless-steel tank partitioned into two approximately equal volumes. A tube connects each volume to one of two ports of a precise volume controller based on a threaded piston with an operating handle. Other tubes connect the two volumes to the ports of the transfer-standard differential-pressure gauge and to the ports of the differential-pressure gauge to be tested or calibrated. The two gauges are connected in parallel; that is, they are exposed to the same differential pressure between the two volumes.

When the operator turns the handle of the volume controller, the volume on one side of the controller decreases, causing an increase in the gas pressure on that side. On the other side of the controller the volume increases, causing a decrease in the gas pressure on the associated side. The technician turns the handle on the volume controller until the transfer-standard gauge indicates the desired differential pressure; when this point is reached, the technician causes the computer to record the readings of the transfer-standard gauge and the gauge under test.

While the decreasing volume (compression) caused an increase in pressure, there was an increase in the temperature. A corresponding decrease in temperature accompanied the decrease in pressure on the other side. In order to determine the value of the pressure he/she has just set, the technician normally has to wait until the temperature differences dissipate. The metal divider in the tank allows this temperature differential to mix at approximately the speed of sound, therefore dissipating the temperature difference during the volume controller adjustment. However, the heat-transfer processes in this apparatus are slow enough that the technician can easily maintain a desired pressure setting by manual adjustment. Moreover, the apparatus is insulated to prevent room air currents and other ambient phenomena from differentially heating or cooling the gases in the two volumes.

The standard differential-pressure gauge is a commercial unit that has been calibrated by use of primary standards that have, in turn, been calibrated by the National Institute of Standards and Technology (NIST). The full-scale reading of this unit is 0.53579 in. of water (about 133 Pa). Tests have shown that with manual adjustment, differential pressure can be regulated to within 5×10^{-6} in. (0.012 Pa), exceeding a design requirement for an accuracy and resolution of 2.5×10^{-4} in. (0.062 Pa).

This work was done by Gregory A. Hall of Kennedy Space Center and Stephen J. Stout, Richard T. Deyoe, James E. Meeks, and Harold E. Crain of I-NET. Further information is contained in a TSP [see page 1].

This invention is owned by NASA, and a patent application has been filed. Inquiries concerning nonexclusive or exclusive license for its commercial development should be addressed to the Patent Counsel, Kennedy Space Center [see page 1]. Refer to KSC-11804.

Procedure for Quick Calculations of Hydroelastic Loads

Effects of sloshing can be estimated faster by use of a simplified mathematical model.

Marshall Space Flight Center, Alabama

A procedure for calculating hydroelastic loads associated with sloshing of liquid in a tank involves the use of (1) a computer code developed previously for finite-element mathematical modeling of hydroelasticity and (2) a finite-element mathematical model of the dynamics of the tank to obtain (3) a simplified (one-degree-of-freedom) approximate mathematical model of sloshing. In comparison with other, more complex mathematical models of sloshing, this approximate model can be

implemented more rapidly and easily and thus more cheaply. The capability afforded by this procedure can be beneficial in analyzing and designing tanks in which sloshing can adversely affect safety and controllability; potential applications include ballast and liquid-transport tanks in ships, fuel tanks in aircraft, and liquid-transport tanks on land vehicles.

The previously developed HYDRO computer program implements the finite-element model of the liquid. This model is based partly on the simplifying assumptions that the liquid is inviscid, incompressible, and irrotational, and that it undergoes only small displacements. The principal unknown quantities that one seeks to compute in HYDRO are pressures in the liquid as functions of position and time. One important consequence of the simplifying assumptions is that one can compute these pressures from displacements of the boundary of the liquid.

In the finite-element modeling of the tank, one seeks to compute the displacements (elastic deflections) of the tank as functions of position and time. Wherever the liquid wets a wall of the tank, the pressure in the fluid and the displacement of the wall affect each other, and the dynamic response of the tank is affected by its elasticity and its distribution of mass.

In the present procedure, HYDRO is used to calculate the slosh frequencies under the initial simplifying assumption that the tank is rigid. Another previously developed computer program called "BEAMER" is then used to obtain a transformation matrix that couples the HYDRO model of the liquid with the finite-element structural model of the tank. The resulting system of equations for the coupled models is solved by use of a third previously developed computer code, namely, MSC/NASTRAN.

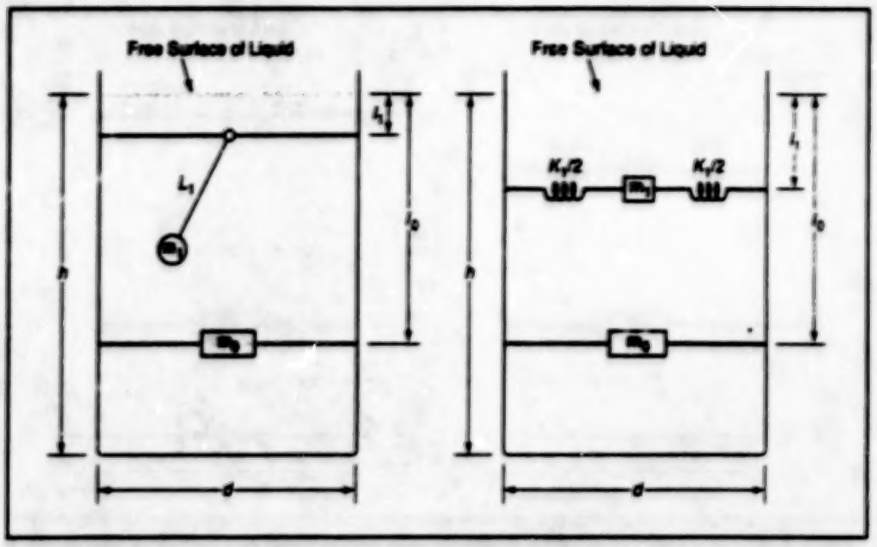

A Pendulum or Spring-and-Mass Model approximates the effects of sloshing of liquid in a tank. Masses m_0 and m_1 represent the nonsloshing and sloshing parts, respectively, of the mass of the liquid. The spring stiffness K_1 or the pendulum length L_1 represents the slosh stiffness.

The last step in the procedure is to generate the approximate single-degree-of-freedom model of sloshing (see figure). Such models have traditionally been used in analyzing control systems that interact with sloshing liquids. To generate data to determine the values of the model parameters m_0, m_1, and either K_1 or L_1, one first models the tank as being subjected to a lateral enforced acceleration. One then finds the values of these parameters that make the oscillations of the model produce net lateral forces and moments equal to those of the first lateral slosh mode. A HYDRO-post-processing code called "SLOSH" has been written for this purpose. SLOSH reads in the results from HYDRO, performs a frequency-response analysis, and solves for parameters of the approximate model.

This work was done by Joseph Brunty and Frank Bugg of Marshall Space Flight Center and Eric R. Christensen of Sverdrup Technology, Inc. Further information is contained in a TSP [see page 1].

Inquiries concerning rights for the commercial use of this invention should be addressed to the Patent Counsel, Marshall Space Flight Center [see page 1]. Refer to MFS-31134.

Mechanisms for Fine Adjustment of Radio-Frequency Reflectors

Differentially pitched inner and outer threads on bushings would produce small differential displacements.

NASA's Jet Propulsion Laboratory, Pasadena, California

A class of simple mechanisms for fine adjustment of the panels of radio-frequency-reflectors is based on the use of two sets of screw threads at slightly different pitches to obtain small differential axial displacements for relatively large rotations. In the original application for which these fine-adjustment mechanisms were devised, reflector panels were adjusted by use of singly threaded adjusters of 20 threads per inch (pitch of 0.05 in. = 1.27 mm). To displace a panel 0.001 in. (0.0254 mm), one would turn one of the older singly-threaded adjusters through an angle of 7.2°. This is too small a turn to control easily by hand, and a slight rotation error could lead to an unacceptably large displacement error; a mechanism with a much larger rotation for the same displacement would make it easier to perform fine adjustments.

A mechanism of the present doubly threaded type provides the desired larger rotation for a given displacement. The figure illustrates a prototype of this type of mechanism installed behind a simple aluminum sheet, which serves as a model of a reflector panel. The edges of the aluminum sheet are bonded to a housing, in which the mechanism is mounted.

The heart of the mechanism is a hollow bushing with an outer thread pitched at 28 per inch (pitch of about 0.0357 in = 0.907 mm) and an inner thread pitched at 32 per inch (pitch of 0.03125 in. = 0.79375 mm). The inner thread of the bushing engages a stud connected to the center of the aluminum sheet, while the outer thread of the bushing engages a threaded hole in the housing behind the sheet.

Turning the bushing to pull down (or to push up) on the stud causes the bushing to ride upward (or downward, respectively) in the threaded hole in the housing, so that the net upward or downward move-

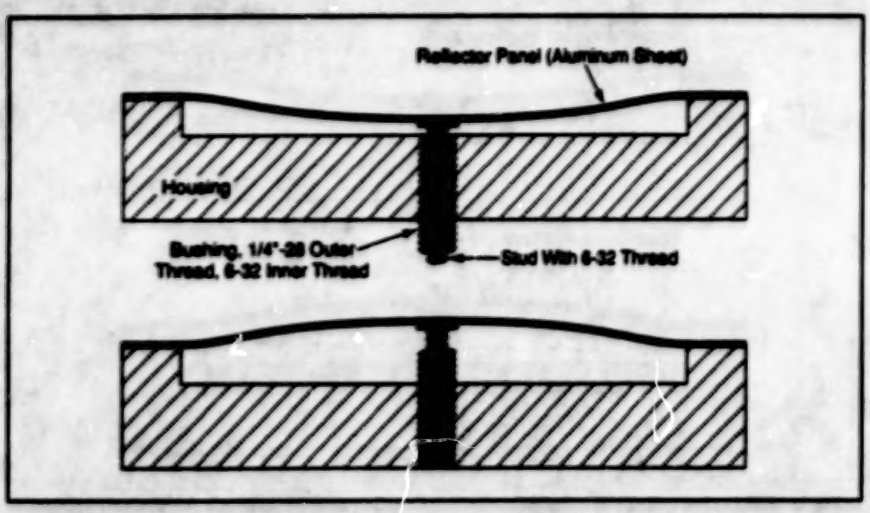

The Deflection of the Reflector Panel in this prototype is adjusted by turning the bushing. A practical reflector structure would include many (48 in the original intended application) such adjustment mechanisms.

ment of the stud and reflector is the difference between these two displacements. The net displacement equals the difference between the two pitches multiplied by the number of turns of the bushing. For example, one full turn of the bushing produces a net displacement of about 0.00446 in. (≈ 0.113 mm). For another example, to obtain a displacement of 0.001 in. (0.0254 mm), one would turn the bushing about 80°; this is ten times the rotation and thus easier to control and less subject to error than is the original single-thread design.

This work was done by Michael P. Moore of Caltech for NASA's Jet Propulsion Laboratory. Further information is contained in a TSP [see page 1].
NPO-19457

Active Suppression of Vibrations in Automobile Drive Trains

Vibrations were reduced substantially in experiments.

NASA's Jet Propulsion Laboratory, Pasadena, California

Feedback control systems for suppression of vibrations in automobile drive trains are undergoing development. Like typical active vibration-suppressing systems designed for other purposes, a system of this type would be based on the general concept of measuring vibrations with an accelerometer, processing the accelerometer output via a suitable compensator to generate a command signal representative of opposing vibrations, and applying an amplified version of the command signal to an electromechanical actuator to generate the opposing vibrations. With proper design of the compensator, actuator, and associated circuitry, the net vibration level could be reduced substantially.

A broadband control system would not perform adequately because it would not focus its energy at the disturbance frequencies, where it would be most needed. Most of the energy of vibrations in an automobile drive train is concentrated at the first few harmonic and subharmonic frequencies of the rotational speed of the engine. Accordingly, the approach followed in the present development is to design a compensator such that the overall effect of the system is that of self-tuning bank of notch filters, with notch center frequencies that are adjusted to track the varying engine speed.

In a vibration-suppression system of this type, the basic engine-rotation signal would be provided by a magnetic pickup device, mounted near the flywheel, that senses the passage of the flywheel teeth. The accelerometer would be affixed to a drive-train-mounting cross member. The electromechanical actuator would also be mounted on the cross member near the actuator. The output of the magnetic pickup device would be digitized and fed to a counter for determination of the number of flywheel teeth that have passed at any given instant of time. The output of the accelerometer would be digitized and fed

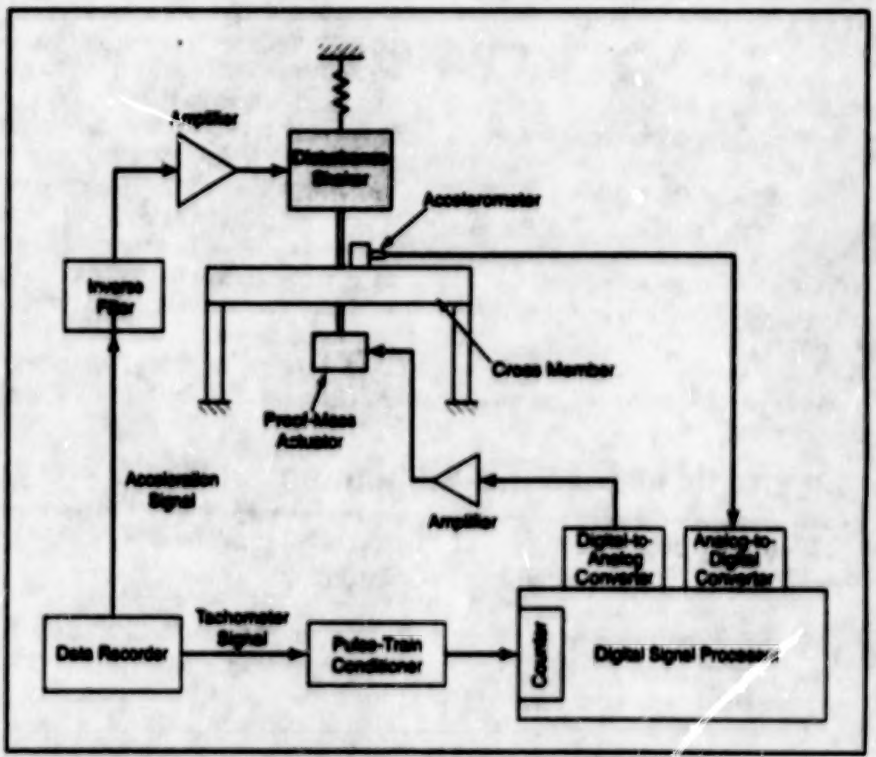

This Laboratory Setup was used to demonstrate the present concept for active suppression of vibrations in an automobile drive train. In a real application, the tachometer signal would be a flywheel-tooth-passage signal from a magnetic pickup device, and the shaker would be replaced by an engine and drive train.

to a digital signal processor (DSP), along with the digital tooth-count signal.

The DSP would use the tooth-count signal to determine the instantaneous engine shaft angle and generate in-phase and quadrature reference signals — synchronized with the engine rotation — for all the harmonic and subharmonic frequencies at which vibrations are to be suppressed. All the reference signals would be generated with little computation, by use of only one lookup table. The DSP would implement the compensator from the reference and acceleration signals by use of a modified version of the Least Mean Squares algorithm. The output of the DSP would be fed through a digital-to-analog converter, then amplified, then applied to the actuator.

The figure schematically illustrates a prototype system in a laboratory setup. The electromechanical actuator used in this setup was of the proof-mass type, with a mass of about 1 kg and the capability to generate forces as large as 40 N at frequencies above 40 Hz. The compensator was implemented in a commercial DSP, which was programmed to suppress vibrations at nine frequencies; namely, the first five harmonics and the four integer-and-a-half harmonics between them. A real engine was not used in this setup: Instead, engine vibrations were synthesized by driving a shaker, via an inverse filter, with a previously recorded vibration signal from a real engine; and flywheel-tooth-passage pulses recorded along with the vibration signal were substituted for the output of a real magnetic pickup device. In experiments on this setup, the vibrations at the nine selected frequencies were attenuated by more than 20 dB when the system was operating.

This work was done by Zahidul H. Rahman and John T. Spanos of Caltech for **NASA's Jet Propulsion Laboratory.** *Further information is contained in a TSP* *[see page 1].*

NPO-20026

Fixture Holds Flexible Waveguide Rigidly After Installation

Spherical ferrules can be clamped in somewhat different orientations.

NASA's Jet Propulsion Laboratory, Pasadena, California

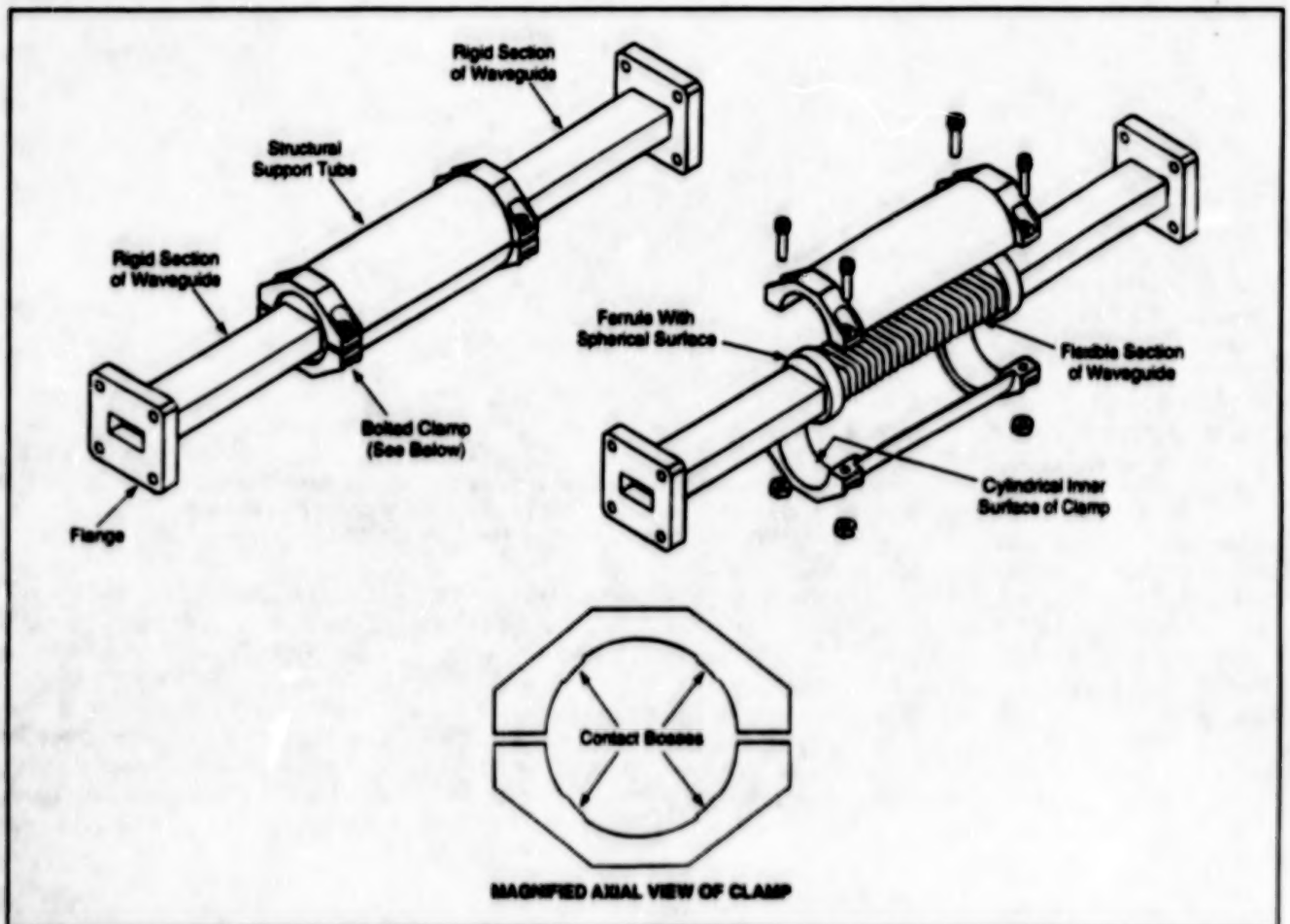

The Ferrules Are Clamped to rigidize the flexible middle section of the waveguide. Contact bosses on the inner cylindrical surfaces of the clamps accommodate manufacturing tolerances.

A fixture called a "lockout device" rigidly holds the ends of a bellowslike flexible section of a waveguide after installation. The flexible section is needed during installation to accommodate small misalignments of the interfacing end flanges (see figure). After installation, the waveguide is required to be rigid to prevent excessive displacements in the flexible section and, ultimately, fatigue failure; this requirement is satisfied by use of the lockout device, which fixes the positions and orientations of the ends of the flexible section with respect to each other while also accommodating misalignments.

The lockout device includes a split tube with bolted frictional clamps at the ends. The clamps engage flangelike ferrules at the ends of the flexible section of the waveguide. The outermost surfaces of these ferrules are spherical, while the inner contact surfaces of the clamps are cylindrical; thus, each clamp can engage a ferrule at any orientation within the range provided by the spherical surface.

This work was done by David J. Levitt and Wesley P. Schmitigal of Caltech for **NASA's Jet Propulsion Laboratory**. *Further information is contained in a TSP [see page 1].*
NPO-19617

Self-Cleaning Spool Valve

Controlled leakage for gradual shutdown is combined with self-cleaning.

Marshall Space Flight Center, Alabama

A spool that places the main actuator in the pneumatic shutdown position and is used to control the rate of shutdown has been modified by the incorporation of a self-cleaning curtain orifice. Helium gas applied to the pneumatic end of the spool places the valve in the pneumatic shutdown position. In this position, the opening cylinder of the main actuator is communicated to the hydraulic return system via a timing orifice in the spool valve sleeve. The shutdown rate is regulated by a sized timing orifice of rectangular cross section. Helium gas, which is also applied to the closing piston of the main actuator (the closing piston is in a push-push configuration with the opening piston), provides the necessary closing force to the main actuator. The hydraulic fluid in the opening cylinder is forced through the timing orifice, therefore controlling the closing rate of the main actuator.

The top part of the figure shows the unmodified version of the valve, without the self-cleaning curtain orifice. In this version, debris are trapped by a filter inside the spool. The oil flows only one way through the filter and only during the shutdown sequence; as a result, there is no convenient way to remove accumulated debris from the filter.

The bottom part of the figure shows the modified version. An annular gap around part of the spool allows some leakage and acts as an oil filter. The radial gap of the annulus is chosen small enough (smaller than the smallest dimension of the timing orifice) to prevent debris from reaching and blocking the timing orifice. The length of the annulus is then chosen so that the rate of leakage through the annulus can be an order of magnitude greater than that through the timing orifice. The annulus is cleaned by the scavenging effect of the normal flow of oil through the valve. The leakage past the annulus is collected by a circumferential channel, which provides for unrestricted flow to the timing orifice.

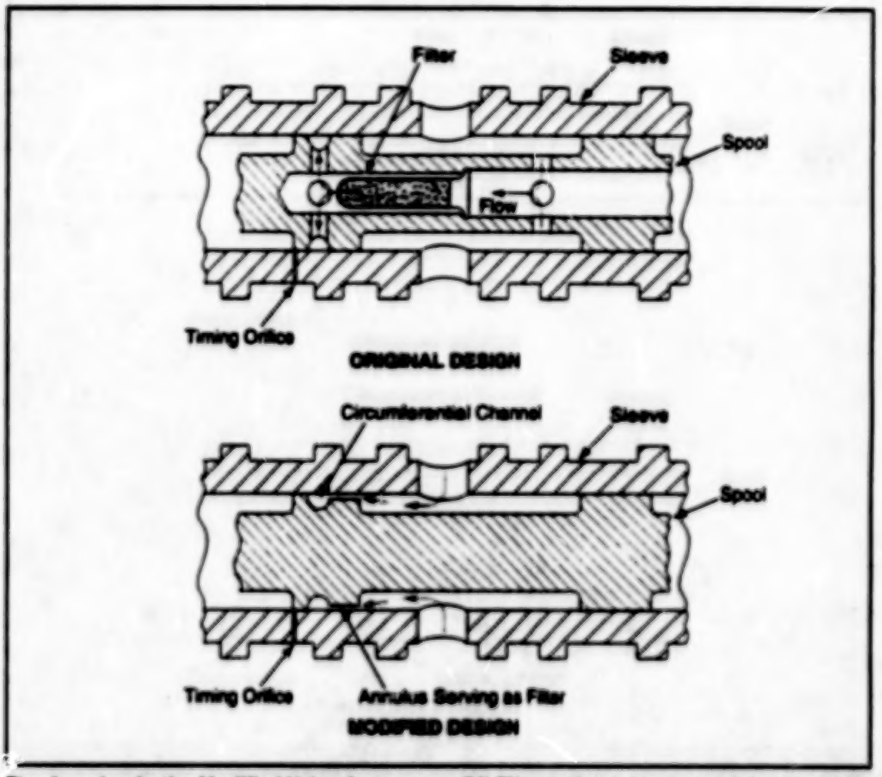

The Annulus in the Modified Valve Acts as an Oil Filter in that it blocks particles too large to travel easily through the timing orifice. The flow of oil through the annulus keeps the annulus clean by sweeping away smaller particles that can travel easily through the timing orifice.

This work was done by Mario Padilla of Rockwell International Corp. for **Marshall Space Flight Center**. *Further information is contained in a TSP [see page 1].*

Inquiries concerning rights for the commercial use of this invention should be addressed to the Patent Counsel, Marshal Space Flight Center [see page 1]. Refer to MFS-30042.

Air-Slide Powder Preblender and Gas Seal

One powder is shaped to block a flow of gas into another powder.

Marshall Space Flight Center, Alabama

The figure illustrates an air-slide apparatus that combines precisely controlled flows of aluminum and iron oxide powders. The apparatus is part of a facility that manufactures solid rocket propellant containing these powders plus other ingredients, but the technological significance of the apparatus goes beyond the rocket propellant application. Apparatuses of this type can be used in processes for making such diverse products as foods, fertilizers, and plastics.

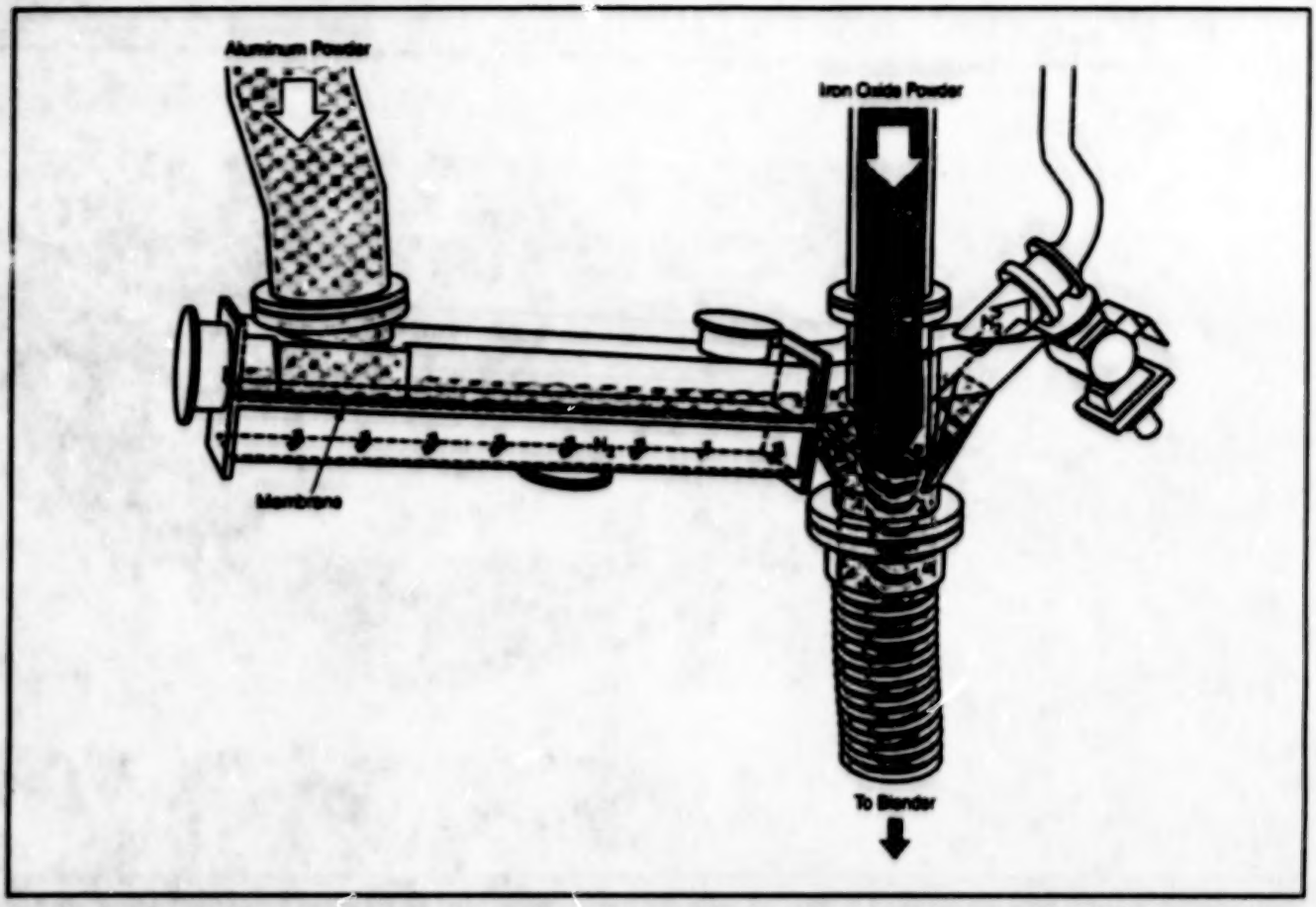

The Aluminum Powder Flows around the iron oxide powder, up to a level above the outlet of the vertical iron oxide duct. The aluminum powder thus blocks any flow of nitrogen through the iron oxide powder, and the iron is encapsulated in the aluminum flow.

The basic task is to combine and preblend two or more weighed quantities of powder in a closed system without degrading their weighment accuracies. Care must be taken to ensure that accuracy is not decreased by either allowing gas pressures to alter precision of upstream weighing equipment or altering the weight of powder that is delivered at the end of the process, by allowing some of it to adhere to interior surfaces of the pipe and process equipment. In designing the apparatus to satisfy these requirements, it was necessary to pay special attention to the unique properties of the aluminum and iron oxide powders:

- To prevent ignition of the highly explosive aluminum powder, it is necessary to maintain an inert (nitrogen) atmosphere in the ducts.
- Iron oxide powder is very adhesive, tending to accumulate on some duct surfaces. To ensure the integrity of the weighment, the accumulation of iron oxide powder on surfaces must be minimized.
- Iron oxide powder comprises submicron-sized particles that could easily be blown away by excessive flows of nitrogen in the ducts, with consequent loss of weighment precision.

In the present apparatus, the accumulation of iron oxide powder on surfaces is prevented by making the powder fall through the center of an oversized vertical duct. The air-slide part of the apparatus is used to convey the aluminum powder across a 4-ft (1.2-m) horizontal distance from the outlet of an aluminum-powder feeder to the inlet of the blender, wherein the two powders are mixed. The slide path has a slight downhill tilt from the aluminum-feeder outlet to the blender inlet. "Air slide" is something of a misnomer in that nitrogen is the gas used in this slide. The upper and lower halves of the slide are separated by a gas-permeable membrane. Compressed nitrogen is introduced below the membrane, flows up through the membrane, fluidizing the aluminum powder, which is fed in on top of the membrane. Fluidization enables the aluminum to flow down very slight inclines, much like a fluid.

Iron oxide and aluminum powder merge and are preblended inside the air slide. The iron oxide inlet to the air slide extends vertically into the aluminum powder discharge. The annulus that forms between the outside diameter of the pipe and the air slide was carefully sized to flood and fill with aluminum powder. Thus, the aluminum powder acts as something of a seal, suppressing pressure fluctuations from the upstream weighing equipment and thus preventing the loss of the smaller iron oxide [illegible] as nitrogen vents from the process. Finally, the adhesive iron oxide becomes encapsulated in aluminum powder, which flushes it through the system.

This work was done by Joel Crook of Thiokol Corp. for **Marshall Space Flight Center**. *Further information is contained in a TSP [see page 1].*

Inquiries concerning rights for the commercial use of this invention should be addressed to the Patent Counsel, Marshal Space Flight Center [see page 1]. Refer to MFS-31129.

Discharge Valve for Gravimetric Feeder

This valve prevents leakage of fluidized powder during filling of a hopper.

Marshall Space Flight Center, Alabama

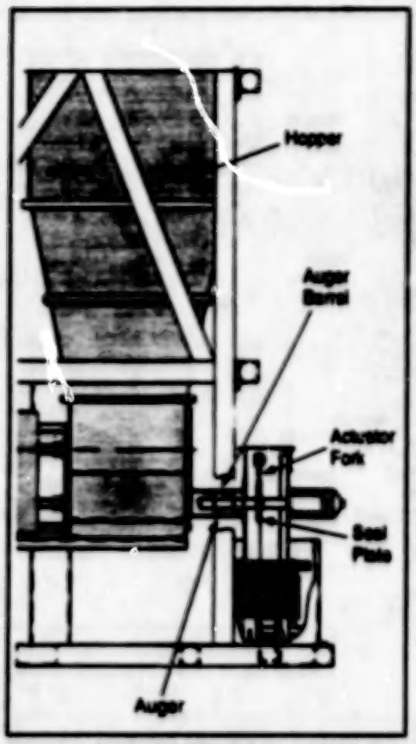

Figure 1. Leakage Occurs as fluidized aluminum flows around the auger helix and through the clearance between the auger (feed screw) and the auger barrel, when the auger is not turning. The valve blocks this leakage during times when powder feed is not desired.

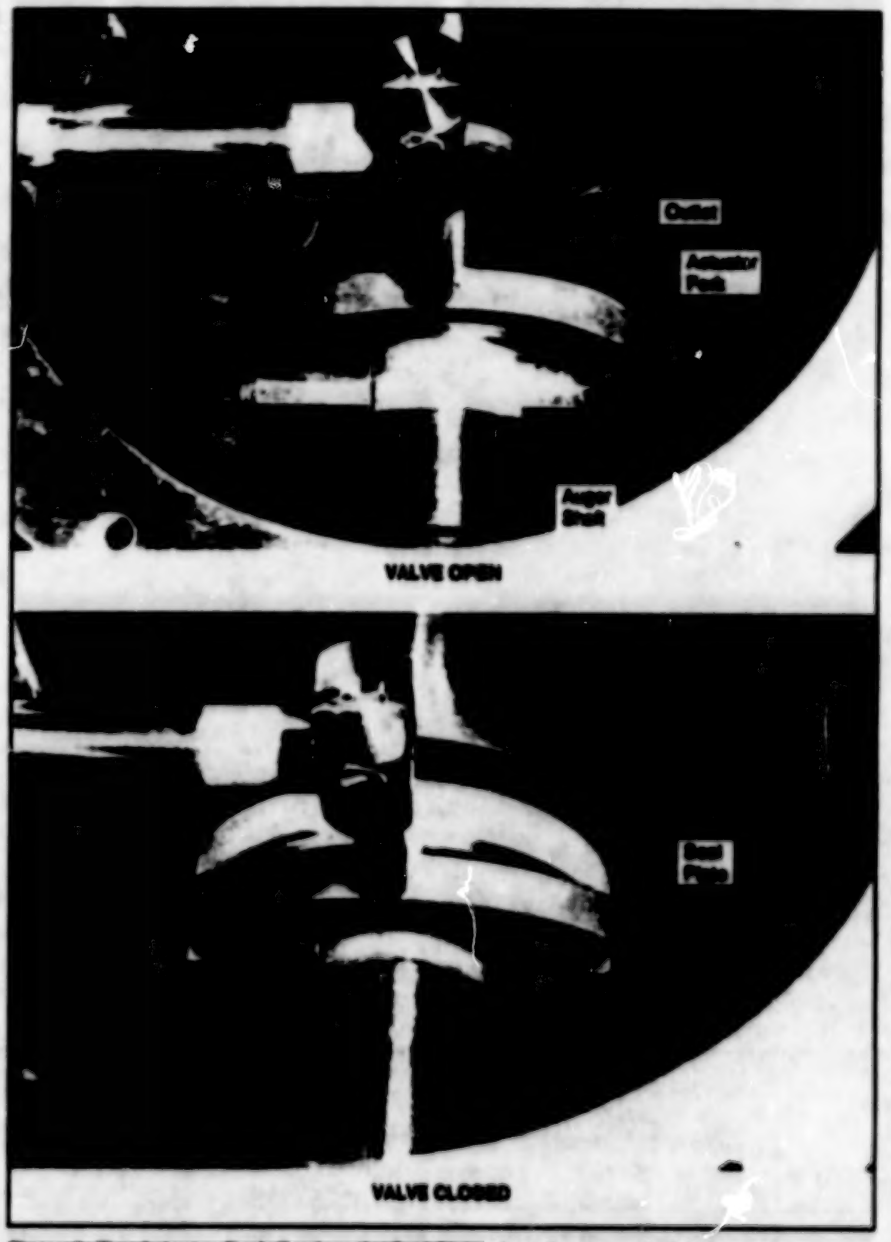

Figure 2. The Actuator Fork Pushes the Seal Plate along the auger shaft between "open" and "closed" positions. The auger shaft runs through the center of the seal plate when the valve is open. The seal occurs around the shaft and also around the auger barrel. The shaft to which the actuator fork is connected is driven by an external pneumatic actuator.

A computer-controlled, pneumatically actuated valve blocks incidental discharge of aluminum powder from the outlet of a gravimetric feeder during batch refills. The feeder is part of a facility that manufactures solid rocket propellant. By preventing small, unintended flows, the valve helps to maintain the precision of metered weights of aluminum powder, as needed for mixing with other constituent materials. This valve concept is not limited to the production of rocket propellant; it could be applied to gravimetric feeders in the food, fertilizer, and plastics industries, for example.

The need for the valve arises largely because of propensity of aluminum to assume fluidlike properties, when moving (fluidized flow). Fluidized flow occurs when particles are separated from each other by cushions of gas. Contact bed flow occurs when particles touch each other and gas is present only in the interstices of the particles. Fluidized flow is preferred for moving powder, within a process, from point A to point B. Contact bed flow is preferable for metering the powder because, in comparison with fluidized flow, it is more controllable.

The gravimetric feeder (see Figure 1) includes a hopper with an auger at its outlet that is used to discharge powder. Initially, free-falling aluminum fills the hopper from the top, and some gas becomes trapped within the powder. After a couple minutes at rest, the weight of the powder will cause much of the trapped gas to permeate out through the top surface of the powder. As aluminum is dropped into the hoper, during refills, the fluidized powder spreads outward as it hits the hopper bottom, rather than forming a pile. Under these conditions, some of the powder spirals through the auger helix and drops into the discharge. Powder following this path is unaccounted for in the batch weighment; this is the unintended flow that the valve is designed to block.

The auger discharge is blocked within a seal plate that slides along the auger shaft. The seal plate is an elastomer

covered disk. During hopper refills, the seal plate is pushed against the outlet of the auger barrel ("closed" position), blocking unintended flow of aluminum powder. The seal plate is moved along the shaft, between the "open" and "closed" positions, by an actuator fork (as shown in more detail in Figure 2), which is connected to an external pneumatic actuator. Under computer control, the actuator closes the valve immediately before the hopper is filled, and opens it immediately before the auger is started to feed powder.

This work was done by Joel Crook of Thiokol Corp. for **Marshall Space Flight Center.** *Further information is contained in a TSP [see page 1].*
MFS-31120

Preventing Fouling of Feeder Mechanisms by Aluminum Powder

Several features prevent powder degradation around rotational components of process equipment.

Marshall Space Flight Center, Alabama

The design of the gravimetric aluminum-powder feeder mentioned in the preceding article incorporates several features to prevent fouling by aluminum powder, an essential ingredient in many solid rocket motors. The particular fouling problem arises because aluminum powder is so soft and fine that it infiltrates small internal openings within the feeder and forms hard foil pieces under very low pressures. Around rotating or sliding parts, such foil pieces accumulate rapidly, so that clearances close and the affected parts seize. The antifouling features prevent the formation of foil by creating a gas pocket around regions where clearances between moving and stationary parts are very small. Similar features might also be useful in gravimetric feeders like those used in the food and chemical industries, where fouling could cause contamination, frictional heating (leading to fire hazards), and possibly other adverse effects, depending on the material(s) being fed.

In the gravimetric feeder, aluminum powder will typically foul where rotating auger and intromitter shafts penetrate the wall of an aluminum-powder-filled hopper. At the wall penetration of each shaft, the interior of the hopper is sealed with graphite packing, a brass lantern ring, and a packing gland, to prevent leakage of aluminum powder. Because of the explosive nature of aluminum powder, an oxygen-free gas (nitrogen) at a pressure of 2 psig (gauge pressure of 14 kPa) is piped directly over the lantern ring. This pressurizes the packing with respect to the environment in the hopper, thereby preventing the flow of aluminum powder into the packing.

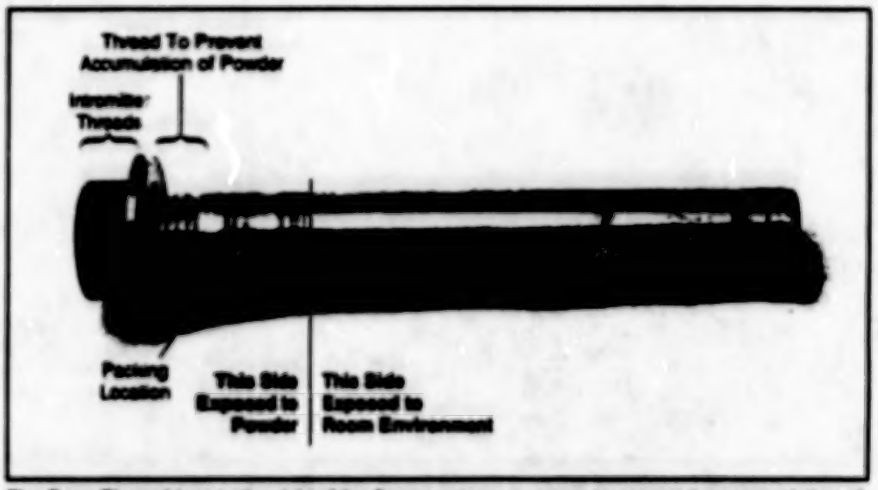
Thread To Prevent Accumulation of Powder
Intromitter Threads
Packing Location
This Side Exposed to Powder
This Side Exposed to Room Environment

The Deep Thread just to the right of the flange acts as an auger to prevent the accumulation of powder inside the hopper near the packing seal.

Additional antifouling features help to prevent the accumulation of aluminum powder around each shaft near the wall penetration. In the case of the intromitter shaft, one of these features is a deep thread, which is cut into the end of the shaft near the wall penetration (see figure). This thread acts as an auger, moving accumulated powder away from the wall penetration. Another antifouling feature is a chamfer around the inside edge of each shaft hole in the hopper wall. The chamfers eliminate what were previously blind holes that trapped powder. A third antifouling feature is a radiused shield that is welded in place on the wall of the hopper just above each shaft. The design of the shield is based on the bulk properties of aluminum powder. A horizontal projection into any vertically flowing powder will create a powder-free area underneath it. The size of this area depends on the physical properties of the material and the geometry of the shield. These antifouling features allow for the shafts to turn inside the powder-filled hopper with little or no powder present in the tight clearances between the shafts and the stationary parts.

This work was done by Joel Crook and Charles D. Fuller of Thiokol Corp. for **Marshall Space Flight Center.** *Further information is contained in a TSP [see page 1].*

Inquiries concerning rights for the commercial use of this invention should be addressed to the Patent Counsel, Marshall Space Flight Center [see page 1].
Refer to MFS-31128.

Inlet Gas Distributor for Pneumatic Powder-Conveying Vessel

Powder in the vessel is fluidized to prevent "ratholing."

Marshall Space Flight Center, Alabama

An inlet gas distributor has been devised to ensure that the entire volume of aluminum powder is conveyed out of a pneumatic conveying vessel during each conveying cycle, thereby increasing the time-averaged conveying rate. The vessel and the rest of the pneumatic conveying system are part of a facility that manufactures solid rocket propel-

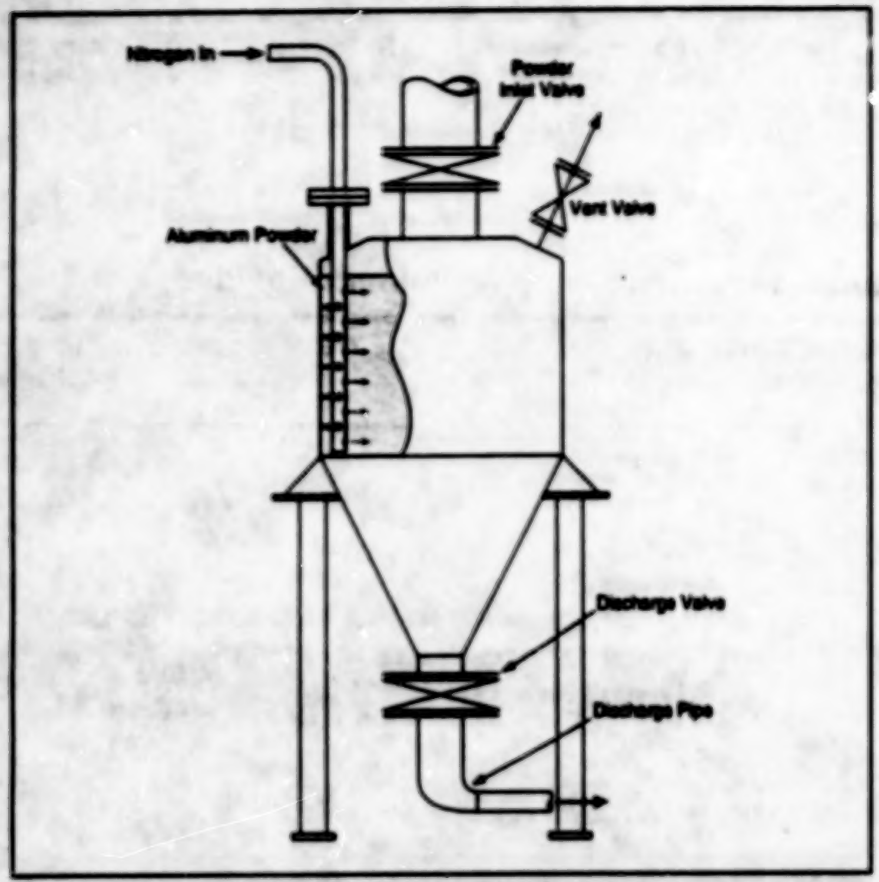

The Pneumatic Conveying Vessel is modified from its original design by substitution of the inlet gas distributor for a nozzle.

tant containing aluminum powder plus other ingredients. Similar inlet gas distributors might also be useful for increasing conveying rates in some of the numerous other industrial processes that utilize pneumatic conveying of materials.

The pneumatic conveying vessel is a hopperlike pressure vessel with a discharge valve connected to a discharge pipe at the bottom (see figure). Each batch of powder is conveyed in the following way: First, the vessel is filled with powder. Next, the powder-inlet valve is closed and the interior of the vessel is pressurized with nitrogen. Once the pressure has risen to a predetermined level, the discharge valve is opened, allowing the pressurized nitrogen to push the powder out through the discharge pipe. During this discharge, pressurized nitrogen continues to flow into the vessel. When the discharge is complete, pressurized nitrogen is supplied for a little while longer to blow the discharge pipe clear.

A phenomenon called "rathoing" occurs during the discharge as a result of the tendency of aluminum powder to settle and consolidate into a weak mass, with just enough strength to hold its shape against gravity. When the discharge valve is opened, only the powder immediately above it is discharged, leaving a thick layer of powder around the periphery of the vessel and a vertical hole (the "rathole") in the middle. Thus, a significant portion of the original powder filling remains in the vessel after discharge. This decreases the effective volume of the vessel, and the time-averaged conveying rate is reduced correspondingly. This problem is further exacerbated when pressure is applied above the powder, just prior to opening the discharge valve. The resultant force from this pressure causes further powder consolidation, which increases the strength of the rathole.

The inlet gas distributor is a capped, perforated pipe that extends along the vertical wall of the vessel. Pressurized nitrogen is fed into the vessel through this distributor. The purpose of the inlet gas distributor is twofold: First, nitrogen pressure is no longer applied directly above the powder. The gas distributor pressurizes the vessel from within the powder mass. This eliminates the differential pressure that can consolidate the material. Second, nitrogen flowing from the distributor fluidizes some of the powder in the vessel along a line that extends vertically through the consolidated ring of powder. The fluidized powder falls out, thereby destabilizing the remaining powder mass enough to make it fall into the discharge pipe.

This work was done by Joel Crook of Thiokol Corp. for Marshall Space Flight Center. Further information is contained in a TSP [see page 1].
MFS-31121

Liners for Inlet Bellows of Gravimetric Feeders

Liners increase weighment accuracy by preventing powder accumulation.

Marshall Space Flight Center, Alabama

Flexible liners have been incorporated into the inlet bellows of gravimetric feeders that are used to meter precise amounts of powders for making solid rocket propellants. The bellows provide freedom of movement between the scale portion of the feeder and the rigid pipe connections at the feeder inlet/outlet. The liners prevent accumulation of powder in the convolutions of the bellows. Before the liners were developed, powders tended to accumulate in the bellows convolutions, causing their stiffness to change. Variations in bellows stiffness degraded metering accuracies.

Each liner is made from a sheet of 5-mil (0.13-mm) thick polyurethane that is cut in a pattern, rolled up, and stitched to form a long, flexible cone that resembles a wind sock (see figure). A neoprene gasket is sewn in place around the hole at the wide end. To install the liner, the gasket is bolted between flanges at the top of the inlet bellows. The liner hangs down from these flanges, extending below the lower end of the bellows and into a hopper that is part of the feeder.

The conical taper prevents the liner from dragging on the inner surface of the bellows and thereby affecting the weight measurement of the feeder. The polyurethane liner material is so slick that even relatively sticky powders like iron oxide do not adhere to it. In operation, the hopper is filled by dropping powder in through the inlet pipe and liner. After the refill is complete, an automatic valve opens, causing compressed nitrogen to flow through four nozzles that penetrate the wall of the inlet pipe, directly beneath the neoprene gasket of the sock. The nozzles sweep the inlet pipe, while vigorously shaking the bellows sock, to remove fugitive dust and powder agglomerations that may be trapped within wrinkles in the sock. Powder that is shaken loose during the compressed-nitrogen sweep falls into the hopper, as desired.

This work was done by Joel Crook of Thiokol Corp. for **Marshall Space Flight Center.** *Further information is contained in a TSP [see page 1].*
MFS-31122

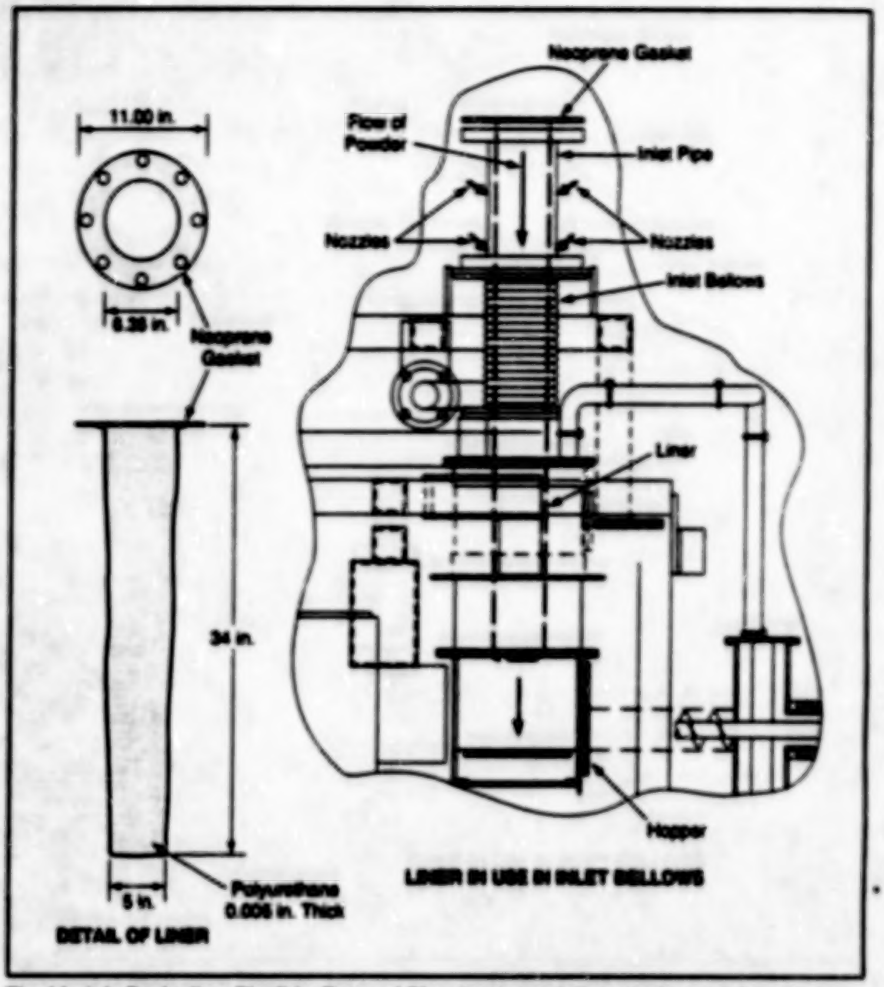

The Liner Is Basically a Flexible, Tapered Pipe that keeps falling powder away from the convolutions of the bellows.

Deflectors for Outlet Bellows of Gravimetric Feeders

These deflectors serve the same purpose as that of inlet-bellows liners.

Marshall Space Flight Center, Alabama

Deflectors have been placed inside the outlet bellows of bulk-powder gravimetric feeders that are used to meter precise weights of powders. Like the inlet-bellows liners described in the preceding article, the outlet-bellows deflectors are used to prevent accumulation of powders in the convolutions of the bellows in order to keep the bellows flexible, as necessary for precise metering of powders by weight.

When powder is discharged from the feed auger, it has a small but significant horizontal velocity. This velocity causes the powder to strike the bellows at some point below and opposite the outlet. The outlet-bellows deflector is a half-cylindrical aluminum shield supported by a flange above the feeder outlet. It hangs down past the outlet and through the bellows to a point somewhat below the lower end of the bellows (see figure). The concave side of the deflector faces the outlet. As powder contacts the outlet-bellows liner, its horizontal velocity goes to zero, and the powder drops vertically through the center of an oversized pipe. Conductive Teflon (or equivalent) is bonded to the surface of the liner to prevent powder adherence and buildup of electrostatic energy.

This work was done by Joel Crook of Thiokol Corp. for **Marshall Space Flight Center.** *Further information is contained in a TSP [see page 1].*
MFS-31124

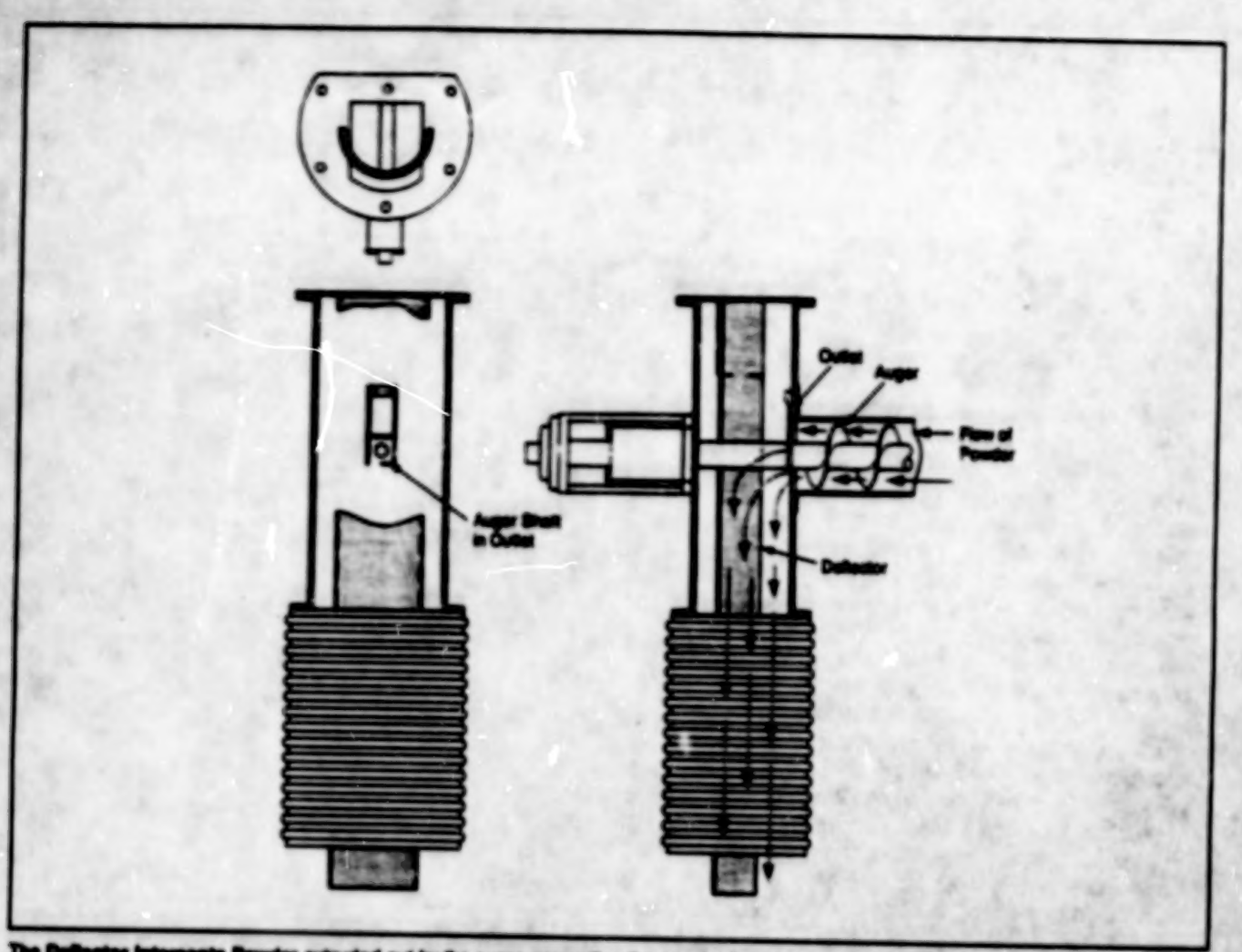

The Deflector Intercepts Powder extruded out by the auger, preventing the powder from striking and getting stuck in the convolutions of the bellows on the opposite side.

Discharge Knife for a Gravimetric Feeder

Discharge weight can be controlled more precisely.

Marshall Space Flight Center, Alabama

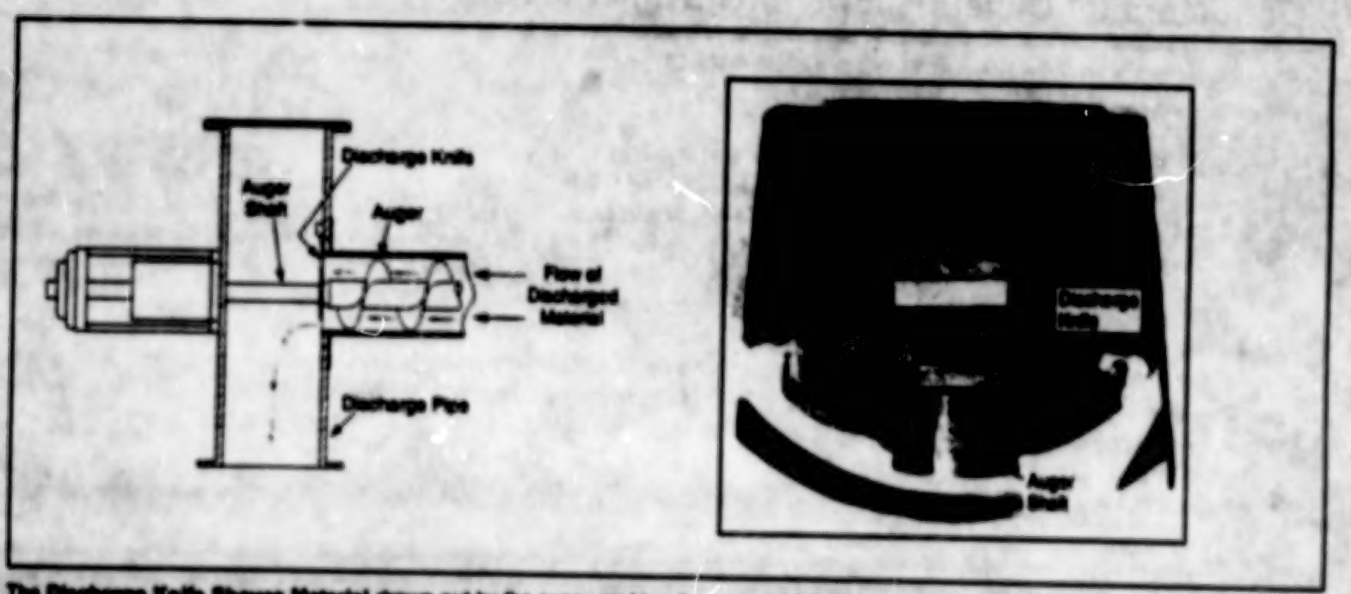

The Discharge Knife Shaves Material drawn out by the auger, making the material fall off the auger in smaller clumps.

The outlet of a gravimetric powder feeder is equipped with a discharge knife that shaves and cuts the material as it is discharged off the end of its auger (see figure). As explained below, the shaving action is needed to increase the accuracy with which the discharged material is weighed out. In this case, the discharged material is iron oxide powder, and the gravimetric feeder is part of a facility that weighs out precise amounts of iron oxide powder that are mixed with other ingredients in making solid rocket propellants. The basic principle of the discharge knife can also be utilized to improve the accuracies of gravimetric feeders that weigh out other materials in the food and chemical industries.

Ideally, the discharged material would not adhere to the auger and would fall smoothly off the auger into the process stream, so that the rate of discharge would be uniform and well controlled by varying the speed of the auger. Unfortunately, iron oxide powder is so cohesive and adhesive that it does not fall off smoothly; instead, it tends to adhere to the auger and itself to form clumps that grow and extend horizontally into the discharge, until they break off under their own weights. This causes the discharge to pulse, and this makes it impossible to precisely weigh a discharged material batch. For example, suppose that the a 20.000-lb (9,071.8-g) batch size is required and the amount weighed out thus far is 19.990 lb (9,067.3 g). If a clump weighing 0.070 lb (31.8 g) breaks off, the amount weighed out suddenly jumps to 20.060 lb (9,099.1 g), so that the batch is now overweight by 0.060 lb (27.2 g).

The auger pushes clumps out with small axial and radial velocities. The discharge knife shaves the clumps as they rotate. Moreover, the design of the discharge knife is such that the portion of discharged material that is not shaved is cut into five roughly equal parts. Thus, the net effect of the discharge knife is to make the discharged material fall off in smaller clumps. This makes it possible to approach the required weight of delivered material in smaller increments, stopping the discharge within a smaller undershoot or overshoot of the required discharge weight.

This work was done by Joel Crook of Thiokol Corp. for **Marshall Space Flight Center**. *Further information is contained in a TSP [see page 1].*

Inquiries concerning rights for the commercial or noncommercial use of this invention should be addressed to the Patent Counsel, Marshall Space Flight Center [see page 1]. Refer to MFS-31123.

Deployable Rigid Wheel

No dedicated deployment actuator is needed.

NASA's Jet Propulsion Laboratory, Pasadena, California

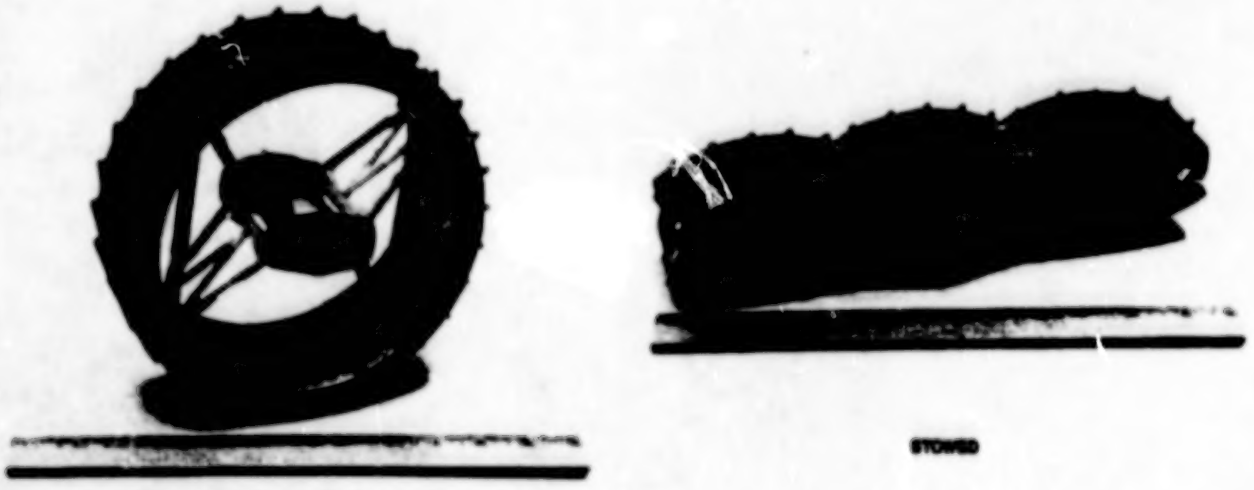

The Deployable Rigid Wheel can be stowed at about one-third its full volume. When released from stowage, it extends itself, then locks itself at full extension.

A rigid wheel for an exploratory robotic vehicle can be folded for stowage at about one-third its full volume, then later deployed for use. Unlike a wheel with an inflatable tire, this deployable rigid wheel can work in extreme temperatures and can survive intense radiation.

The wheel (see figure) includes six rigid outer segments that are hinged together and connected to a hub via pin-ended spokes. No dedicated actuator is needed for deployment; instead, to initiate deployment, one simply releases some restraints. Deployment force and locking are derived from pin-ended extension springs. When deployment is complete, the spokes rest on mechanical stops at the hub; this establishes the load path for transmission of torque.

This work was done by Lee F. Sword, Geoffrey D. Hervey, and Jack A. Frazer II of Caltech for **NASA's Jet Propulsion Laboratory**. *No further documentation is available.*
NPO-19982

Turbine-Blade Radial Damper With Offset Center of Gravity

A device suppresses radial vibrations of a turbine blade, thereby helping to reduce fatigue and prolong the life of the blade. The device is a damper that is pressed outward against the turbine-blade platform by centrifugal force. The damper is shaped and positioned with its center of gravity offset from the radial line through the point of contact with the blade platform, so that centrifugal force applies a torque about this point. The torque is reacted by contact between a radial leg of the damper and the sides of a radial slot into which the leg extends. The circumferential force of contact gives rise to a radial frictional force whenever the blade platform and thus the damper move radially. Thus, kinetic energy of radial vibrations is damped by friction, with consequent reduction of the amplitudes of the vibrations. The heat generated by the frictional dissipation of energy is removed by the turbine flow.

This work was done by Charles A. Bulgrin and John O. Struthers of United Technologies Pratt & Whitney for **Marshall Space Flight Center**. *Further information is contained in a TSP [see page 1].*

Inquiries concerning rights for the commercial use of this invention should be addressed to the Patent Counsel, Marshall Space Flight Center [see page 1]. Refer to MFS-31177.

Books and Reports

Crack-Propagation Studies of Failure Modes in Thin-Rim Gears

A report describes theoretical and experimental studies of the effects of rim thicknesses on the propagation of cracks in thin-rim gears, which are used in advanced aircraft because they weigh less than conventional gears do. The goal of the studies was to determine whether cracks grow through gear teeth (a relatively benign failure mode) or through the rims (a catastrophic failure mode) at various rim thicknesses. The theoretical studies included finite-element computer simulations of gear-tooth bending, fatigue, and propagation of cracks based on linear elastic fracture mechanics. In the experimental studies, gears with various backup ratios (rim thickness ÷ tooth height) were tested in the NASA Lewis Spur Gear Fatigue Rig to validate the theoretical crack-path predictions. In both the theoretical and experimental studies, it was found that tooth fractures occurred in gears with backup ratios of 3.3 and 1.0, and rim fractures occurred in gears with a backup ratio of 0.3. For gears with a backup ratio of 0.5, the experiments revealed rim fractures, whereas the theoretical study showed instability; that is, the possibility of either tooth or rim fracture, depending on initial conditions. Thus, it appears that the theoretical point of transition from tooth to rim failure should be viewed with conservatism to produce a safe design.

This work was done by David G. Lewicki of the Vehicle Propulsion Directorate of the U.S. Army Research Laboratory for **Lewis Research Center**. *To obtain a copy of the report, "Crack Propagation Studies to Determine Benign or Catastrophic Failure Modes for Aerospace Thin-Rim Gears," see TSP's [page 1].*

Inquiries concerning rights for the commercial use of this invention should be addressed to NASA Lewis Research Center, Commercial Technology Office, Attn: Tech Brief Patent Status, Mail Stop 7-3, 21000 Brookpark Road, Cleveland, Ohio 44135. Refer to LEW-16436.

Machinery

Hardware, Techniques, and Processes

57 Apparatus for Access to a Confined Space From Above
58 Reducing Gear-Mesh Vibrations With Piezoelectric Actuators

Books and Reports

59 Coupled Fluid-Dynamic and Thermal Effects in a Turbomachine

BLANK PAGE

Apparatus for Access to a Confined Space From Above

Telescoping tubes, a ladder, and platforms would fit through a narrow opening.

John F. Kennedy Space Center, Florida

A proposed apparatus called an "access kit" would enable technicians and equipment to enter and leave a confined space through a relatively narrow opening in the ceiling. The apparatus is undergoing development; its original intended application is in the installation and removal of refrigerator and freezer components in a spacecraft module through a 50-in. (126-cm) square hatch on top of the module. Similar apparatuses could be designed to provide access to other confined spaces through narrow top openings for purposes of manufacturing, maintenance, and rescue. Large confined spaces such as chemical tanks, vats, and silos could be easily accessed from above. The access kit is unique in that it does not touch the room interior and is entirely supported from above.

The apparatus (see figure) would include three rectangular-cross-section telescoping tubes, a ladder, platforms, and hoists. For compactness, the telescoping motions of the tubes would be actuated by a single wire-rope-drive hoisting mechanism. This mechanism would be strong enough to raise and lower not only the platforms, tubes, and ladder, but also the technicians.

Initially, the apparatus would be maneuvered into position above, and aligned with, the hatch. The telescoping tubes would then be extended by a single actuator down through the hatch into the room below. The telescoping tubes would provide support for the platforms as they were lowered through the hatch and set up for use.

The platforms would include a fixed access platform and several flip platforms, all combined into an assembly at the bottom of the telescoping tube assembly. Once the platform assembly was lowered to the desired position, a technician would climb down the ladder to the platform assembly, then deploy the flip platforms to cover the entire open area and thereby provide a safe work platform. Other technicians, if needed, would then climb down the ladder to the work platform.

Two small jib hoists would be available for lowering and raising components and other equipment and, if necessary, for raising injured technicians.

This work was done by Scott T. Colorado and Alan C. Littlefield of **Kennedy Space Center** *and Scott Strickland of McDonnel Douglas Corp. Further information is contained in a TSP [see page 1].*

Inquiries concerning rights for the commercial use of this invention should be addressed to the Patent Counsel, Kennedy Space Center [see page 1]. Refer to KSC-11848.

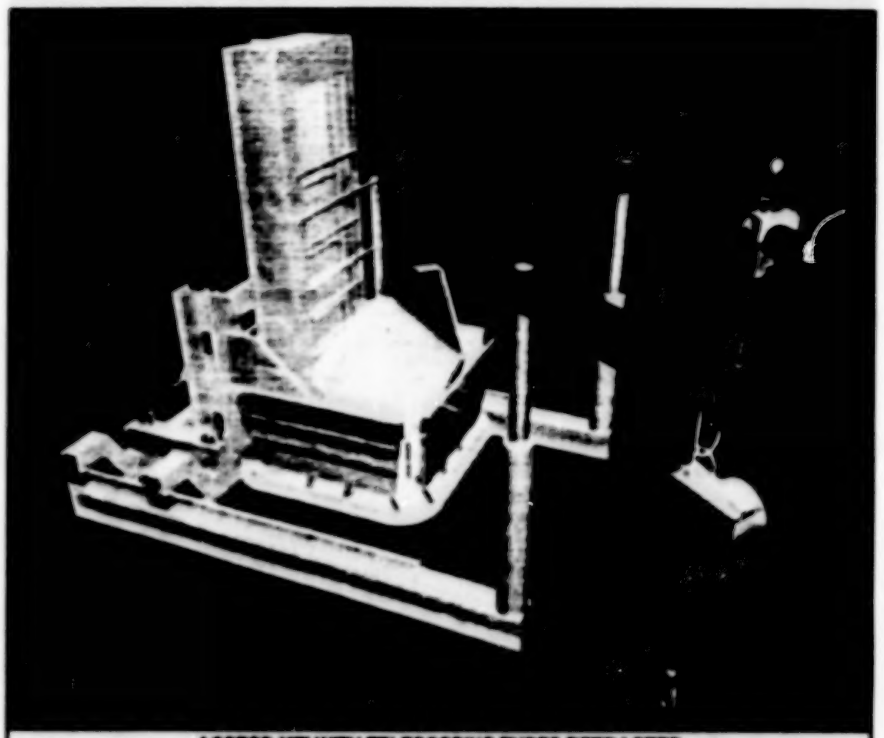

ACCESS KIT WITH TELESCOPING TUBES RETRACTED

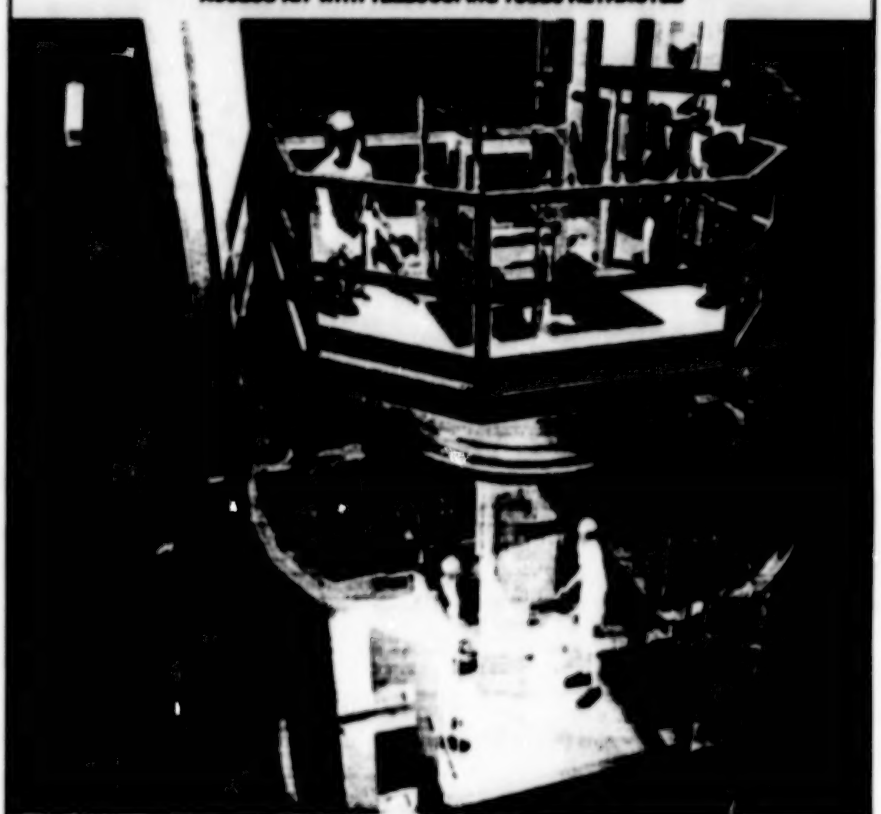

ACCESS KIT IN USE

The Access Kit Would Be Fairly Compact when the flip platforms were folded inward and the telescoping tubes retracted for assembly. In use, the telescoping tubes would be extended downward and the flip platforms deployed to form a work platform.

Reducing Gear-Mesh Vibrations With Piezoelectric Actuators

Opposing vibrations are introduced in a feedforward control scheme.

Lewis Research Center, Cleveland, Ohio

Experiments have demonstrated the feasibility of a feedforward scheme for reducing gearbox vibrations by introducing opposing forces at the gear-mesh frequency, using piezoelectric actuators coupled to the outer races of some of the gear-shaft bearings. The need to consider the introduction of opposing vibrations arises because even in the presence of the most careful design and precise fabrication, the variation in gear-tooth stiffness with motion of the meshing point along the gear-tooth profile makes it impossible to eliminate gear-mesh vibrations completely. The vibrations are transmitted through the gear shafts and bearings to the gearbox housing.

The basic concept of reducing vibrations in the gear box housing by use of opposing, piezoelectrically actuated vibrations has been investigated previously, but with a view toward suppressing synchronous, subsynchronous, and transient vibrations of rotors. In engineering disciplines concerned with vibrations of rotating machine elements, "synchronous" means at the frequency of rotation. Typically, frequencies of rotation are of the order of tens to hundreds of hertz. One of the novel aspects of the present development is the choice of the gear-mesh frequency (typically of the order of several kilohertz) rather than the lower frequencies addressed previously. Another novel aspect is the particular design for coupling between the actuators and the bearing races.

Figure 1 illustrates the arrangement of gears, bearings, and piezoelectric actuators in a test rig used in the experiments. The actuators at an angle that is collinear with the gear-tooth contact force; in the particular gear design, this angle is 20° off the centerlines of the shafts. Cone washers and a threaded plug preload a push rod between each actuator and its respective bearing race. A small accelerometer is mounted on each actuator. Not shown in Figure 1 are a mechanism for applying a static preload torque to the low-speed shaft, four accelerometers mounted on the gearbox housing to measure vibrations.

Figure 2 shows the major functional blocks of the feedforward control scheme to illustrate the principle of operation. An eddy-current displacement sensor is mounted to detect the passage of the teeth of one of the gears. As the gear

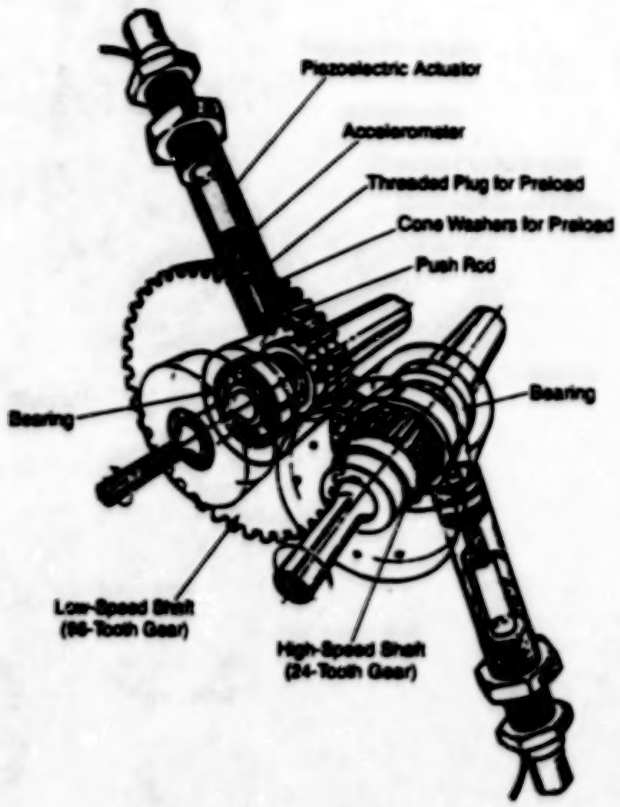

Figure 1. Piezoelectric Actuators Generate Forces to counteract gear-mesh vibrations. The off-center mounting scheme makes the actuator force collinear with the gear-mesh force.

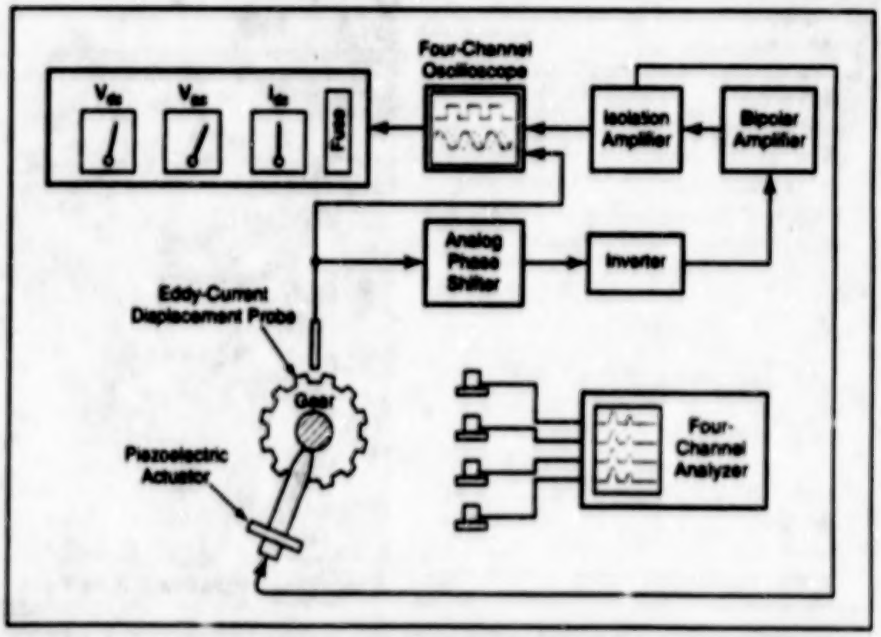

Figure 2. Feedforward Excitation for the Piezoelectric Actuators is generated from the displacement-probe output, which is a pulse wave synchronous with the meshing of the gear teeth.

rotates, this probe produces a pulse wave at the gear-mesh frequency. A feedforward circuit converts the pulse wave to a sinusoid of equal frequency. The phase of the sinusoid for each actuator can be adjusted manually, by use of a phase shifter and an inverter, over the full range of 360°. The feedforward circuit has a separate manual control to adjust the amplitude of the sinusoid.

An oscilloscope is used to monitor the gear-tooth pulse wave and the amplified feedforward sinusoid for each actuator. The voltage and current of the feedforward sinusoid is monitored by analog meters. A four-channel dynamic signal analyzer monitors the frequency responses of four accelerometers. In operation, the phase and amplitude of the feedforward sinusoid(s) are adjusted manually to minimize the amplitude of the gear-mesh-frequency component of the vibration amplitudes indicated by the signal analyzer.

This work was done by Albert F. Kascak and Gerald T. Montague of the Vehicle Propulsion Directorate of the U. S. Army Research Laboratory and Alan Palazzolo, Daniel Manchala, and Erwin Thomas of Texas A&M University for **Lewis Research Center**. *Further information is contained in a TSP [see page 1].*

Inquiries concerning rights for the commercial use of this invention should be addressed to NASA Lewis Research Center, Commercial Technology Office, Attn: Tech Brief Patent Status, Mail Stop 7–3, 21000 Brookpark Road, Cleveland, Ohio 44135. Refer to LEW-16070.

Books and Reports

Coupled Fluid-Dynamic and Thermal Effects in a Turbomachine

Effects that cause fatigue and reduce operating life are studied by numerical simulation.

A report summarizes a study of coupled fluid-dynamic and thermal effects that affect the performance and longevity of the fuel turbine of the Space Transportation main engine. The fuel turbine is a two-stage transonic turbine designed to produce a power of approximately 60,000 hp (=45 MW) and drive a three-stage turbopump that pumps cold hydrogen. The complex flows of hot turbine gas, of cold hydrogen (which leaks into the forward turbine-disk cavity), and of heat in each turbine-disk cavity were simulated numerically by use of advanced techniques of computational fluid dynamics: the equations for the transfer of heat coupled with the Navier-Stokes equations of flow in a flux-element-based, finite-volume formulation were solved numerically. A method called "conjugate heat transfer analysis" was used to solve equations for the flows in all three cavities and for the conduction of heat in each disk: this method involves mathematically treating all the disks and the flows in the cavities as being coupled together into one system (as they are in fact). The computed flows and distributions of temperature were used in the study to address such issues as thermal gradients, the resultant stresses in and distortions of disks, loss of performance through loss of sealing caused by thermal distortions that exceed dimensional tolerances of critical seal clearances, fatigue cracks caused by cyclic thermal stresses, and combined effects of thermal stresses and embrittlement by hydrogen. The goal of this and similar studies is to design a disk-cooling scheme that yields an acceptable thermal environment throughout the turbine.

This work was done by George Bache, Richard Swaim, and Robert Blumenthal of Gencorp Aerojet for **Marshall Space Flight Center**. *To obtain a copy of the report, "A Numerical Procedure for Coupled CFD/Thermal Conduction Analysis of Turbine Disks and Disk Cavities," see TSP's [page 1].*
MFS-28935

BLANK PAGE

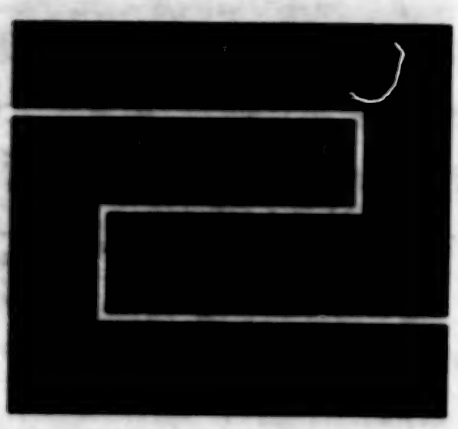

Fabrication Technology

Hardware, Techniques, and Processes

63 Back-Surface Relief To Enhance Friction Stir Welding

64 Desktop Manufacturing of Silicon Nitride Components

BLANK PAGE

Back-Surface Relief To Enhance Friction Stir Welding

Sensitivity to depth of penetration is reduced, and strength is increased.

Marshall Space Flight Center, Alabama

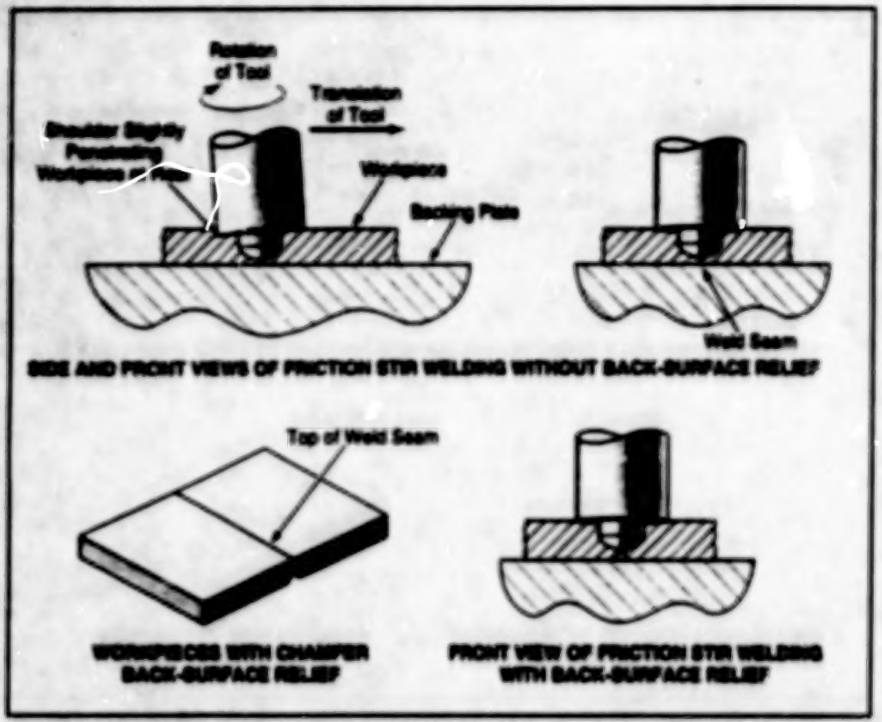
Rotation of Tool
Translation of Tool
Shoulder Slightly Penetrating Workpiece or Plate
Workpiece
Backing Plate
Weld Seam
SIDE AND FRONT VIEWS OF FRICTION STIR WELDING WITHOUT BACK-SURFACE RELIEF
Top of Weld Seam
WORKPIECES WITH CHAMFER BACK-SURFACE RELIEF
FRONT VIEW OF FRICTION STIR WELDING WITH BACK-SURFACE RELIEF

Figure 1. Friction Stir Welding can be performed without or with back-surface relief. Although the back-surface relief shown here is in the form of an inverted V groove, other relief cross sections could also be used.

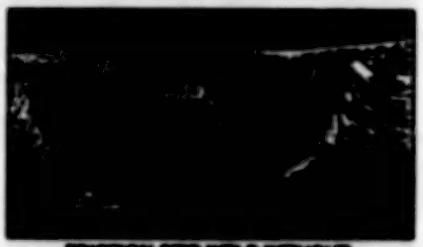

Figure 2. These Cross Sections of FSW Specimens exhibit different distributions of fine-grain structure. In the specimen made with back-surface relief, the distribution extends to the bottom and is more nearly even. These differences are associated with differences in mechanical properties.

An improved version of friction stir welding (FSW) incorporates a weld-preparation step in which a groove of suitable cross section is machined into the back surface, straddling the weld line between two workpieces to be joined (see Figure 1). This groove, known in the art as back-surface relief, offers two advantages: (1) it makes the overall FSW process more controllable by decreasing the sensitivity of the resulting weld quality to variations in the depth of penetration of the welding tool into the workpieces, and (2) the fracture strength and toughness of the weld exceed those of a similar weld made without back-surface relief.

The tool used in FSW comprises a shoulder and a probe. The tool is rotated, moved along the weld line, and pushed into the workpieces with considerable force. The force and motion plasticize and forge the parent material under the tool. The quality of the resulting weld is highly dependent on the depth of penetration of the probe, making it necessary to control the depth of penetration precisely by use of rigid structures to support the tool and the workpieces. In principle, the depth could be measured and controlled actively, but this would entail great expense.

In the absence of back-surface relief, plasticized material is forged between the probe tip and the bottom of the parent material. In the presence of back-surface relief, forging occurs between the probe tip and the backing plate, so that forged material is pushed into the relief volume. Back-surface relief thus redefines the nature of the FSW process. Though the precise physics of the improvement may be difficult to explain, it is apparent that back-surface relief makes the depth of penetration of the tool less critical, and there is apparently some optimal relationship between the geometry of the relief and the amount of parent metal pushed into the relief volume.

In an experiment to demonstrate this concept, 0.250-in. (6.35-mm)-thick workpieces of Al/Li alloy 2195 were joined by FSW, both with and without back-surface relief (see Figure 2). The specimens made with back-surface relief exhibited higher fracture strengths and greater elongations than did the specimens made without back-surface relief. Moreover, the standard deviations of the fracture strengths of the specimens made with back-surface relief were an order of magnitude smaller than those of the other specimens. These data indicate that back-surface relief results in stronger, more consistent welds.

This work was done by Jeff Ding of **Marshall Space Flight Center**, *Peter Oelgoetz of Boeing North American, Rocketdyne Division, Peter Romine of Florida International University, and Glynn Adams of the University of Arkansas. Further information is contained in a TSP [see page 1].*

Inquiries concerning rights for the commercial use of this invention should be addressed to the Patent Counsel, Marshall Space Flight Center [see page 1]. Refer to MFS-30134.

Desktop Manufacturing of Silicon Nitride Components

Three-dimensional components are built up layer-by-layer.

Marshall Space Flight Center, Alabama

A proprietary "desktop" laminated-object-manufacturing process has been used to rapidly fabricate silicon nitride components. The finished components are based on a computer-generated model and built without any mold or dies, so the design can be easily changed, providing engineers and designers with a very flexible and rapid prototyping process. The process has been used previously for rapid fabrication of prototype components from other ceramic materials besides silicon nitride. It has also been successfully used to create metal prototypes.

The first step in the process involves taking the ceramic powder and forming it into thin, flexible tape. The tape is used in special-purpose, computer-controlled equipment that laminates one layer of tape to a stack of previously laminated and cut layers. The new layer is then cut to form one cross-section of the part being built. In this manner, the desired three-dimensional components are built up layer-by-layer. After the part is finished, it is heat treated to complete the process.

This work was done by Curtis W. Griffin of Lone Peak Engineering for **Marshall Space Flight Center**. *No further documentation is available.*

MFS-26467

Mathematics and Information Sciences

Hardware, Techniques, and Processes

67 Double-Difference Precoding and Postdecoding

68 Optimization of Particle-in-Cell Codes on RISC Processors

69 Flexible Software Processes Telemetric Data

BLANK PAGE

Double-Difference Precoding and Postdecoding

This method improves data-compression performance for multiple and time-shifted sets of data.

Goddard Space Flight Center, Greenbelt, Maryland

A method of increasing the efficiency of data-compression coding involves precoding and postdecoding via double-difference computations. The method is particularly suitable for data from multiple and/or time-shifted sources; for example, image data from the same scene observed in different spectral bands and/or observed at different times.

The precoding and postdecoding amount to additional stages of compression and decompression, respectively. Like other data-compression schemes, this one reduces the volume of data to be transmitted by removing some of the correlated and redundant components of successive original data, so that successive transmitted data samples contain a higher proportion of uncorrelated and nonredundant data. Also as in other schemes, the redundant and correlated components are reconstructed, during decoding, from information contained in both current and previously transmitted coded data samples.

Of the various types of double-difference schemes that could be used, the one preferred in the present method is called "cross-adjacent" and is illustrated schematically in Figure 1. This scheme applies to two original sets of data: $(a_i) = (a_1, a_2, a_3, \ldots)$ and $(b_i) = (b_1, b_2, b_3, \ldots)$ where successive subscripts denote successive original data and where a_i corresponds to b_i. For example, a_i and b_i could represent original spectral intensities from the same location (the ith pixel) in the same image at two different wavelengths. First, for each (ith) pair of original data, one computes the cross-difference

$$\Delta_i^{b\,a} = b_i - a_i .$$

Next, one computes the differences between successive (adjacent) cross-differences; that is,

$$\Delta_i = \Delta_{i+1}^{b\,a} - \Delta_i^{b\,a} .$$

This is the desired set of double differences.

Straightforward algebraic manipulation of the double-difference equations yields recursive equations for reconstruction of one of the original sets of data from the other original set of data, the double differences, and the zeroth cross-difference term. That is, one obtains equations for reconstructing (b_i) from (a_i), (Δ_i), and $\Delta_0^{b\,a}$. Thus, it suffices to transmit the precompressed set of data $((a_i), (\Delta_i), \Delta_0^{b\,a})$.

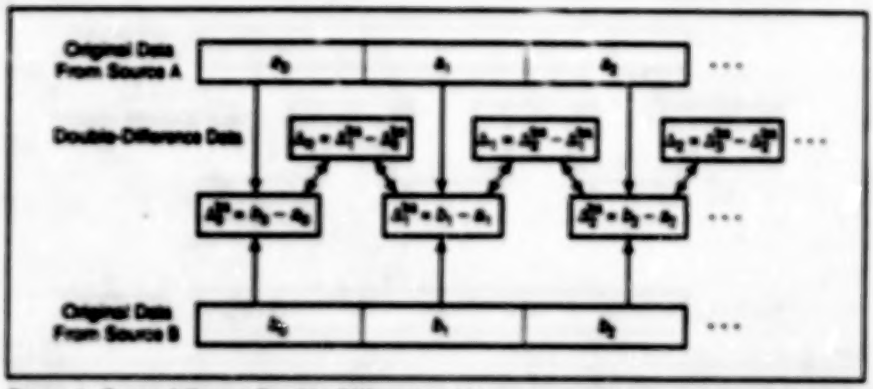

Figure 1. Cross-Adjacent Double Differences (Δ) are computed from sequences of corresponding original data (a) and (b).

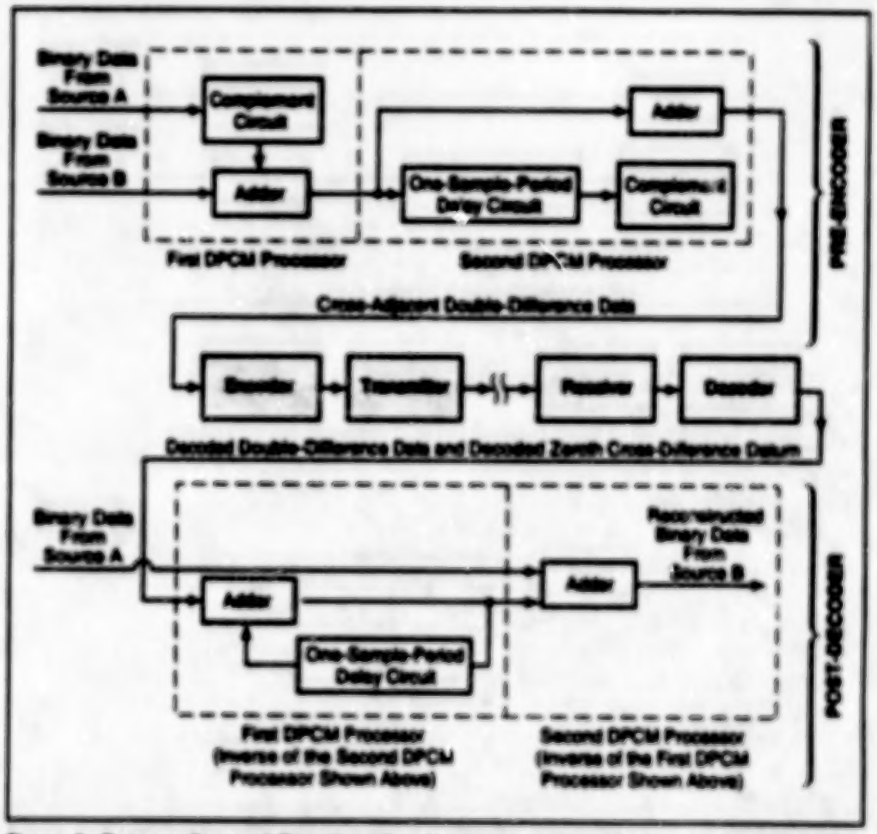

Figure 2. Precoding and Postdecoding Hardware that implements the cross-adjacent double-difference scheme consists of DPCM functional blocks.

Accordingly, in operation the original data are precompressed via the double-difference equations, and the precompressed data are fed to a standard lossless or lossy data-compression encoder suitable for the specific application. Following transmission, reception, and decoding, the complete original data are reconstructed from the decoded precompressed data via the recursive equations.

Typical electronic hardware for double-difference precoding compression and postdecoding reconstruction consists of several differential pulse code modulation (DPCM) processors (see Figure 2.) In precoding, binary data (a_i) from source A are fed to an arithmetic-complement circuit, while binary data (b_i) from source B are fed to one of the two input terminals of an adder. The output of the arithmetic-complement circuit is fed to the other input ter-

minal of the adder. The output of the adder is the cross-difference data (Δ_i^0 ^{a}). This output is fed directly to one of the input terminals of a second adder; it is also delayed by one data-sample period, then complemented, then fed to the other input of the second adder. Thus, the output of the second adder computes differences between successive cross-differences, yielding the stream of double-difference data, (Δ_i).

The postdecoding hardware, shown at the bottom of Figure 2, includes logic circuitry similar to that of the precoding hardware, except that it does not include a complement circuit. The decoded binary data (a_i) from source A are fed to one of two inputs of the right adder. The decoded double-difference data (Δ_i) and the zeroth cross-difference (Δ_0^0 ^{a}) are fed to one of the two input terminals of the left adder. The output of the left adder is delayed by one data-sample period and fed back to the other input terminal of the left adder. The output of the left adder is also fed to the other input terminal of the right adder. The output of the right adder is the stream of reconstructed data (b_i) from source B.

This work was done by Pen-Shu Yeh of **Goddard Space Flight Center**. *Further information is contained in a TSP [see page 1].*

This invention is owned by NASA, and a patent application has been filed. Inquiries concerning nonexclusive or exclusive license for its commercial development should be addressed to the Patent Counsel, Goddard Space Flight Center [see page 1]. Refer to GSC-13552.

Optimization of Particle-in-Cell Codes on RISC Processors

A combination of strategies yields appreciable speedup.

NASA's Jet Propulsion Laboratory, Pasadena, California

Several strategies for maximizing the speed of execution of particle-in-cell (PIC) codes on reduced-instruction-set-computer (RISC) processors have been developed. PIC codes have long been used in plasma physics to compute motions of charged particles in electric and magnetic fields generated by themselves. Algorithms for efficient execution of PIC codes on parallel processors were available prior to the development of the present strategies, but these algorithms do not address the efficient implementation of the codes on individual processors. The present strategies are intended to fill this gap.

The strategies were evaluated in computational experiments, using an established and previously well-tested Fortran electrostatic-field/charged-particle PIC code. The particular code was chosen because it is conceptually simple yet adequate for demonstrating the strategies. The time step in an electrostatic PIC code comprises three main parts: deposit, field solve, and push. In the deposit step, charge is deposited from the particles onto a grid to find the charge distribution. Each particle deposits charge to several nearby grid points and many particles deposit charge to each grid point. In the field-solve step, a Poisson equation is solved on the grid to find the electric field. In the push step, the electric field is interpolated to the particles to find their accelerations. Each particle reads the electric field from several nearby grid points and each grid point is read by many particles. These three main parts are repeated for as many time steps as desired. The deposit and push steps are characterized by memory references that are effectively random and

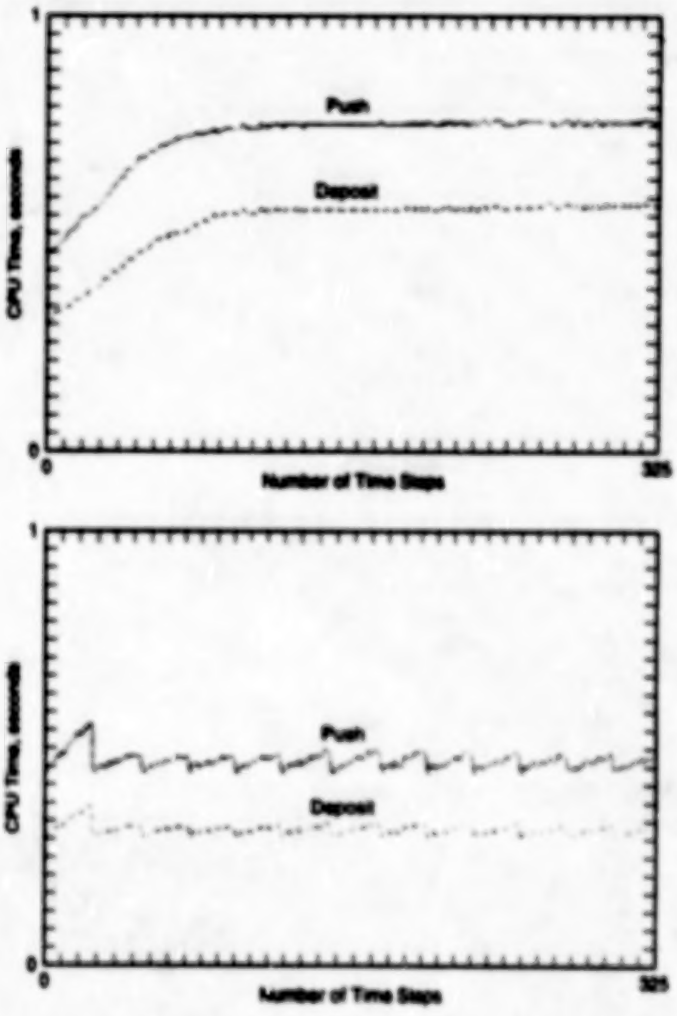

Central-Processing-Unit (CPU) Time for the push and deposit steps in a test case involving 327,680 particles tended to increase, in the absence of sorting, as particles became randomized by the computation. A simple bin sorting routine applied every 25 time steps proved effective in limiting the increase in CPU time without incurring excessive sorting overhead.

change from one time step to the next, making these steps challenging for computer-memory systems that are optimized for regular reference patterns.

The optimization strategies fall into two categories, one of which involves reorganization of data to improve utilization of cache memory. This category includes strategies for storing data on particles, or on both particles and fields, at contiguous memory locations. Also included in this category is a strategy for improving reuse of cache memory by occasional sorting of particles (see figure).

The second category involves reorganization of code to increase the efficiency of pipelined arithmetic. Strategies in this category include removing "IF" statements, reordering calculations, precalculating integer conversions, using one-dimensional addressing, and separation of "load" and "store" operations in the deposit step.

The results of the tests showed that no single strategy made a huge difference when applied alone, but that substantial improvements in performance (in terms of increases in processing speed) were achieved by aggregating the strategies. The amounts of improvement differed among processors and ranged between factors of 1.38 and 3.43.

This work was done by Viktor Decyk, Steve R. Karmesin, and Paulett C. Liewer of Caltech and Aeint de Boer of UCLA for **NASA's Jet Propulsion Laboratory**. *Further information is contained in a TSP [see page 1].*
NPO-19866

Flexible Software Processes Telemetric Data

This software provides a less-expensive alternative to ASIC telemetry-processing hardware.

Goddard Space Flight Center, Greenbelt, Maryland

The Software Telemetry Processing System (STPS) is a computer program that performs telemetric-data-processing functions that, heretofore, have been performed by custom-designed application-specific integrated circuits (ASICs). The cost of using the STPS in a given application ranges between one-tenth and one-fifth that of using ASICs. Originally designed to process data from spacecraft telemetry as specified by the Consultive Committee for Space Data Standards (CCSDS), the STPS can also be used, with little or no modification, to process non-CCSDS data.

In comparison with older telemetric-data-processing hardware and software, the STPS offers greater portability, scaleability, and flexibility. Portability is achieved by use of the C language, which can be compiled and installed on most computers. Scaleability is a consequence of portability in the sense that one can take advantage of portability to select a computer capable of handling data at the required rate for a specific application. Flexibility is achieved by incorporating the main data-processing capabilities into three software modules that can readily be customized for specific applications; an additional degree of flexibility is the possibility of using the computer for other tasks when there is no need to process telemetry.

The STPS performs the functions of a traditional frame synchronizer with an embedded Reed-Solomon Decoder and service processor. The first of the three software modules is functionally equivalent to an ASIC frame synchronizer that follows a "search, check, lock, and flywheel" synchronization strategy. It features programmable frame length, synchronization pattern, and tolerance settings. When executed on a Sun Microsystems Ultra 1-170 (or equivalent) computer with 32MB of random-access memory, this module can process data at a rate up to 18 Mb/s.

The second software module is functionally equivalent to an ASIC Reed-Solomon decoder. High-speed operation is achieved by clever use of registers and pointers in a highly optimized version of the Reed-Solomon decoding algorithm. This module features programmable virtual fill and interleaving settings. It can decode any Reed-Solomon code with a symbol length up to eight bits. When executed on a computer like the one mentioned above, this module can function at a data rate up to 2.55 Mb/s for data with a bit-error rate < 10^{-6}, or at a somewhat lower data rate for data with a higher bit-error rate.

The third software module — functionally equivalent to an ASIC service processor — accepts a stream of synchronized, decoded data from the preceding modules in a CCSDS format called "Channel Access Data Units" (CADUs). The data are subjected to either of two CCSDS processes called "Virtual Channel Data Unit Service" ("VCDU Service" for short) and "Path Service," respectively. The output of this module is in the form of data packets or VCDUs that do not include synchronization markers but do include headers that describe the processing that was performed and, optionally, descriptions of the data. The performance of this module depends on the lengths of packets; typical rates for execution on the previously mentioned computer are 10 Mb/s or 4×10^4 packets per second.

This work was done by Steve Duran, Chris Wilkinson, Tom Grubb, Karen Michael, Alex Krimchansky, John Park, and Greg Henegar of **Goddard Space Flight Center**, *and Jay Masino of Lockheed Martin. Further information is contained in a TSP [see page 1].*
GSC-13826

END

12-22-99